"Your eyes can eject tears [during grad school] to reflect any number of lesser emotions. Here's how to stop these involuntary shows of feeling [and weakness]:

**Tears of Sadness:** To stop yourself from crying, just remember that no matter how bad things seem, they would be even worse if you were a dinosaur—because you would be dead.

**Tears of Joy:** To throw off predators who will not hunt sad animals, your body may leak tears even if you are happy. Regain your composure by reflecting on a serious loss of life, such as the dinosaurs.

**Tears of Hunger:** If you haven't eaten in a few hours, you will start crying.

**Tears of Passion:** When your soul is enraptured by lust, your eyes will bleed tears to reflect the "ocean of love" you're swimming in. And then one day? BOOM! The whole world gets blown up by an asteroid, dinosaur-style."


- Groupon Cat




*"If you wish to make an apple pie from scratch, you must first invent the universe. "*

*"Matter is composed chiefly of nothing "*

*"The fossil record implies trial and error, an inability to anticipate the future, features inconsistent with an efficient Great Designer. "*

*- Carl Sagan*

# University of Alberta

Synthetic Main Group and Transition Metal Targets for Electronic and Photovoltaic Applications

by

## Adam C. Malcolm

A Thesis submitted to the Faculty of Graduate Studies and Research in partial fulfillment of the requirements for the degree of

## Master of Science

Department of Chemistry

©Adam C. Malcolm
Fall 2012
Edmonton, Alberta, Canada

*Dedicated to Jenna Marbles*

**Abstract**

The work presented herein is focused on the synthesis and characterization of inorganic materials for potential use in electronic and photovoltaic applications.

Platinum containing complexes of the form $L_xPt(SC_4H_2Br)_2$ (x = 1, L = dppe, dppp; x = 2, L = PBu$_3$, PAr$_3$), were synthesized using methods adapted from established literature procedures. The complexes were tested for their ability to undergo polymerization using known cross-coupling techniques. The ultimate goal of this study was to prepare photovoltaic polymers in polymer-based solar cells. For the complex $(Bu_3P)_2Pt(SC_4H_2Br)_2$, it was found that polymerization was possible, with crude materials having molecular weights ranging from 3500 - 38 000 g/ mol. We were unable to purify the polymeric materials due to high solubility of the crude product in all organic solvents. For the cases involving dppe and dppp, polymerization was not achieved, and simple cross-coupling reactions involving monofunctional thienyl-Br linkages were attempted. Preliminary synthetic routes towards sterically bulky Pt complexes were also attempted.

Boron nitride (BN) is a ceramic with hardness akin to diamond in its cubic form, and has an exceptionally high thermal conductivity, making it ideal as a heat transfer agent in microelectronics. We began looking at molecular boron nitride systems by isolating inorganic analogues of ethene ($H_2BNH_2$), in the form of donor-acceptor adducts of the form LB-$H_2BNRR'_2$-$BH_3$ (LB = DMAP, IPr, IPr=CH$_2$ and R, R' = H, H; Me, Me; H, $t$Bu). Preliminary dehydrogenation chemistry was performed with [Rh(COD)Cl]$_2$ and MBr$_2$ (M = Cu, Ni), to yield borazine as a byproduct, suggesting the presence of HBNH as an intermediate species. The efficacy of these adducts to yield parent iminoboranes and molecular boron nitride was also explored.

**Acknowledgements**

While completing this Master of Science degree, my near 3 year tenure at the University of Alberta has been filled with life changing experiences that I hope to convey the importance of with this fact:  grad school is not a glorious life, and it is seemingly seldom rewarding. Given the time input and the paltry salary a graduate student gets paid, one ultimately works for approximately $8/hr. The other side to this story is that this graduate degree has allowed me to rub shoulders with some of the most talented scientists I've ever met in my life, many of whom are a constant source of inspiration and guidance. I've been able to establish life-long connections with people and places that I likely would not have made otherwise. I also learned more in any 1 year of this degree, than I did in the entirety of my undergraduate studies, and I was given the opportunity to publish scientific papers in some of the most respected journals in my field. These are experiences I hold dear. I discovered though, that this path is not meant for me at this time. For those taking the path that I didn't: good luck.

I would like to first thank my supervisor Dr. Eric Rivard, a person who took a physical undergraduate chemist on as an inorganic graduate student, even though I hadn't even heard the term *Schlenk* before starting my work in his lab. When your graduate student's iPod contains a playlist of Slayer, Glee, Megadeth and Justin Bieber, and he hasn't even heard of "*n*BuLi", you are taking a huge gamble. Also, "The Rivarmy" is ©Adam Malcolm. I get $2 in non-negotiable royalties for every use.

I would also like to thank my partners in crime who helped make carrying out my sentence at the U of A worthwhile. Steve "Black Steve" Dempster, you made many of the most frustrating days just bearable enough that I didn't spontaneously combust. The Lofstrands Verner, Erika and Simon: you  both taught me many important life lessons including how to maintain a work/life balance, use a wet tile saw and breastfeed a cat. Sarah Theodore Regli, we will forever be locked in mortal kombat, akin to Yoda and Emporer Palpatine; 4 out of 5 Rebel Alliance scientists agree that you are a Sith Lord. Melanie "Melony" Hoffman, I am so thankful I was able to infiltrate your

secret circle, and become friends with a U of A celeb. Yours and Theodore's support were crucial to my survival, our Alliance of Awesome (including Dr. Matt "Who Has Hair Like That?" Zamora) has been impenetrable and invaluable to me over the last year. Kyle "Chelay" Sabourin, the process of obtaining waffles and consuming carbonated beverages is still unclear to me, but I am hoping that our friendship lasts long enough for you to show me, and for you to get me another publication. Marie Barnes, you terrify me but you make me cupcakes, which is the equivalent of a blood pact in many cultures. Shaleh Mohammed Ibrahim Al-Rafia, you were the best part of working in the Rivard lab, and I am thankful we had the chance to work together on so many projects. To the CSA: Consisting of Kyle Sabourin, Marie Barnes, Jason Brandt, Amber Shukaliak, Cameron S. Mullen, Leah Gaskin, Janelle Smiley-Wiens, Kevin Haggerty and many others; your group has been instrumental in allowing me to consume copious litres of ethanol and still have a place to sleep at the end of the night on Superbed. Sean Jien Hao Liew and William Ramsay, you guys were a pleasure to work with, and you taught me a lot, especially on the days when my patience seemed at an all time low. Everyone here has been my covert support team, helping me to evade capture, and stay on course. Not even divine animal sacrifices can repay the debt I owe you.

The following is a list of people who helped me come to terms with the cold and unrelenting universe: Dr. Matt Zamora, Christine Dunbar, Adam Park, Jenna Marbles, Rebecca Black, Kevin Zheng, E. Honda, Drs. Mike Ferguson and Bob McDonald, Dr. Kyle Wells, Dr. Joel Kelly, the Internet, Kyle Manchee, Tony Stark, Groupon, Katie Nizio, Jeremy Gauthier, Master Splinter, Sean Hoffman, Shaun McKinney, Alpha Five, Justin Thuss, left-handedness, Greg Kaufman, Amber Shukaliak, Rhett Clarke, Azuret Zuniga, Prof. Jon Veinot, Jeff Bunquin, Mark Miskolzie, Barney Stinson, Jessica Day, Dave Mustaine, Red Ranger, Erin Faught, Green Ranger, Leanne Laboissiere, Black Ranger, Arthur Mar, Jason Brandt, James Cameron, Michael Reed, Shawn "Ice Spiders" Compton, Amelia Walker, British Columbia, Earth, Jupiter, the Yukon, Pluto, gravity, Albert Einstein, Aunts and Uncles Malcolm, Matt Zamora again, Wegli, the Doppler effect, ethanol, caffeine, Japan, Craig Rutt, Diana of Themyscira, Briana Raposo, Ned Stark, Wanda, Ezio, Altair

**Table of Contents**

**List of Tables**

## List of Figures

**List of Schemes**

**List of Symbols, Nomenclature and Abbreviations**

$E_g$: Band-gap energy

$E_c$: Conduction band energy

$E_v$: Valence band energy

PCE: photovoltaic conversion efficiency

TW: Tera-watt

MWh: Mega-watt hour

PBSC: Polymer-based Solar Cell

P3HT: poly-3-hexylthiophene

PPV: poly(phenylvinylene)

PTB: poly(benzodithiophene)

PCBM: phenyl-C61-butyric acid methyl ester

HOMO: Highest occupied molecular orbital

LUMO: Lowest unoccupied molecular orbital

eV: Electron-volt

PVP: poly(vinylpyridine)

BN: molecular formula of boron nitride

SATP: Standard Ambient Temperature and Pressure

NMR: Nuclear Magnetic Resonance spectroscopy

MAS NMR: Magic Angle Spinning NMR

IR: infrared spectroscopy

AB: Ammonia Borane

LB: Lewis Base

LA: Lewis Acid

NHC: N-heterocyclic Carbene

IPr: 1,3-diisopropylphenylimidizol-2-ylidene

CAAC: Cyclic Alkyl Amino Carbene

MLCT: Metal-to-Ligand  Charge Transfer

DSSC: Dye Sensitized Solar Cell

MHJ: Multi-heterojunction

DCM: dichloromethane

THF: tetrahydrofuran

COD: 1,5-cyclooctadiene

$PBu_3$: tri-*n*-butylphosphine

dppe: bis(diphenyphosphino)ethane

dppp: bis(diphenylphosphino)propane

ppm: parts per million

$M_w$: molecular weight

ε: molar absorptivity

PDI: Polydispersity Index

GPC: Gel Permeation Chromatography

$IPrCH_2$: 1,3-diisopropylphenylimidizol-2-methylidene

DMAP: p-dimethylaminopyridine

MO: molecular orbital

HOMO-*n*: the *n*'th orbital below the HOMO

SHELXS-97: X-ray crystallography software

a, b, c, α, β, γ: unit cell vector and angle parameters

$ρ_{calcd}$: calculated density

μ: absorption coefficient

Δρ: electron difference map

DFT: Density Functional Theory

B3LYP: Becke, 3-parameter, Lee-Yang-Parr

cc-pVDZ: correlation consistent basis set

NBO: Natural Bonding Orbital

# Chapter 1

# Introduction

<div align="center">**Chapter 1**</div>

<div align="center">**Introduction**</div>

**1.1 Foreword**

The primary focus of the research presented in this Thesis involves the synthesis of materials for potential applications in solar cell and microelectronics technologies. Specifically, the first research chapter of this Thesis (Chapter 2) describes the attempted synthesis of new platinum-containing polymers for use in solar cells. The second research chapter (Chapter 3) involves the synthesis of donor-acceptor adducts of inorganic ethene derivatives ($H_2BNR_2$, R = H, Me, $t$Bu) and the exploration of these species as precursors for boron nitride (BN), a useful thermal conductor in microelectronics. In particular, the attempted dehydrogenation of these adducts to give complexes of inorganic ethyne (HBNR) and BN was explored. The relevant background material for Chapters 2 and 3 is described in sections 1.2 and 1.3, respectively.

**1.2 Platinum-containing polymers for use in polymer-based photovoltaics**

The term "solar cell" is conventionally used to describe a device that takes energy in the form of photons, and transforms it into electrical energy. This phenomenon can be traced back to what is most famously described as the photoelectric effect, where a photon impinges energy upon a material, ejecting an electron from the surface, inducing a form of photoconductivity. Discovered by Hertz [1] and described by Einstein [2], this phenomenon began what would later develop into solar cell technology. While Hertz and Einstein are considered some of the forefathers of photovoltaics, Smith [3], Adams and Day [4] were the first to observe the "effect of light on selenium" in 1873 and 1876 respectively. These bodies of work are responsible for discovering and laying the groundwork for what is now the modern field of photovoltaics.

**1.2.1 Current solar-cell technology**

Solar cells work on the simple principle of excitation of electrons from the valence band of a semiconducting material into the conduction band. The valence band can be described as a linear combination of the highest occupied molecular orbitals of the base unit of any material (in the case of bulk silicon, the 2p orbitals on Si atoms; in the case of a polymer, the HOMO of the monomer unit). In the same sense, the conduction band can be described as a linear combination of the lowest unoccupied molecular orbitals of the base unit. The energy difference between the two is known as the band-gap, which can be measured as the energy difference ($E_g$) between the highest occupied level of the valence band ($E_v$) and the lowest unoccupied level of the conduction band ($E_c$), such that the following relation is true: $E_g = |E_c - E_v|$. The primary function of a solar cell is to use electrons that have been photoexcited across the band-gap for work in photovoltaic cells [5a].

While solar cells were first developed on the principles of bulk semiconducting materials like Se and Si [5b], the technology has diversified into several sub-categories. The most prevalent types of solar cell under investigation as of 2012 are crystalline Si, semiconducting thin-film, quantum dot based, dye-sensitized, organic / inorganic polymer based, and multijunction cells [5]. While each type of cell has their strengths and weaknesses (which will be discussed later), all solar cells are bound by the physical limits of photoconductivity. An ideal solar cell would take in all usable energy from the sun, and convert it into electricity, which can be measured as the ratio of usable electrical energy output to solar energy input from the sun, giving a photovoltaic conversion efficiency (PCE); i.e., $E_{in} = E_{out}$, therefore $E_{out}/E_{in} = 100\%$. However, the physical limits of solid state p-n junctions and device limitations prevent this from happening, giving the more realistic relation: $E_{in} >>> E_{out}$. In 1961, it was first predicted by Shockley and Queisser that for a single p-n junction (a boundary between p-type (electron poor) and n-type (electron rich) semiconducting materials), the maximum amount of solar energy that can be converted into electric energy is 30%. This is limitation is refered to as the Shockley-Queisser limit, or more appropriately, the detailed

balance limit [6].

The described efficiency losses stem from three key physical events. The first involves the blackbody nature of all matter, whereby radiation emission above 0 K prevents absorption in the emitted energy range. The second involves electron-hole recombination, where an excited electron recombines with a  positive lattice hole instead of moving to the electrode, re-emitting the absorbed energy. The last form of efficiency loss arises from portions of the solar spectrum energetically insufficient to excite an electron from the valence band to the conduction band. This is the most significant source of loss, as any photon with energy less than the band-gap of the material, will not result in photocurrent, and is reflected as light or emitted as heat through non-radiative rovibrational decay. It was later calculated by De Vos in 1980 [7], that for an infinite series of p-n junctions, the maximum theoretical efficiency of such a cell is 86%. In a more pragmatic calculation, it was proven that the maximum for two and three tandem junction cells is 42% and 49%, respectively. However, if a solar cell can be manufactured at, or better than, grid parity (a measure that indicates whether a new form of electricity can match or decrease the current infrastructure's cost per watt) with today's means, an efficiency of even half of these theoretical maxima would allow for the optimal absorption of the 120 000 TW of power the sun provides daily; of note, global energy requirements comparitively are minimal, at needs of 15 - 20 TW [8].
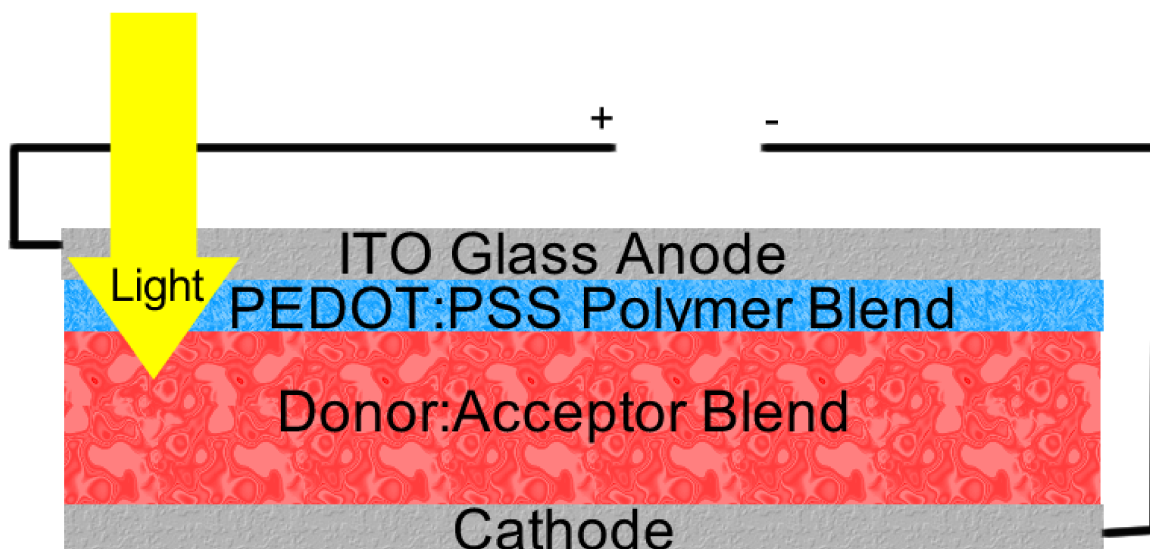
**Figure 1.2.1**: General schematic for a polymer-based bulk heterojunction solar cell device (top). The relative energy levels of the HOMO and LUMO levels for the relative components are shown (bottom). The HOMO-LUMO level for PEDOT:PSS is not shown, as it is not required for a standard solar cell to function, and this is meant for illustrative purposes only. [15]

The most widely used bulk material in solar cells is single crystal silicon (c-Si). Even though the cost of producing solar cell grade c-Si is high ($210/MWh as opposed to $86/MWh for hydroelectricity), the power conversion efficiency of these cells has increased rapidly over the years to 25.0% [9]; moreover when a concentrated sunlight source was used, a maximum reported efficiency of 27.6% was reported [10]. Producing large quantities of crystalline silicon at this high cost is a significant challenge, therefore there is a focus on preparing solar cells consisting of thin-films of semi-conductors that are cheaper and easier to produce. Currently, thin-films of semi-conductors based on Cu, Ga, In, As, and several pnictides and chalcogenides are the most efficient materials in thin-film semiconductor solar cells. Gallium arsenide (GaAs) is currently the gold standard for thin-film solar cells, with a maximum reported efficiency of 28.2% for unconcentrated sunlight, and 29.1% with concentrated sunlight [11]. When different semi-conducting thin-films are grown epitaxially on top of one another, an increasing number of p-n junctions can be obtained, resulting in cell efficiencies that can increase to over 40% [12]. The highest recorded PCE for a

solar cell is held by a three junction cell, composed of GaInP, GaAs, and GaInNAs layers. An efficiency of 43.5% was achieved when highly concentrated sunlight was used (418 suns; 1 sun represents the amount of solar radiation that strikes the earth per unit area [~930 W/m$^2$]) [13].

While the solar cell efficiencies offered by thin film or crystalline Si are impressive, the primary drawback is that they all require flat surfaces to prevent surface imperfections or extensive breaking of the crystalline phases, that degrade device performance. This creates a niche where organic and inorganic based polymers can be used, since polymeric materials do not require a flat surface as they are not by necessity regioregular and are soluble in most organic solvents, making them easily processable. Due to the increase of heterogeneous supermolecular disorder, light absorption is less uniform, thus power conversion efficiencies for polymer-based solar cells (PBSCs) are comparitively low (between 1% and 8%) [14], but this is balanced by the opportunity to incorporate PBSCs onto non-uniform or highly disordered substrates. The basic design of a PBSC is given in Figure 1.2.1 (note that a homogeneous donor-acceptor blended material is used). This is required to separate charges generated by the excited conductive polymer. Donor materials are conjugated polymers with a low band gap that generate excited state electrons when irradiated. Acceptor materials (typically fullerene derivatives) are those that funnel electrons away from the donor polymer towards the electrode, to prevent excited electron-hole recombination. Both materials are intimately mixed in the device, in order to promote electron-hole separation that is homogeneous throughout the donor:acceptor polymer layer of the device. Examples of donor materials are given in Figure 1.2.2.

The polymers shown in Figure 1.2.2 have lead to the production of devices with a variety of photovoltaic conversion efficiencies (PCEs, examples shown in later sections). In general, the PCE of a solar cell (defined as η) is calculated using the following equation.

$$\eta = \frac{V_{oc} I_{sc} FF}{P}$$

The variables $V_{oc}$, $I_c$ and $P$ represent the open circuit voltage, short circuit current and power input

respectively. The fill factor (FF) is a measure of how closely the power output of a cell matches the theoretical maximum (i.e., FF = $[P_{out}]^{measured}$ / $[P_{out}]^{theory}$) [15]. Polyphenylene vinylene (PPV) was the first polymer used in a photovoltaic device, and its derivatives have since been used to develop devices with PCEs between 0.75 and 2.5% [16] and, perform similarly to devices fabricated with polyfluorenes [17]. Poly-3-hexylthiophene (P3HT) is an alternative cost-effective polymer that can be synthesized from materials obtained from crude petroleum feedstocks. P3HT has been used to construct devices with common power conversion efficiencies between 3 and 4% [18]. Organic polymers have in recent years replaced or enhanced other components of the solar cell. For example, the polymer blend of poly(3,4-ethylenedioxythiophene) (PEDOT) and poly(styrenesulfonate) (PSS) has been used as a hole transport layer in devices with PCEs between 2% and 5% [18b, 19]. Nanowires of CdSe encapsulated in P3HT [20] and functionalized benzodithiophene polymers (PTBs) [21] have been able to achieve PCEs of between 6 and 7%, while 9.8% is the highest verified PCE for a polymeric solar cell derived from a P3HT variant [22].

A common trait amongst nearly all PBSCs in production today (i.e., Heliatek, Konarka, etc.)



**PPV**                **P3HT**                **PTB**
                                              **R = alkyl group**
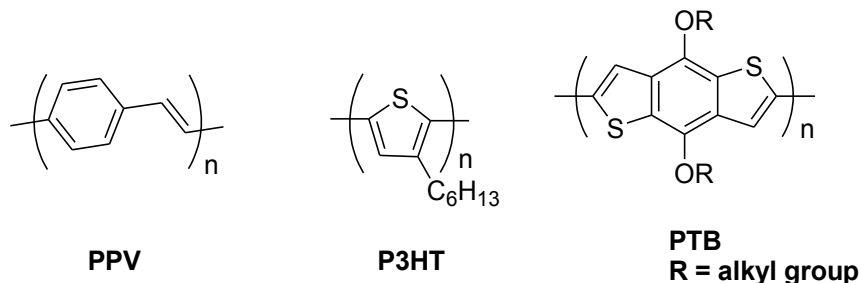
**Figure 1.2.2**: Common polymers used in PBSCs. PPV = poly(phenylvinylene), P3HT = poly(3-hexylthiophene), PTB = poly(benzodithiophene).

is the use of a specific electron acceptor material called phenyl-$C_{61}$-butyric acid methyl ester (PCBM). The parent material, fullerene ($C_{60}$) was first studied using PPV derivatives [23], and PCBM, this soluble derivative of $C_{60}$ has been shown to take on as many as 6 electrons in a reversible fashion [24, 25]. Due to the low efficiencies associated with PBSCs, the synthesis of thermally stable low-cost polymers of high molecular weight with an appropriately small band-gap

7

are required for widespread use of polymer-based devices. In 2006, Scharber and co-workers designed a theoretical experiment to predict the necessary HOMO and LUMO levels of a donor polymer to most efficiently work in tandem with PCBM, based on optimized polymer film thicknesses, fill factors and average charge mobilities of previously fabricated devices. It was predicted that the maximum single junction device efficiency using PCBM was between 10 and 11%, based on the limitations of the empirical factors inherent to the model, and the corresponding donor polymer would need a bandgap of <1.74 eV and a LUMO level of <-3.94 eV [26]. Furthermore, to achieve a modest efficiency range of 4 - 8%, the corresponding polymer will need a LUMO level between -3.2 and -3.7 eV, and a bandgap between 1.9 and 1.7 eV. With these parameters in mind, it is possible to predict at a glance if a polymer is appropriate for PCBM-based solar cells, without having to build costly prototype devices.

### 1.2.2 Metallopolymer chemistry

Metallopolymers are materials that contain metal atoms in the repeating monomer unit, and are a growing class of polymer for consideration in PBSCs. While not all metallopolymers are suitable for solar cells, there is a commonality in the synthetic methodologies used to prepare these materials. The presence of transition metals in a polymer backbone allow for a rich variety of bonding and reactivity due to the greater number of orbitals available to transition metal complexes with respect to organic counterparts. In addition, the nature of the valence shell of most metals allow for synthesis of highly coloured electron-rich materials. The following section comprises an overview of some of the key metallopolymer work relevant to the synthesis of Pt-containing polymers presented in section 1.2.3 and Chapter 2. Some of the first metallopolymers incorporated ferrocene ($Cp_2Fe$) as a building block ($Cp = \eta^5\text{-}C_5H_5$) [27], and in recent years, Manners and co-workers have explored the ring-opening polymerization (ROP) of dimethylsilaferrocenophane to form polymers (such as **1**) with controllable molecular weight distributions (Scheme 1.2.1).

Reactions of **1** with 2-vinylpyridine and N-trimethylsilyl(trichlorophosphoranimine) lead to the formation of the block co-polymers **2** and **3**, respectively [28, 29]. Notably, homopolymer **1** is useful as a charge dissipation coating for satellites [30]. Moreover when ferrocene is incorporated as a pendant group, highly coloured polymers can be obtained (Scheme 1.2.2, e.g., polymer **4**), with applications in chemosensing [31].
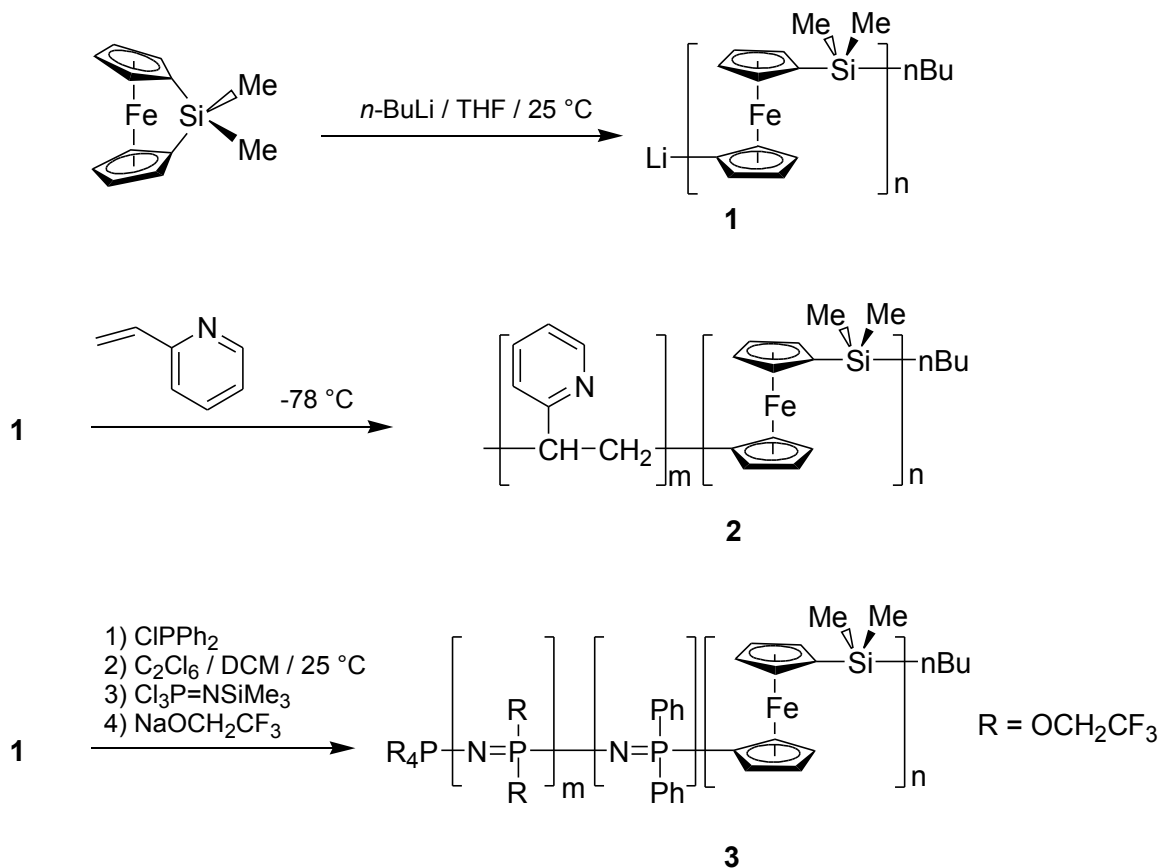


**Scheme 1.2.1**: Ring-opening polymerization of dimethylsilaferrocenophane, followed by formation of block co-polymers (**2** and **3**).
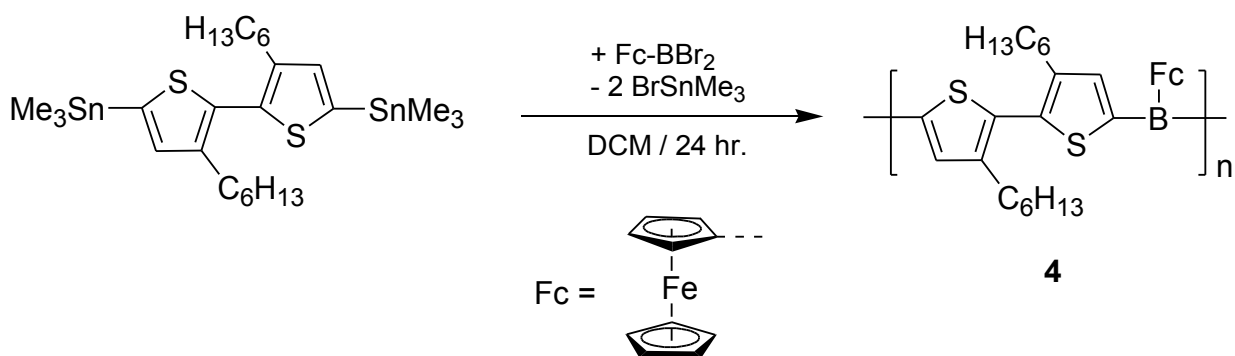
**Scheme 1.2.2**: Synthetic approach to building ferrocenyl boron-modified polybithiophene (**4**), a highly coloured material [31].

Another common type of metallopolymer are those generated by the cyclization of diynes using $Cp_2ZrCl_2$ (polymer **5**, Scheme 1.2.3) [32]. The use of $R_xECl_2$ type compounds (E = S, P, Ge, As, Sb, Bi, Si; R = Ph, Me) to replace Zr in heterocycles has been used before to generate phospholes, thiophenes, germoles, arsoles, etc. for molecular systems [33], but was extended to polymeric systems in this work, and later applied to macrocycles of similar structural nature [34]. Polymers of this form were first introduced in 1997 by Tilley and others, which emitted blue-light (Scheme 1.2.4, compound **6**) when Zr was replaced with phosphorous and sulfur (polymers **7** and **8**). It was found that polyphospholes synthesized using this method (e.g., **8**) had broad absorptions centred around 400 nm [35]. This strategy has more recently been used to modify existing polymer systems like polyfluorenes, to generate the organometallic polymer precursor **9** (Scheme 1.2.5), which can be used to generate many polymer variants rapidly by exchanging Zr with many different heteroatoms: this alone increases the scope of polymers that can be tested in photovoltaic applications [36].
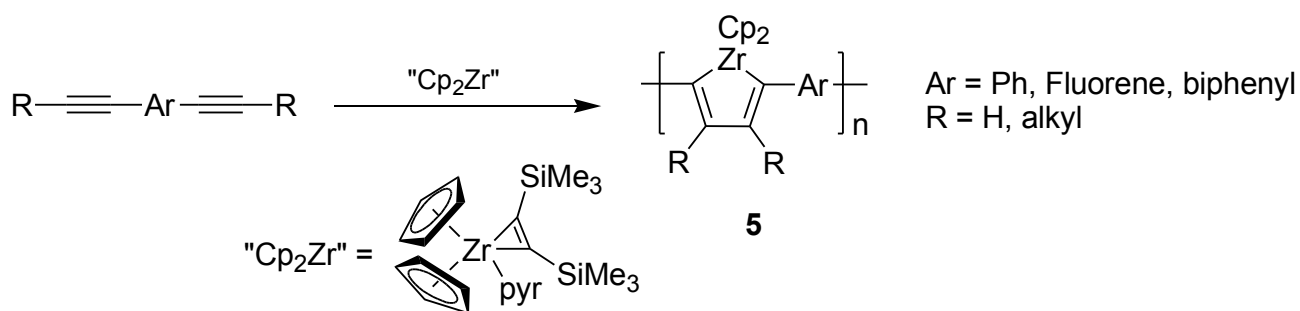
**Scheme 1.2.3**: General approach for the coupling of aromatic diynes to form zirconocene polymers.
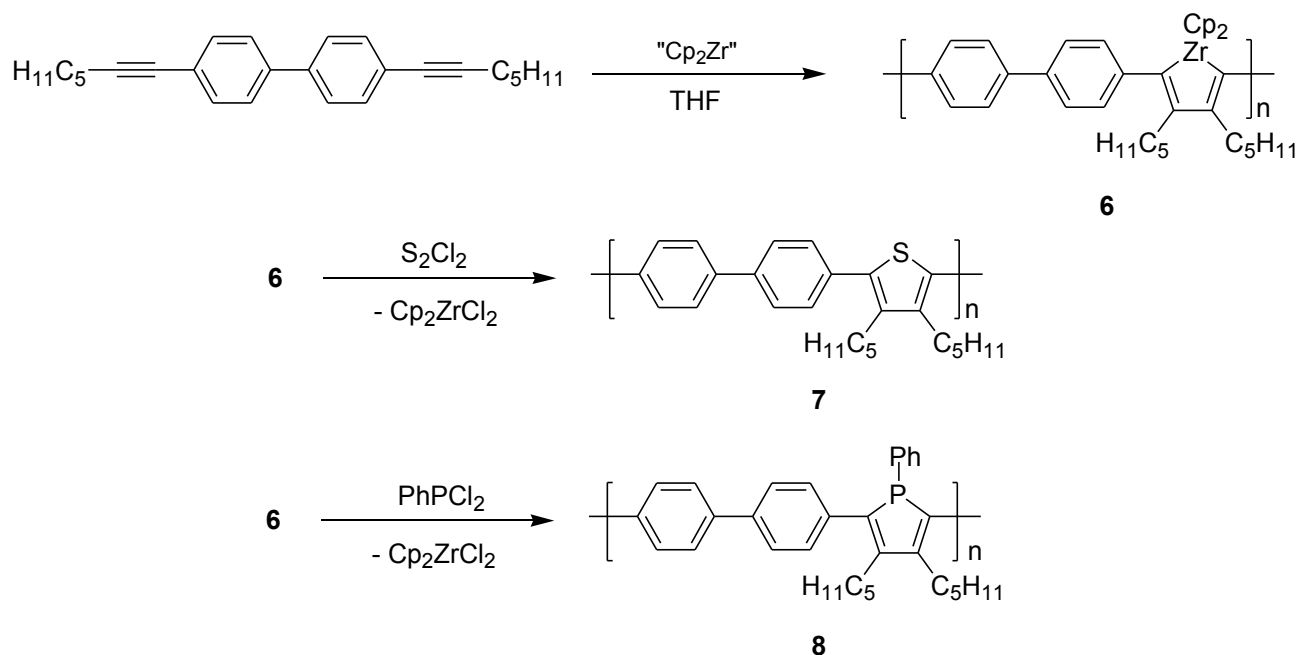


**Scheme 1.2.4**: Formation of Zr containing polymer (**6**) by coupling of an aromatic diyne using the Negishi reagent "Cp$_2$Zr", followed by metallacycle transfer to form polymers **7** and **8**.
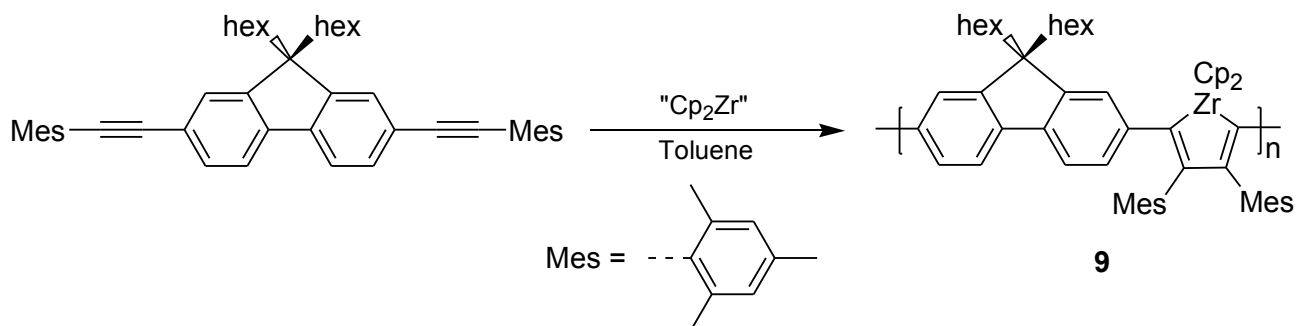


**Scheme 1.2.5**: Formation of the precursor polymer **9**, which can be used to generate a series of polymer variants via metallacycle transfer.

The ability of transition metals to take on many electrons and ligands into their coordination spheres allow for a broad range of bonds forming synthetic opportunities to form polymers. Coordination polymers are materials that feature metal atoms in either the main chain or as a pendant group in the repeating unit of the polymer, linked by coordinating ligands. Transition metals can be found in a variety of oxidation states and are typically electrophilic. Scheme 1.2.6 shows the synthesis of a polymer with Cu and Zn coordinated by two aromatic bidentate ligands, and because each side of the aromatic unit contains bidentate functionality, long chains of coordinated Cu and Zn atoms can be formed (compounds **10** and **11** [37]). Note that $Cu^{2+}$ and $Zn^{2+}$ are charge balanced by 2 $Cl^-$ anions in the inner coordination sphere. Another example is that shown in Scheme 1.2.7, where bis(bipyridyl)alkanes can form extended chains with $Fe(ClO_4)_2$ and $Co(ClO_4)_2$ (by the same reaction pathway as **10** and **11**), but also allows for the cross-linking of polymer chains due to the flexibility of the alkyl spacer between each pyridyl function, forming **12** and **13**. Other types of coordination polymers are those with pendant metal complexes that are not incorporated into the polymer backbone. Compounds **14** and **15** are representative examples of this type of polymer. Polymer **14** was synthesized by grafting vinyl functionality onto one of the bipyridine rings around Ru, followed by co-polymerization with other vinyl functionalized monomers, such as N,N′-methylenebis(acrylamide) [38]. In a different synthetic route, polymer **15** is prepared when pure poly(vinylpyridine) (PVP) is mixed with $Os(bpy)_2Cl_2$, which can coordinate to the pyridinyl nitrogen via cleavage of the Os-Cl bond. Due to the bulk of such a coordination complex and the short distance between pyridinyl groups, not all monomer units are metallated, thus a statistical polymer made up of PVP and $[PVP-Os(bpy)_2Cl]Cl$ units results [39]. In this case, one of the $Cl^-$ ligands was dissociated from the inner shell of Os to make room for pyridine, but remains in the outer shell for charge balance.
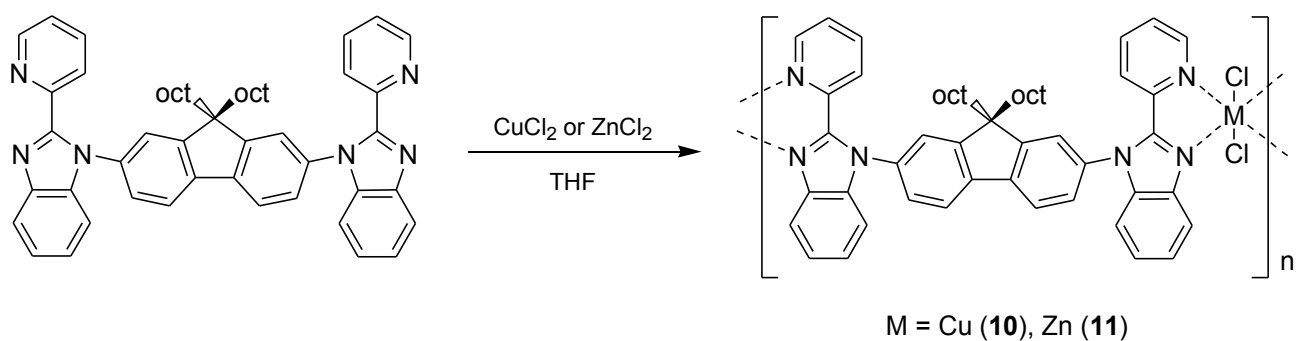
**Scheme 1.2.6**: Synthesis of a coordination polymer with Cu and Zn in the backbone.
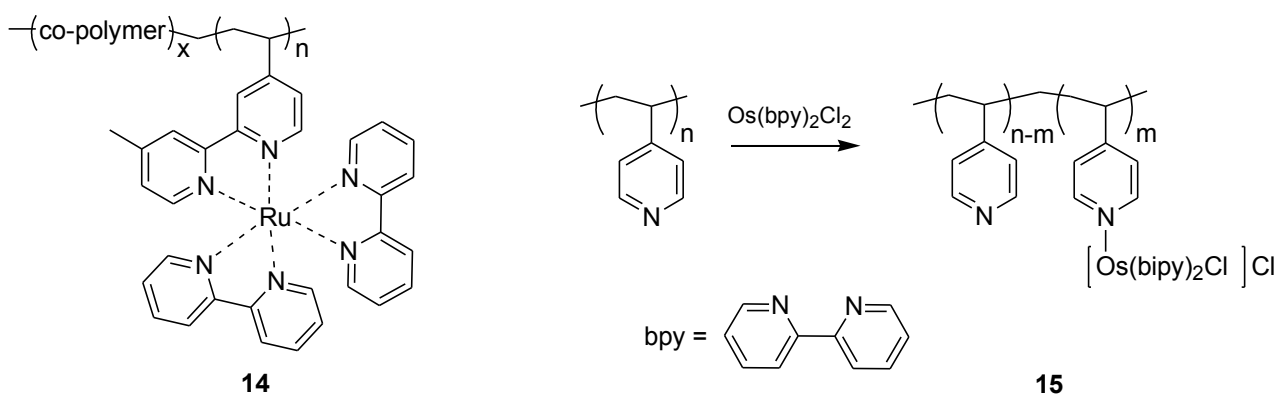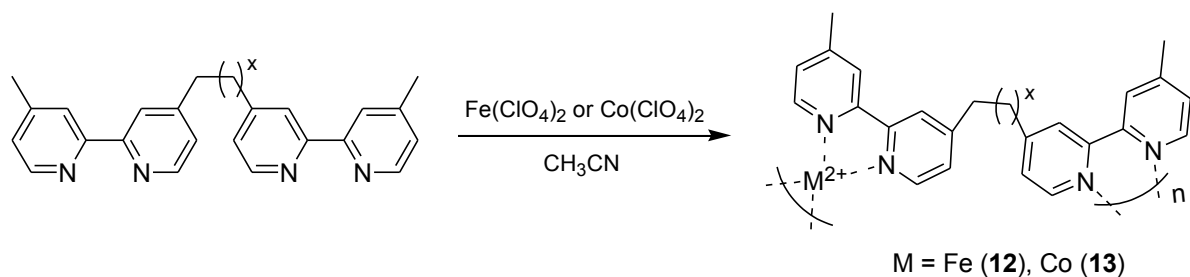


**Scheme 1.2.7**: Examples of coordination polymers with metals in the main polymer chain (**12**, **13**) and as pendant complexes (**14** and **15**).

The last type of metallopolymer to be discussed in this introduction are the rigid-rod acetylide polymers. In general, their defining trait is the placement of a metal atom between two acetylide units in the polymer chain, where the structural inflexibility of sp hybridized carbon atoms gives rise to the descriptor: rigid-rod. This type of polymer is synthesized from the Cu(I) catalyzed condensation of ligand stabilized transition metal dichlorides with aromatic diynes. The first

polymers of this type contained only Group 10 metals (e.g., polymer **16**), as metals in this chemical group readily form coordinatively unsaturated $d^8$ square planar arrangements, stabilized by a variety of neutral pnictine donors (Scheme 1.2.8) [27, 40]. It was also found that mixed metal polymers could be obtained by using a mixture of group 10 metal complexes (i.e., $L_2PtCl_2$ and $L_2PdCl_2$). Molecular weights of the air-stable polymers produced using this method can range from 1000 to 35 000 g/mol.



Ar = [benzene-1,4-diyl] or [biphenyl-4,4'-diyl] or [2,5-diethylbenzene-1,4-diyl]

L = $PMe_3$, $PBu_3$, $AsBu_3$

M = Pd, Pt, Ni

**Scheme 1.2.8**: General approach to polymerization of aryl diynes and the Group 10 metals.

Historically, there was some difficulty expanding the polycondensation route illustrated in Scheme 1.2.8 to include metals from Group 8 or 9, as many of the complexes necessary were not stable enough under the stated reaction conditions. However, as shown in Scheme 1.2.9, oxidative addition of the terminal C-H bond of an alkyne to the group 9 complex $Rh(PBu_3)_4(CH_3)$, can occur to give the Rh(III) complex **17a**. This complex subsequently reductively eliminates $CH_4$, allowing for another oxidative addition event to occur resulting in the formation of the diyne substituted Rh complex, **17b**. Successive reductive elimination and alkyne coupling events then transpire to yield a high molecular weight polymer, **18** (Scheme 1.2.9). The advantage of this method relative to prior routes is that it proceeds uncatalyzed, and forms volatile products that are easily removed *in vacuo* [41]. This class of metal-acetylide polymer has been shown to exhibit liquid crystalline behaviour

and non-linear optical properties [41b,c].
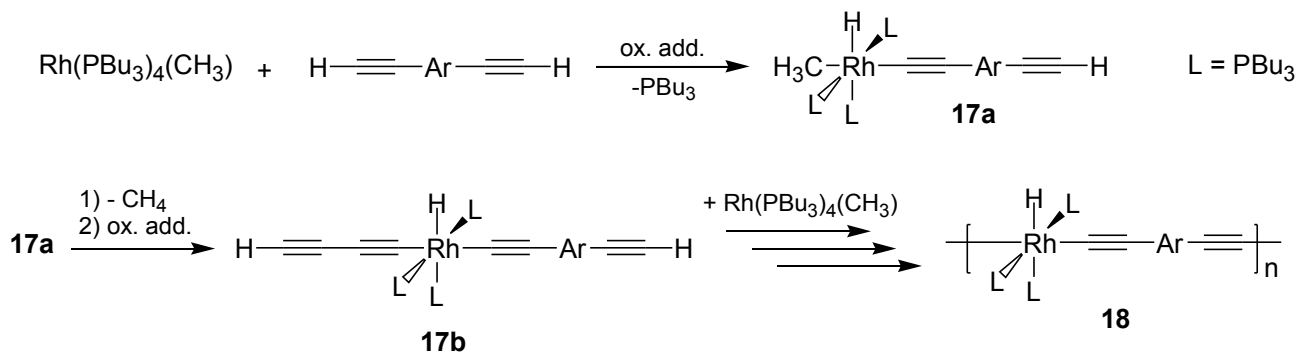


Scheme 1.2.9: An example synthesis of a rigid-rod Group 9 metallopolymer. Successive oxidative addition and reduction steps yield the polymer (18).

The above review of metallopolymers is far from exhaustive, as many of the polymer types described above have been investigated for almost 30 years, thus many variants with unique and specialized applications have been discovered [27]. What follows is a brief review that demonstrates how the previously described polymerization techniques and bonding motifs have been applied to platinum-based materials, and their more recent use in solar cell technologies.

### 1.2.3 Platinum-based complexes and conjugated polymers for solar cell applications

It is possible to extend the techniques described in the previous section to develop many different families of platinum-containing polymers. Organometallic complexes of heavy 2nd and 3rd row transition metals (even lanthanoid and actinoid metals) can exploit the ability of heavy atoms to stabilize and promote the formation of photoinduced high-spin excited states, via relativistic effects from the nucleus or intersystem crossing, which has been found to be especially true for platinum. This allows for a broad range of accessible excited states, and thus correspondingly broad light absorption profiles [42].

Platinum has been in widespread use outside of materials chemistry for many years. One of the most famous uses for platinum complexes is in the treatment of tumours with cisplatin [43]

(compound **20**, Figure 1.2.3). In recent years, **21** has been used to greater effect than **20** in deep tissue tumours, due to its photoactivity, a result of increased conjugation between Pt and its ligands [44]. Platinum complexes can have highly tunable absorption and emission spectra with substantial spectral changes induced by modifying the ligand structure around Pt. Compound **22** represents a recent example of a Pt complex whose luminescence undergoes a vapochromic shift in the presence of CHCl$_3$ vapour, simply by changing the position of the aryl-bound F atom on the phenylacetylide ligands. This phenomenon was attributed to the different ways in which **22** and its substitutional isomers pack during crystallization [45]. Platinum-acetylide compounds (such as **23**) are of special relevance as they are the building blocks of some of the first Pt-containing polymers. They are easily synthesized by reacting alkynes with L$_2$PtCl$_2$ type compounds (**19**) (see Scheme 1.2.8). The first Pt complex featuring thienyl groups bound directly to the metal centre was synthesized by Sonogashira (**24**), and the presence of thiophene groups were shown to greatly extend the conjugation length and the absorption profile of the complex relative to commonly synthesized platinum acetylides like **23** [46]. Compound **24** forms the basis for the monomers developed in Chapter 2, as it represents the convergence of Pt organometallic complexes and the established thiophene polymer chemistry already in use in PBSCs.
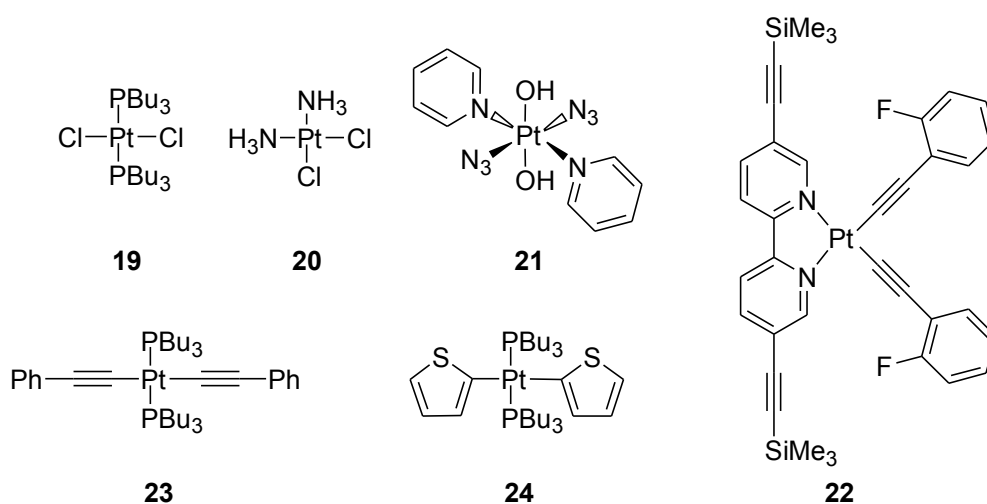


**Figure 1.2.3**: Selected examples of different types of organoplatinum complexes.

Many platinum polymers have been developed using the methodology described in section 1.2.2, and some selected examples are given in Figure 1.2.4. Compounds **25** and **26** represent typical Pt based polymers, where the phenyl and dioctyloxyphenyl spacer that bridges the diyne functionality has been varied to an exhaustive degree [47]. Many other examples exist where non-aromatic spacing groups have been used, such as **27**, which was synthesized using CuI catalyzed cross-coupling of **19** and diethynyldimethylsilane [48]. The molecular weights of **25 - 27** range from 5000 to 120 000 g/mol, with a wide range of polydispersities and degrees of polymerization [45b, 47, 48]. Polymer **29** is a unique example that combines two different metal centres within the same polymeric structure. It is synthesized from the monomer **28**, and contains Pt in the backbone chain of a rigid-rod polymer, with pendant ferrocene complexes on the stabilizing phosphines. Incorporation of ferrocene into the backbone of a polymer allows for enhanced redox chemistry and photoconductivity via enhanced MLCT events. Molecular weights as high as 88 000 g/mol have been recorded for **29** [49].
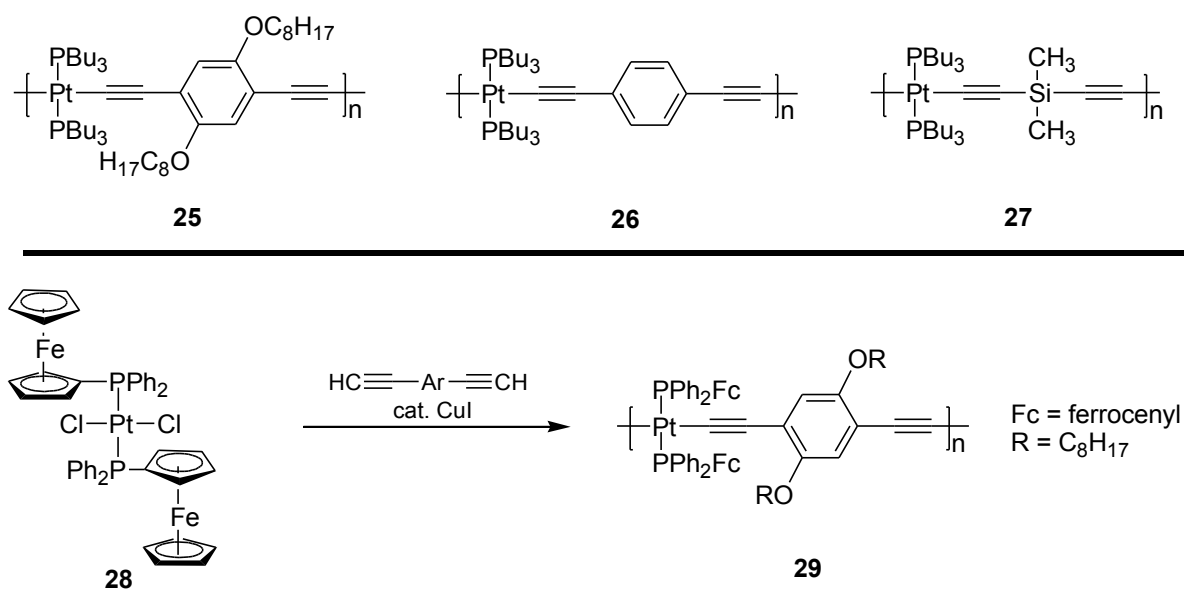


**Figure 1.2.4**: Representative examples of Pt-containing polymers from the scientific literature.

More recently researchers have focused efforts towards incorporating Pt-containing polymers in polymer based photovoltaics. Figure 1.2.5 contains selected examples of Pt-based polymers that have been tested in solar cell devices. Because of their historical usage in PBSCs, optical absorption profile, thermal stability and relatively low cost of fabrication, thiophene and thienyl variants are often incorporated into metallopolymer arrays as evidenced by polymers **30** - **32** (Figure 1.2.5). Not surprisingly the highest PCE for platinum polymer-based devices are most frequently obtained when Pt-complexes are joined by thiophene-containing bridging units. Polymers **30** and **31** have conversion efficiencies of 2.5% [50] and 2.41% [51] respectively, the higest recorded values for Pt-based PBSCs thus far. The effect of thiophene can be seen by comparing the observed PCEs of **32** and **33**, where the efficiency drops significantly  (from 1.29% to 0.41%) upon moving from thienyl to fluorenyl based co-monomers [52]. Apart from **32** and **33**, most Pt-based polymers contain bridging acetylide groups, due in great part to their ease of synthesis. Because of the presence of acetylide spacing groups, the conjugated thiophene units have the ability to freely rotate, which disrupts the π-system of the backbone, and reduces the conjugation length of the polymer.
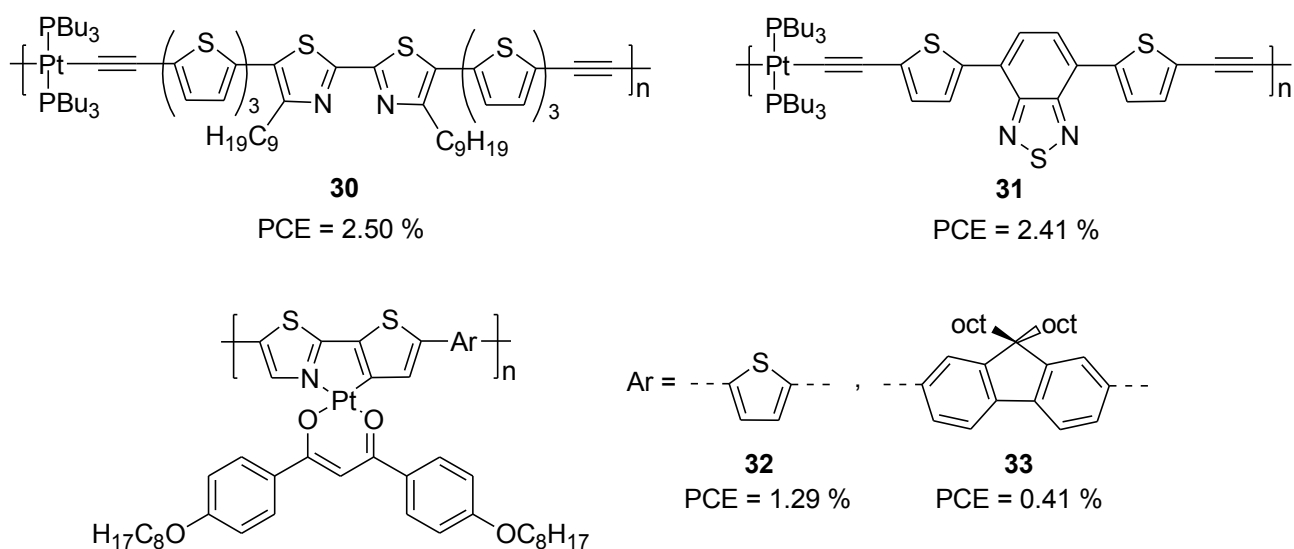


**Figure 1.2.5**: Selected Pt-based polymers that have been tested for use in polymer-based photovoltaics (with power conversion efficiencies (PCEs) shown).

It is hypothesized that the direct binding of thiophene rings to a Pt centre will introduce enough steric bulk from the proximal Pt-bound ligands that free rotation will be inhibited, while potentially encouraging additional backbone conjugation through $Pt(d_\pi)$ - thiophene($p_\pi$) interactions [46]. The synthetic methodology to prepare such a polymer has yet to be explored, and thus the goal of the work presented in Chapter 2 of this Thesis was to explore the synthesis and polymerization of Pt complexes with directly bound thienyl groups in order to generate high performance PBSC materials.

**1.3 Isolation of inorganic ethene ($H_2BNH_2$) for the mild synthesis of boron nitride**

Molecular boron nitride (BN) can be regarded as an inorganic equivalent of the dimeric carbon allotrope ($C_2$). Much like the alloptropic behaviour of carbon, boron nitride can exist in many different polymorphic phases. The molecular form of boron nitride is BN, and has only been observed fleetingly in the gas phase [53] and at very low temperatures in neon matrices [54]. It has been observed to exist in both its singlet and triplet states, with the triplet state being the most stable ground state [54,55]. The most common polymorphs of BN include hexagonal (graphitic) and cubic (diamond) forms. Cubic boron nitride (c-BN) is of great interest in electronic and mechanical applications, because it has a hardness similar to that of diamond [56, 57], and has an experimentally determined thermal conductivity of 7.4 W cm$^{-1}$ K$^{-1}$ (by comparison, Cu, Ni, and Au have thermal conductivities of 3.5, 0.9 and 3.1 W cm$^{-1}$ K$^{-1}$, respectively) [58]. What sets boron nitride apart from diamond is its thermal stability. Diamond readily oxidizes and decomposes when heated between 700 - 1700 °C, as diamond is itself only a metastable crystal form of carbon. Boron nitride does not decompose under such conditions, is stable to temperatures of 2000 °C under inert atmosphere, and is thermodynamically stable at room temperature [59]. It is with this material in mind that the work reported in Chapter 3 was done.

**1.3.1 Current methods for synthesizing boron nitride**

Amorphous boron nitride (a-BN) and hexagonal boron nitride (h-BN) are the most easily synthesized polymorphs of BN. a-BN can be synthesized by reacting $B(OH)_3$ under an atmosphere of $NH_3$ at 900 °C, which upon annealing at 1600 °C under $N_2$ atmosphere, forms the hexagonal phase [60]. While the energy requirements for synthesizing h-BN are seemingly high, given the low cost and availability of the starting materials, the costs of producing it are outweighed by potential applications. h-BN is a graphite-like substance that is already used as a high-end lubricant, and sees use in various cosmetics as it is transparent to colour additives, lubricious, and mixes well with

naturally occurring oils such that it easily applied to human skin [61]. It is also used as a primary feedstock for synthesizing cubic boron nitride (c-BN), which as mentioned, is a highly sought after material. Cubic boron nitride was first discovered in 1957, and later explored in detail by Wentorf and co-workers [59a, 62].  It was first synthesized by compressing an h-BN pellet at 1500 °C under 45 000 atm of pressure, using a "Belt" apparatus, designed to operate at ultra-high pressure and high temperature [63]. Addition of alkali metals and alkaline-earth metals were found to catalyze the transformation, yielding higher quantites of crystalline c-BN. Wurtzite BN (w-BN), another polymorph, is also obtained by this method, however it is highly unstable and slowly converts into c-BN at SATP, even though w-BN has been determined to be harder and tougher (Mohs and Vickers hardness) than its cubic form [64]. It was later discovered that the h-BN phase was obtained again if c-BN was heated above 1000 - 2000 °C at pressures higher than 10 GPa [65]. Other boron and nitrogen sources have since been used, as illustrated by the reaction between $B_2O_3$ and urea, $O=C(NH_2)_2$, to give h-BN [66]. Diamond has been used as an abrasive coating due to its hardness, thus c-BN is sought after as a synthetic cost-effective alternative. In addition, due to its high thermal conductivity and stability, it is a promising candidate as a heat transfer interface for micro- and nano-electronics, as it can absorb and dissipate heat very rapidly [58]. In light of these useful properties, much work has been done to synthesize c-BN using more cost-effective methods. An ideal synthesis would produce c-BN at a greatly lowered temperature and pressure.

Since the initial discovery of c-BN, several new techniques were found to produce high quality crystals of the material. For example, Yazu and co-workers used a temperature gradient approach, where a-BN or h-BN was heated in alkaline earth metal fluxes to 1600 K at 5.5 GPa to produce thermally mobile BN, which was grown on c-BN seed crystals at 1300 K [67]. This method does not improve the energy input requirements, but high quality crystals of varying sizes could be grown this way. Other gas phase methods of c-BN growth involve the use of ablation or ionization methods which convert h-BN or its precursors into gaseous BN molecules, which can be

crystallized as c-BN on various substrates. Shanfield and co-workers were able to deposit c-BN on ceramic or glass substrates by neutralizing an ion beam generated from a borazine ((HBNH)$_3$) plasma [68], and Vankar and co-workers were able to achieve the same result by sublimating B(OH)$_3$ into an NH$_3$ plasma [69]. Schulze and co-workers were able to deposit c-BN thin films by ablating h-BN with a KrF laser, and generating an ion beam by directing BN particles into an Ar/N$_2$ plasma, and later depositing c-BN onto silica or stainless steel substrates [70].

Dry chemical methods for synthesizing c-BN are the most prevalent in the scientific literature [71,72], however many other wet chemical and lower-temperature methods exist for producing boron nitride from molecular and polymeric precursors. Paine and others were able to synthesize h-BN at relatively low temperatures by pyrolysis of the boron and nitrogen rich material, poly(borazinylamine) (compound **35**, Scheme 1.3.1). Reacting **34** with HN(SiMe$_3$)$_2$ in diethylether at -78 °C formed **35** in high yield [73]; pyrolysis of **35** under vacuum at 900 °C, followed by annealing at 1200 °C in open air yielded h-BN. These temperature and pressures are significantly lower relative to the methods described earlier. The Paine group was also able to achieve the same result by starting with tris(dimethylamino)borazine (**36**) [74]; more recently the same group have also developed a method to generate hollow spheres of a-BN at low temperature (600 °C) by reacting liquid aerosols of aqueous B(OH)$_3$ with a gaseous stream of NH$_3$ [75].

While pristine samples of c-BN are difficult to make, polycrystalline and mixed phase of BN has been readily synthesized at low temperatures using the poly(aminoborane) **37**, followed by thermolysis at only 200 °C. Kim and co-workers detected the formation of fused B$_3$N$_3$ rings and small domains of amorphous BN by MAS NMR spectroscopy when samples of **37** were heated to 200 °C; full conversion to h-BN was then achieved when the samples were heated further to 1200 °C under N$_2$ (Scheme 1.3.1) [76]. One of the most interesting synthetic methods was developed by Strongin and co-workers, who were able to form h-BN by photolysing a condensed mixture of B$_2$H$_6$ and NH$_3$ gasses at 78 K, with 1000 eV synchrotron radiation. The mechanism by which this process

occurs is not fully understood, but characterization of the resulting BN film confirmed that the hexagonal phase was generated, though it remains unclear why such high energy photons were required to induce this chemistry [77]. This represents one of the very few, truly low temperature and pressure syntheses of BN, however the required use of synchrotron radiation still impedes the widespread use of this synthetic method by the chemical community. Many of the above mentioned methods utilize cyclic amino-borane precursors to form bulk boron nitride from controlled dehydrogenation reactions. Therefore it is plausible that molecular BN could be prepared directly from ammonia borane ($H_3N \bullet BH_3$) via dehydrogenation chemistry (Scheme 1.3.2).
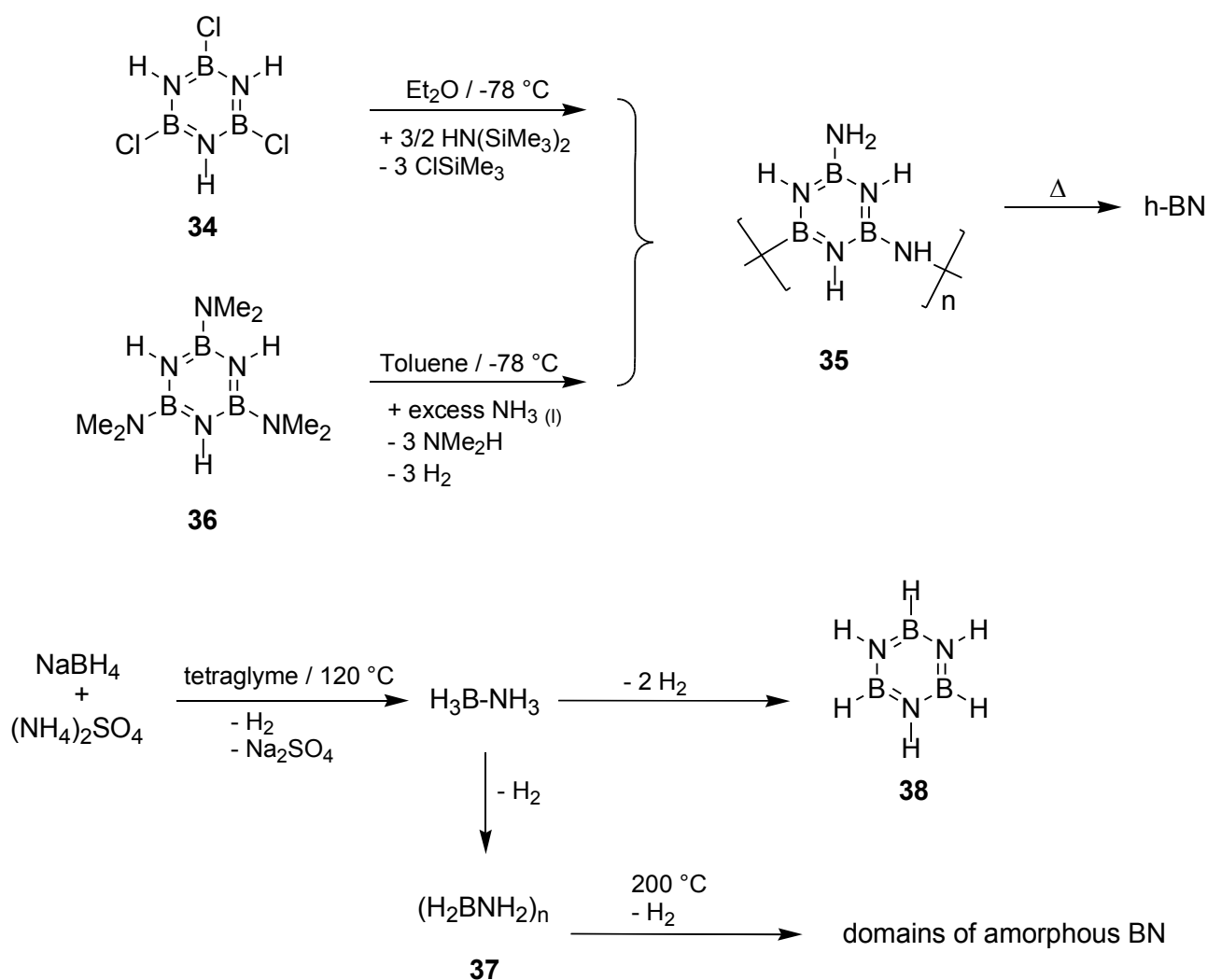


**Scheme 1.3.1**: Synthetic routes towards molecular precursors of boron nitride.

$$\text{H}_3\text{BNH}_3 \xrightarrow[\text{- H}_2]{} \text{H}_2\text{BNH}_2 \xrightarrow[\text{- H}_2]{} \text{HBNH} \xrightarrow[\text{- H}_2]{} \text{BN}$$
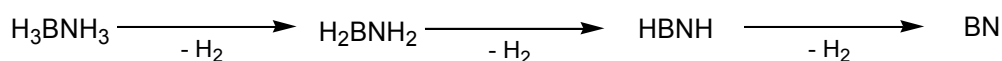
**Scheme 1.3.2**: Successive dehydrogenations of ammonia borane (H₃B•NH₃) to form molecular boron nitride.

### 1.3.2 Ammonia boranes as precursors for molecular boron nitride

Ammonia borane (AB, $H_3B•NH_3$) was recently termed "the hydrogen source par excellence" [78], as it contains 19.4 wt% of hydrogen stored in the form of N-H and B-H chemical bonds. The pathway for the release of hydrogen from AB involves the elimination of successive equivalents of $H_2$ gas, passing through oligomers of $H_2BNH_2$, HBNH, and finally an extended structure of BN as products. Unfortunately, the energetic requirements to achieve complete dehydrogenation were prohibitive, and recycling of the products was difficult, thus making it impractical as a hydrogen fuel source. The proposed mechanism of dehydrogenation is however useful as a model for developing materials for boron nitride synthesis. AB is isoelectronic with ethane, although its chemical reactivity is significantly different. Ethane ($H_3CCH_3$) is a neutral, dipole-less molecule, composed of poorly polarized covalent bonds, and is thus unable to form significant intermolecular hydrogen bonds. Ammonia borane is formally a coordination compound, formed by $NH_3$ donating its lone pair into the empty p-orbital of boron, datively binding to $BH_3$. The B-N bond is extremely polar (based on the difference in Pauling electronegativities) [79]. The B-H and N-H bonds are also very polar, leading to hydridic B-H bonds, and acidic N-H bonds; this bonding characteristic of ammonia borane allows for the release of hydrogen gas to transpire in a thermodynamically favourable manner [80]. These polar bonds also allow for significant intermolecular bonding, in the form of $H^{\delta+}•••H^{\delta-}$ interactions [79]. As a result, AB exists as an air-stable solid at room temperature, while ethane is a gas. The difference between ethane and AB can also be seen by examining the computed enthalpies of hydrogen release for the respective molecules (Figure 1.3.1).

|  | $\Delta H_{rxn}$ (kJ/mol) |  |  | $\Delta H_{rxn}$ (kJ/mol) |
|---|---|---|---|---|
| $H_3BNH_3 \longrightarrow H_2BNH_2 + H_2$ | -21.3 | | $H_3CCH_3 \longrightarrow H_2CCH_2 + H_2$ | 136.4 |
| $H_2BNH_2 \longrightarrow HBNH + H_2$ | 131.4 | | $H_2CCH_2 \longrightarrow HCCH + H_2$ | 175.8 |
| $HBNH \longrightarrow BN + H_2$ | 562.1 | | $HCCH \longrightarrow CC + H_2$ | 609.9 |

**Figure 1.3.1**: Comparison of reaction enthalpies from elimination of $H_2$ gas from ammonia borane and ethane. [78 and 80].

Dixon and Gutowski [80] calculated the reaction enthalpy ($\Delta H_{rxn}$) of $H_2$ loss from AB forming $H_2BNH_2$ to be -21.3 kJ/mol, while the related conversion of ethane to ethene is considerably endothermic ($\Delta H_{rxn}$ = 136.4 kJ/mol) [78]. The subsequent dehydrogenations of $H_2BNH_2$ and ethene are considerably endothermic (Figure 1.3.1), however catalysts have been developed which promote further dehydrogenation of amine-boranes, thus reducing the energy input required [80, 81]. For the case involving $H_2BNH_2$, polarization of the B-H and N-H bonds via electron donating or withdrawing groups may also aid in the further dehydrogenation. This behaviour of AB makes it a suitable precursor for boron nitride materials, and even the elusive BN molecule. In order to achieve this, simple $B_xN_xH_{2nx}$ molecules (analogous to hydrocarbons) must be synthesized using AB or similar materials.

### 1.3.3 BN analogues of hydrocarbons

The isoelectronic and isolobal nature of BN compounds with hydrocarbons [82] has led to the discovery of several new BN compounds. The most famous of which is borazine (**38**, Figure 1.3.2), the BN analogue of benzene. Many other BN analogues of hydrocarbon rings exist, despite having fewer practical uses than borazine iteself. Borazylene (**39a**, $[BH_2NH_2]_3$), is the inorganic equivalent of cyclohexane, and is formed by trimerization of $H_2BNH_2$ after dehydrogenation of AB. Similarly, the extended borazacycles $(BH_2NH_2)_4$ (**40a**) and $(BH_2NH_2)_5$ (**41**) have also been observed, albeit poorly characterized due to their very low solubilities in conventional solvents [83].

The heavier phosphinoborane congeners bearing aryl groups at P have been prepared by Manners and co-workers (**39b** and **40b**). Furthermore, the groups of Denis and Manners have synthesized the polyborophosphanylenes **42** and **43**, respectively [84]. The Manners group has also developed quantitative methods for synthesizing aminoboranes such as **44** from $Me_2HNBH_3$ with the aid of the dehydrocoupling catalysts $[CpFe(CO)_2]_2$ [85], $Ni^{(0)}$ [81], colloidal Rh and $[Rh(COD)Cl]_2$ (COD = 1,5-cyclooctadiene) [86]. The unusual aminoborane **45** has been synthesized as a byproduct from the catalytic dehydrocoupling of AB using $Ni^0$ catlysts, and thought to be produced by the reaction of transient $H_2BNH_2$ with $H_3B-NH_2-BH=NH_2$, an inorganic isomer of 1-butene (**46**) [87].
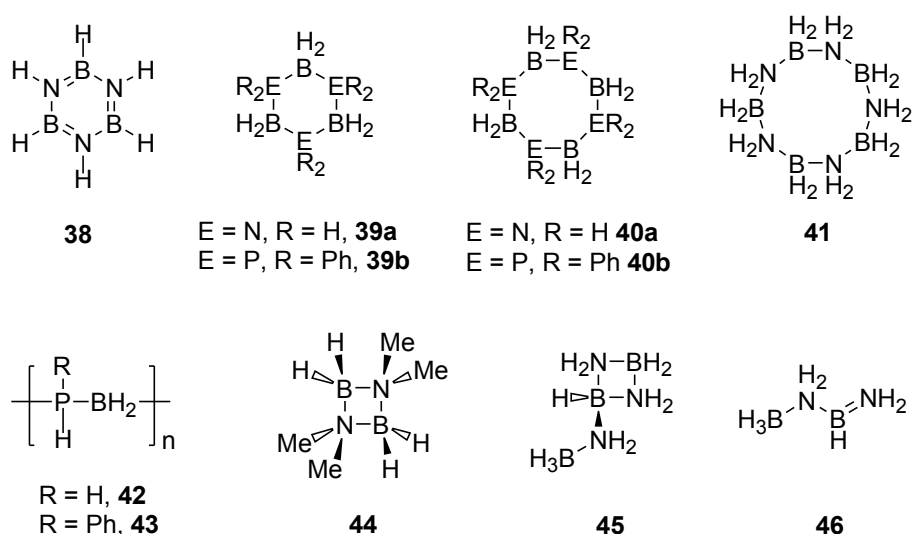


**Figure 1.3.2**: Inorganic (p-block) analogues of hydrocarbon rings, chains and macromolecules.

While BN analogues of hydrocarbon rings are thermodynamically stable at room temperature, many of the BN analogues of linear alkanes, alkenes and alkynes exist either transiently, or at very low temperatures. Other than AB, the next simplest linear BN hydrocarbon analogues are $H_2BNH_2$ (**47**), and HBNH (**48**), which are isoelectronic with ethene and ethyne [88]; in theory both of these species can be produced from the dehydrogenation of AB as outlined Scheme 1.3.3. While these molecules are highly unstable and cannot be isolated in the condensed phase, by substituting the hydrgogen on nitrogen for alkyl groups, many derivatives can be made

that are stable under ambient conditions. Dehydrogenation of secondary amine-borane adducts ($HR_2N \cdot BH_3$) can yield monomeric aminoboranes or oligomers, depending on the steric bulk of the N-substituent (Scheme 1.3.3). As discussed previously, when R = H, tetramers and pentamers are observed (**40a**, **41**), however when R = methyl, the dimer (**44**) is the major species found [86]. When the bulk of the substituents at nitrogen are increased (R = *i*Pr (**49**), Cy (**50**)), monomeric aminoboranes of the form $R_2N=BH_2$ are formed [85].
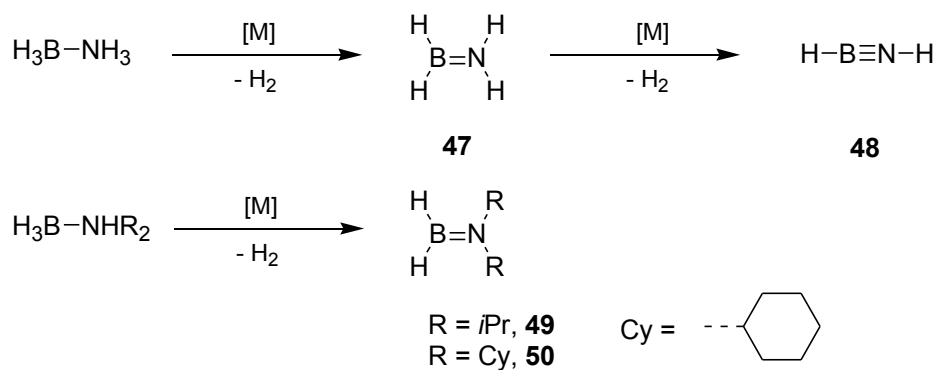


**Scheme 1.3.3**: Dehydrogenation of ammonia borane and secondary amine-borane adducts.


Due to the fact that $CH_2CH_2$ is isoelectronic with $BH_2NH_2$, only pairs of B-N bonds are strictly isoelectronic and isolobal with hydrocarbons. Thus the next highest BN chain analogue is that of butane ($H_3NBH_2NH_2BH_3$, **51**), which was only very recently synthesized [89] via the route shown in Scheme 1.3.4. The only other known 4-chain analogue is that of 1-butene (**46**, $BH_3NH_2BH=NH_2$) mentioned previously [87]. As of this writing, the largest observed straight chain BN analogue is that of butane (**51**), however the 6, 8, 10, and 12 atom chains $[H(BH_2NH_2)_nH]$ have already been investigated by theoretical methods [90]. The next largest analogue, BN-hexane (Scheme 1.3.4, compound **52**), has been predicted to form straight chains in the solid phase and is thermodynamically stable. This is not true in the solution phase, where borazylene formation is predicted to be favourable due to coiling and dehydrocyclization of **52** [91] (Scheme 1.3.4), hence BN-hexane has not yet been isolated.

$H_3B-NH_3$ + $BH_3 \cdot THF$ $\xrightarrow[-H_2]{THF}$ [cyclic B–N–B structure] $\xrightarrow{+NH_3}$ $H_3B$–$\overset{H_2}{N}$–$\overset{NH_3}{B}$ (**51**)

BN-hexane, **52** $\xrightarrow[-H_2]{\text{coiling in solution}}$ borazylene, **39**
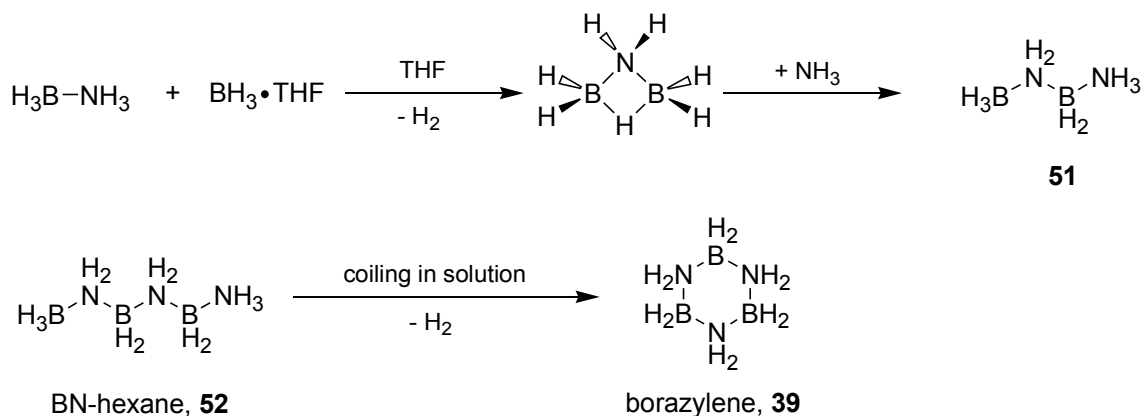
**Scheme 1.3.4**: Synthesis of BN-butane and dehydrocyclization of BN-hexane.

The simplest boron-nitrogen species, BN, is also one of the most elusive. In the formal Lewis structure, BN has a B-N triple bond, with a lone pair on N ($B\equiv N:$). While this compound has been observed in matrix isolation and plasma discharges, no stable complexes of this molecule have been synthesized yet. Iminoboranes ($R-B\equiv N-R$) are the closest class of compound to molecular BN as these species have bonding that is formally derived from the donation of the N lone pair into the empty p-orbital on B (Scheme 1.3.5). The first isolated example of an iminoborane, $C_6F_5$-$B\equiv N$-Mes (Mes = 2,4,6-$Me_3C_6H_2$) (**53**), was discovered by Paetzold in 1967 [92], with the tert-butylated analogue, $t$Bu-$B\equiv N$-$t$Bu (**54**), being the most well-studied system. Compound **54** is chemically versatile with numerous cycloaddition reactions known and coordination chemistry with transition metals reported (e.g., compound **55**) [93] (Scheme 1.3.5).
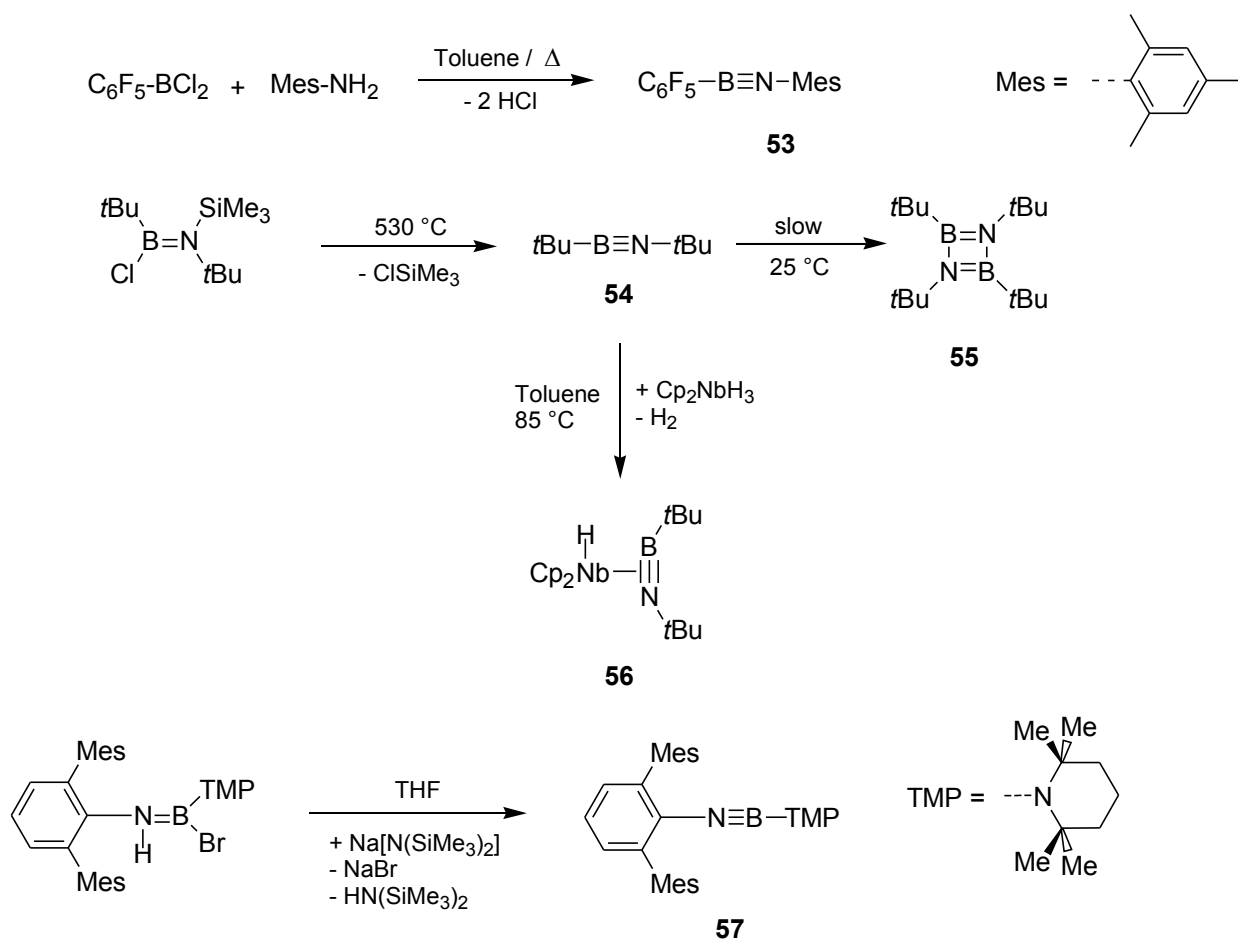
**Scheme 1.3.5**: Synthetic routes towards iminoboranes, (RB≡NR).

In recent years, the Power group synthesized an iminoborane using bulky terphenyl substituents on nitrogen (**57**) via dehydrohalogenation [95]. It is worth noting no examples of the parent iminoborane (HB≡NH) have been stabilized at room temperature, likely due to the propensity of this molecule to oligomerize [96]. Iminoboranes are the most logical precursors to molecular boron nitride (B≡N:), it is therefore of great interest to discover a methodology for stabilizing such a molecule in its monomeric form.

### 1.3.4 Donor-acceptor stabilization of reactive molecules

Often molecules predicted to be stable in the gas phase will decompose in the liquid or solid

state because of weak or polar bonds and the presence of reactive sites such as lone pairs on an electronegative atom, or vacant orbitals that allow for further reaction in low energy pathways. While stable in the absence of strong σ-donors, boron containing molecules are often prone to nucleophilic attack, because boron has an electron deficient valence shell (a trait of the triel elements), with an empty p-orbital perpendicular to the $sp^2$ bond plane of boron in the commonly observed $BR_3$ systems. This reactivity pathway can often be shut down by occupying the orbital with a neutral, closed-shell donor to form a coordinative donor-acceptor adduct ($R_3B•LB$; LB = Lewis basic lone pair donor).

A classic example of a borane adduct was discovered in 1809 when Gay-Lussac and Thenard stabilized the reactive gas, $BF_3$, with the lone pair of $NH_3$, to give $H_3N•BF_3$ as a stable solid [97]. Since this time many other examples of boron based adducts compounds have been discovered, including those of the parent borane ($BH_3$) and many derivatives thereof [98]. In addition, adduct formation can enable isolation of species that are highly reactive. An excellent example of this principle is the formation of a stable complex of diborene (HB=BH, **58**) by Robinson and co-workers (Scheme 1.3.6); notably HBBH is a highly reactive triplet molecule in the absence of the donor IPr (1,3 - diisopropylphenylimidazol-2-ylidene) [99, 100]. Braunschweig and others were able to use a similar method to intercept the parent borylene (:BH) using N-heterocyclic carbenes (NHCs) and sodium naphthalide, however the borylene fragment was never truly isolated, and only invoked as a plausible intermediate in the examined reactions. In 2011, Bertrand and co-workers were finally able to isolate HB: coordinated by two NHCs to form **59** [101] (Scheme 1.3.5). This result is especially significant because it is the first isolation of a neutral nucleophilic source of boron. Other excellent examples of stabilized reactive molecules include dialane ($H_2AlAlH_2$) [101c], silanones ($R_2Si=O$) [101d], diphosphorus ($P_2$) [101e], digermene ($H_2GeGeH_2$) [101f], and the formal complexation of phosphorus nitride (PN) [101g]. One of the best examples of carbene stabilization comes from the Robinson group, who stabilized the elusive disilene

complex(LB-:Si=Si:-LB, **60**, LB = Lewis base), which has both a vacant orbital and lone pair on each silicon atom [102].

Similar to disilene, some molecules are bifunctional, in that they contain both a vacant orbital (Lewis acidic site), and lone pair (Lewis basic site). Many such molecules have also been stabilized with NHCs, however a Lewis acid is also added as a capping agent to prevent reaction of the nucleophilic lone pair. Using both a Lewis acid and a Lewis base to stabilize these bifunctional molecules has been termed donor-acceptor stabilization. This technique has been used by our research group to generate the first stable complexes of the parent heavy methylenes [103], :SiH$_2$ (**61**), :GeH$_2$ (**62**), and :SnH$_2$ (**63**) (Scheme 1.3.7). These molecules are often invoked as intermediates in the decomposition pathways of metallanes, EH$_4$ (E = Ge, Si), and have been trapped at low temperatures [104], but were first isolated at room temperature here in the form of stable adducts.
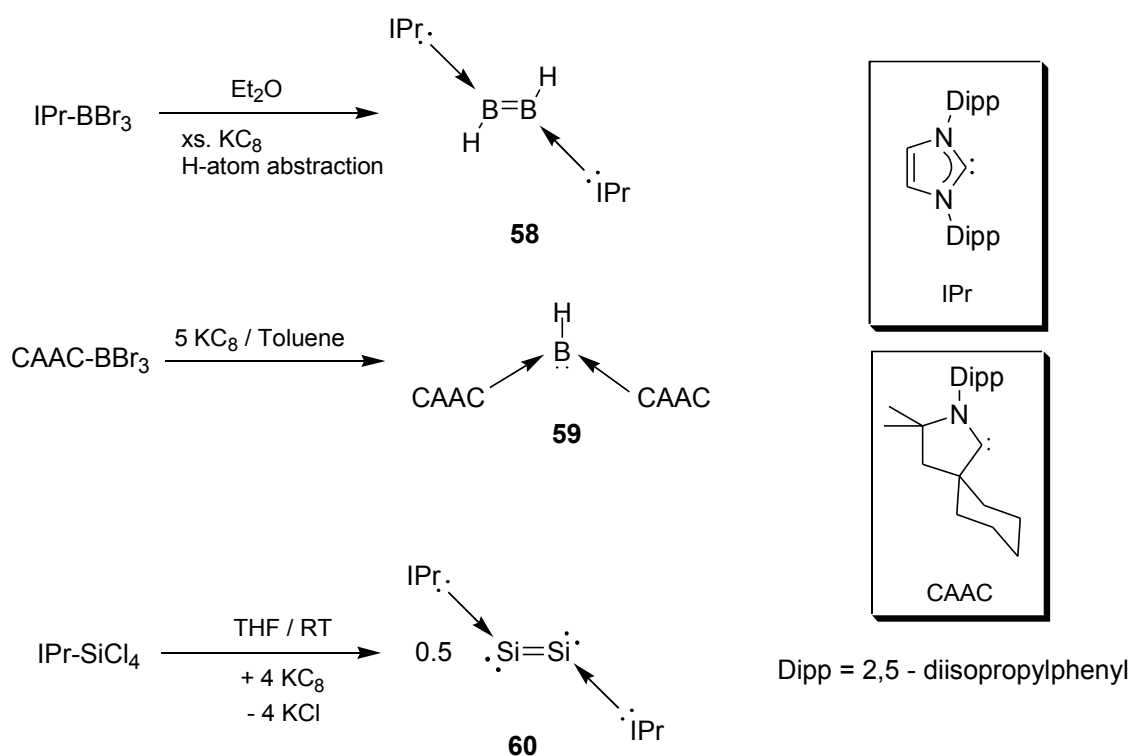


**Scheme 1.3.6**: Stabilization of diborene (**58**), the parent borylene (**59**), and disilene (**60**) using NHC ligands.

31
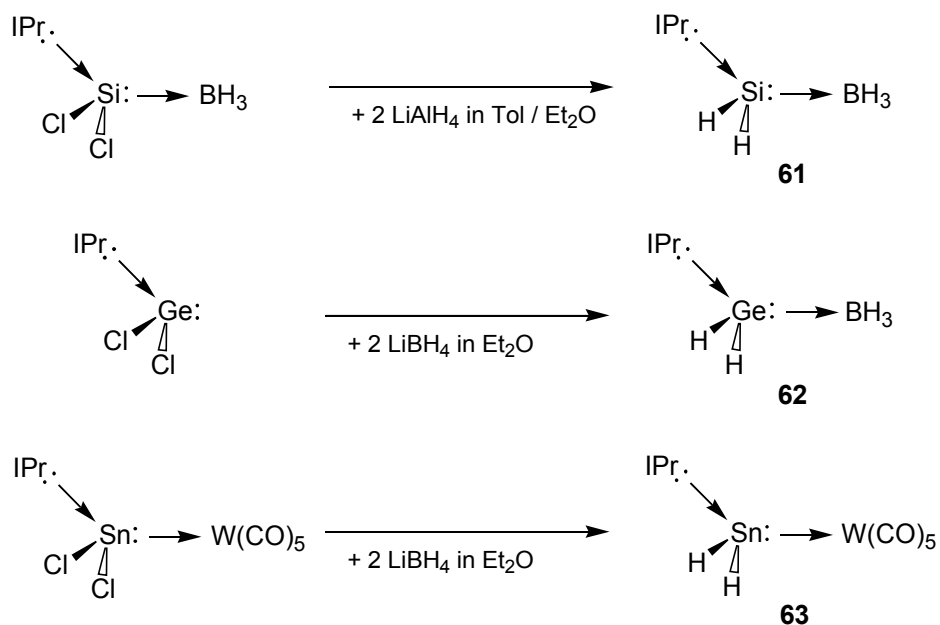
**Scheme 1.3.7**: Trapping of the parent heavy methylene analogues :EH$_2$ (E = Si, Ge, Sn).

The lone pair functionality on these low oxidation state hydrides (:EH$_2$) can also be used to construct molecular chains, allowing for the formation of the heavy inorganic ethylene adducts, H$_2$Si=GeH$_2$ (**64**), H$_2$Si=SnH$_2$ (**65**) [105], and H$_2$Ge=GeH$_2$ (**66**) [106] (Figure 1.3.3). An especially relevant example to the abovementioned work is the donor-acceptor stabilization of H$_2$PBH$_2$, H$_2$PAlH$_2$ and H$_2$PGaH$_2$ by Scheer and co-workers [107]; the pnictogen-triel bonding motif in these group 13/15 species best reflects the compounds characterized in Chapter 3 of this Thesis (Compound **67**, **68a-c**, Scheme 1.3.8).
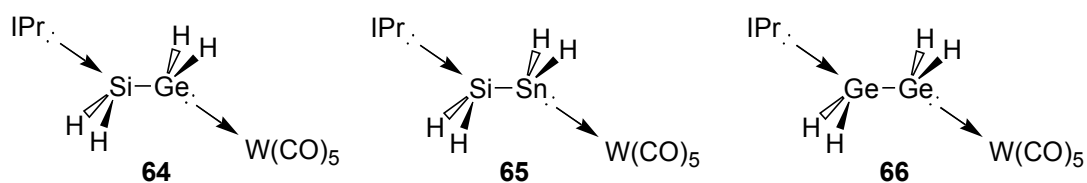


**Figure 1.3.3**: Heavy inorganic congeners of ethylene, synthesized by the Rivard group.

$$H_2P-BH_2 + Fe_2(CO)_9 \xrightarrow[- Fe(CO)_5]{toluene,\ 50\ °C}$$

with NMe$_3$ donor below H$_2$P−BH$_2$; product **67**: (CO)$_4$Fe coordinated to H$_2$P−BH$_2$ with NMe$_3$.

$$LA \leftarrow :PH_2Li + ClH_2B \leftarrow :NMe_3 \xrightarrow[- LiCl]{}$$

LA = W(CO)$_5$, Ga(C$_6$F$_5$)$_3$, B(C$_6$F$_5$)$_3$

product **68a**: LA coordinated to H$_2$P−BH$_2$ with NMe$_3$.

$$(CO)_5W \leftarrow :PH_3 + H_3E \leftarrow :NMe_3 \xrightarrow[- H_2]{pentane}$$

E = Al, Ga

product: (CO)$_5$W coordinated to H$_2$P−EH$_2$ with NMe$_3$;
E = Al, **68b**
E = Ga, **68c**
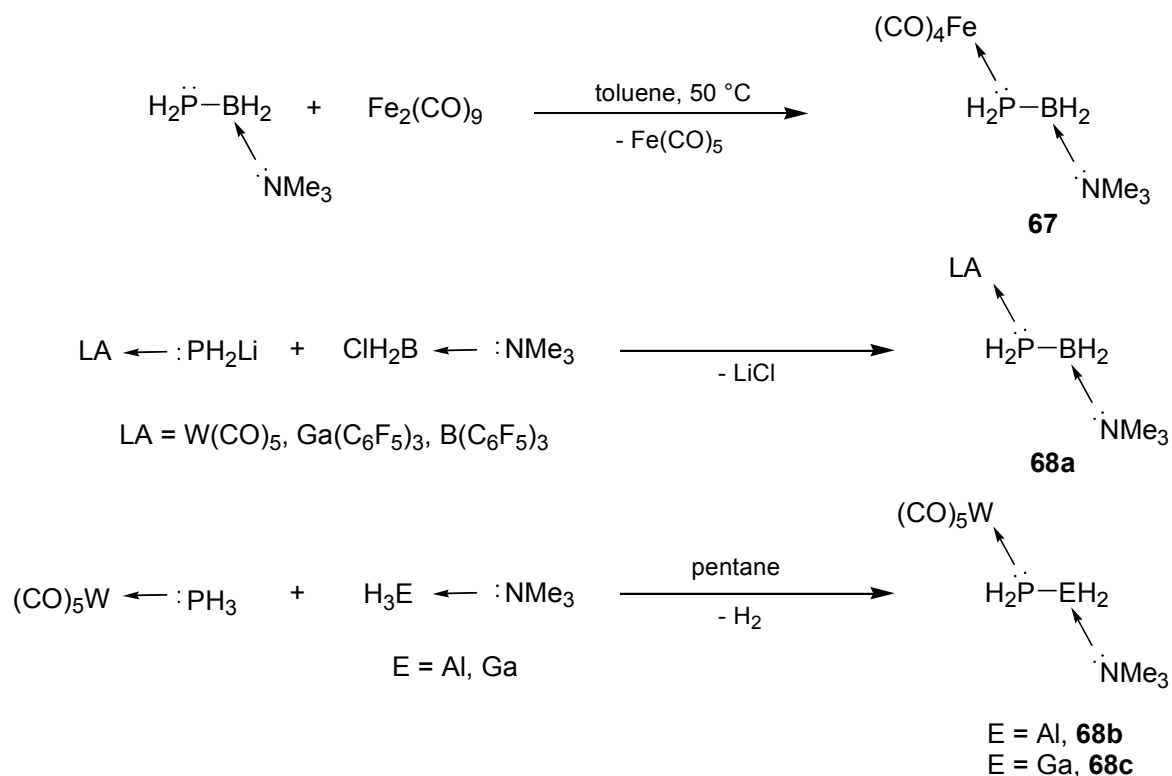
**Scheme 1.3.8**: Synthesis and stabilization of H$_2$PBH$_2$, via donor-acceptor stabilization.

It is with these compounds in mind that this methodology can be extrapolated to isolating the BN analogues of ethene. Molecules of the form H$_2$BNR$_2$ (R = H, alkyl) have an empty p-orbital on boron, as well as a lone pair on nitrogen. One can draw two canonical forms for H$_2$BNH$_2$, using the lone pair to π-bond with boron (Scheme 1.3.9, **I**), or remain on nitrogen, creating a Lewis basic and acidic molecule (**II**), which is theorized to be stabile by the same donor-acceptor motif shown below (Scheme 1.3.9). The research contained in Chapter 3 is centred around stabilization of Lewis base stabilized adducts of the parent inorganic ethene, H$_2$BNH$_2$, in the form LB-H$_2$B=NR$_2$-LA (**69**, LA = Lewis acid), and exploration of dehydrogenation chemistry as a means of obtaining the parent iminoborane and molecular boron nitride.
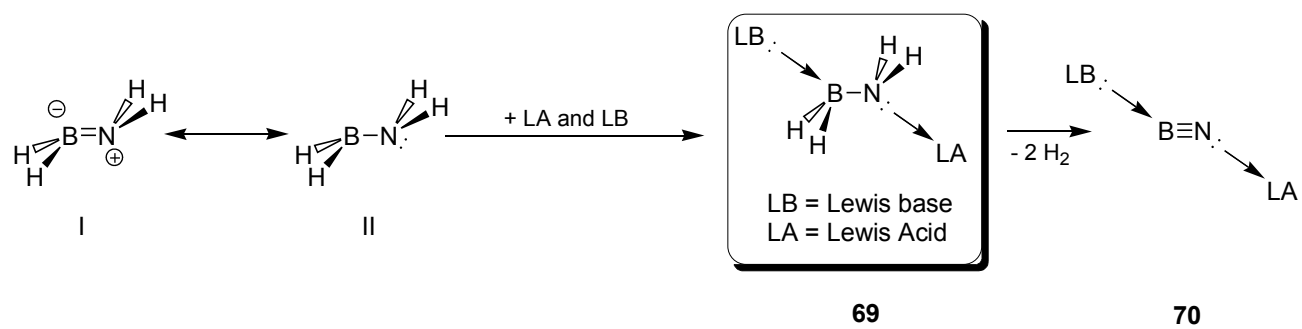
**Scheme 1.3.9**: Resonance forms of H$_2$BNH$_2$, and its potential interception in the form of a stable donor-acceptor adduct.

**1.4 Summary of Thesis Content**

This Thesis is comprised of two research chapters, wherein the work was completed over the course of 26 months between January 2010 and February 2012, each of which is presented with the goal of designing materials or material precursors for electronic or photovoltaic applications.

Chapter 1 is focused on platinum-containing polymers for use in polymer-based photovoltaic devices. Specifically, the target polymers are comprised of Pt-based monomers with directly bound thienyl residues ($-SC_4H_2Br$), as there is no precedent for such polymers, as described herein, in the scientific literature. Utilizing aryl-bromide coupling and cross-coupling techniques, the ability of Pt-thienyl monomers to polymerize was tested. It was found that the polymeric materials could be obtained through Yamamoto homo-coupling, however the purity of the polymers and the overall platinum content are still a subject of investigation.

Chapter 2 involves the synthesis of donor-acceptor adducts of the parent inorganic ethene, $LB-H_2BNH_2-LA$ (LB = Lewis base, LA = Lewis acid), as precursors for boron nitride. Using strong nucleophilic donors such as N-heterocyclic carbenes (NHCs), phosphines and aromatic amines, the parent inorganic ethene and the associated alkyl functionalized derivatives [$H_2BNMe_2$ and $H_2BNH(t\text{Bu})$] were stabilized using our donor-acceptor approach. Initial dehydrogenation attempts yielded both the parent and *tert*-butyl substituted iminoboaranes, which oligomerized into borazines. The mechanism of dehydrogenation as well as the lability of the terminal Lewis acid are an areas of research still under investigation.

## 1.5 Acknowledgement of Collaborators

Portions of the work discussed in this Thesis were completed in collaboration with other group members or researchers within the Department of Chemistry at the University of Alberta.

In Chapter 2, the syntheses and initial cross-coupling of $(dppe)Pt(SC_4H_2Br)_2$ and $(dppp)Pt(SC_4H_2Br)_2$ were performed by Mr. Kyle Sabourin. Growth of crystals suitable for X-ray crystallography of **2**, **4** and **5**, were also carried out by Mr. Sabourin. The synthesis of tris(3,5-diisopropylphenyl)phosphine was carried out by Mr. Paul Lummis, while the synthesis of **9** was carried out by Mr. Sabourin. All X-ray crystallographic analyses were performed by Dr. Robert McDonald and Dr. Michael Ferguson, including mounting of crystals, setup and operation of the diffractometer, refinement of structures and preparation of all crystallographic data tables.

In Chapter 3, all X-ray crystallographic analyses were performed by Dr. Robert McDonald and Dr. Michael Ferguson, including mounting of crystals, setup and operation of the diffractometer, refinement of structures and preparation of all crystallographic data tables. All $^{11}B$ decoupled $^1H$ NMR spectra were run and recorded by Mr. Mark Miskolzie, Ms. Nupur Dabral, Ms. Mickey Richards, and Dr. Tiffany McDougall. Computational analysis was made possible by valued discussions with Dr. Alex Brown and Dr. Mariusz Klobukowski.

As is policy in our research group, each chapter of this Thesis is written as a self-contained paper, prepared for publication in peer reviewed journals. All chapters were drafted by myself, and as of submission of this Thesis, no portions have yet been submitted for publication.

## 1.6 References

[1] H. Hertz. *Annalen der Physik* **1887,** *267*, 983.

[2] A. Einstein. *Annalen der Physik* **1905,** *322*, 132.

[3] W. Smith. *Nature* **1873**, *7*, 303.

[4] W. G. Adams, R. E. Day. *Proc. R. Soc. Lond.* **1876**, *25*, 113.

[5] a) M. A. Green. *Prog. Photovolt.: Res. Appl.* **2001**, *9*, 137. b) D. M. Chaplin, C. S. Fuller, G. L. Pearson. *J. Appl. Phys.* **1954**, *25*, 676.

[6] W. Shockley, H. J. Queisser. *J. Appl. Phys.* **1961**, *32*, 510.

[7] A. De Vos. *J. Appl. Phys.* **1980**, *13*, 839.

[8] a) O. Morton. *Nature* **2006**, *443*, 19. b) International Energy Angecy. "2010 Key World Energy Statistics". Available online at http://www.iea.org/textbase/nppdf/free/2010/key_stats_2010.pdf, accessed Mar 2012.

[9] a) U.S. Energy Information Administration. "Levelized Cost of New Generation Resources in the Annual Energy Outlook 2011", press release November 2010, accessed online at **http://www.eia.gov/oiaf/aeo/electricity_generation.html** on Mar 2012. b) M. A. Green. *Prog. Photovolt: Res. Appl.* **2009**, *17*, 183.

[10] A. Slade, V. Garboushian. "27.6% efficient silicon concentrator cell for mass production." Technical report, *15th International Photovoltaic Science and Engineering Conference*, Shanghai, October **2005**. Available online at: http://amonix.com/technical_papers/2005/Paper%20for %20PVSEC-15%20proceedings%20.pdf, accessed Feb. 2012.

[11] a) Single junction thin-film record PCE (unconcentrated sunlight): http://spectrum.ieee.org/green-tech/solar/solar-cell-breaks-efficiency-record, accessed on Feb 2012., b) Single junction thin-film record PCE (concentrated sunlight): M. A. Green, K. Emery, Y. Hishikawa, W. Warta, E. D. Dunlop. *Prog. Photovolt: Res. Appl.* **2011**, *19*, 565.

[12] For a comprehensive list, see the solar cell efficiency tables, published by Progress in

Photovoltaics: Research and Applications; For 2011, Version 37 see: M. A. Green, K. Emery, Y. Hishikawa, W. Warta. *Prog. Photovolt: Res. Appl.* **2011**, *19*, 84.

[13] www.sj-junction.com, "*Solar Junction Breaks World Record with 43.5% Efficient CPV Production Cell*", http://www.sj-solar.com/downloads/Solar_Junction_World_Record_%20Efficiency_14April11.pdf, access Feb. 2012.

[14] For a review on common polymer-based solar cell materials, see the review: A. C. Mayer, S. R. Scully, B. E. Hardin, M. W. Rowell, M. D. McGehee. *Materials Today* **2007**, *10*, 28 (and references therein).

[15] S. Günes, H. Neugebauer, N. S. Sariciftci. *Chem. Rev.* **2007**, *107*, 1324.

[16] a) S. E. Shaheen, C. J. Brabec, N. S. Sariciftci. *Appl. Phys. Lett.* **2001**, *78*, 841. b) G. Yu, J. Gao, J. C. Hummelen, F. Wudl, A. J. Heeger. *Science* **1995**, *270*, 1789. c) J. J. M. Halls, C. A. Walsh, N. C. Greenham, E. A. Marseglia, R. H. Friend, S. C. Moratti, A. B. Holmes. *Nature* **1995**, *376*, 498. d) S. C. Veenstra, W. J. H. Verhees, J. M Kroon, M. M. Koetse, j. Sweelssen, J. J. A. M. Bastiaansen, H. F. M. Schoo, X. Yang, A. Alexeev, J. Loos, U. S. Schubert, M. M. Wienk. *Chem. Mater.* **2004**, *16*, 2503.

[17] M. Svensson, F. Zhang, S. C. Veenstra, W. J. H. Verhees, J. C. Hummelen, J. M. Kroon, O. Ingandäs, M. R. Andersson. *Adv. Mater.* **2003**, *15*, 988.

[18] a) F. Padinger, R. S. Rittberger, N. S. Sariciftci. *Adv. Funct. Mater.* **2003**, *13*, 85. b) P. Schilinsky, C. Waldauf. *Appl. Phys. Lett.* **2002**, *81*, 3885.

[19] a) Y. H. Kim, C. Sachse, M. L. Machala, C. May, L. Müller-Meskamp, K. Leo. *Adv. Funct. Mater.* **2011**, *21*, 1076. b) D. Mühlbacher, M. Scharber, M. Morana, Z. Zhu, D. Waller, R. Guadiana, C. Brabec. *Adv. Mater.* **2006**, *18*, 2884.

[20] W. U. Huynh, J. J. Dittmer, A. P. Alivisatos. *Science* **2002**, *295*, 2425.

[21] Y. Liang, Z. Xu, J. Xia, S.-T. Tsai, Y. Wu, G. Li, C. Ray, L. Yu. *Adv. Mater.* **2010**, *22*, E135.

[22] S. Rhor. *Heliatek achieves new world record for organic solar cells with certified 9.8% cell*

*efficiency.* Technical report for Heliatek organic based photovoltaics. Dresden, Germany. December 2011.

[23] N. S. Sariciftci, L. Smilowitz, A. J. Heeger, F. Wudl. *Science* **1992**, *258*, 1474.

[24] a)  R. E. Haufler, J. Conceicao, L. P. F. Chibante, Y. Chai, N. E. Byrne, S. Flanagan, M. M. Haley, S. C. O'Brien, C. Pan, Z. Xiao, W. E. Billups, M. A. Ciufolini, R. H. Hauge, J. L. Margrave, L. J. Wilson, R. F. Curl, R. E. J. Smalley. *J. Phys. Chem.* **1990**, *94*, 8634. b) P.-M. Allemand, A. Koch, F. Wudl, Y. Rubin, F. Diederich, M. M. Alvarez, S. J. Anz, R. L. Whetten. *J. Am. Chem. Soc.* **1991**, *113*, 1050. c) D. Dubois, K. M. Kadish, S. Flanagan, R. E. Haufler, L. P. F. Chibante, L. J. Wilson. *J. Am. Chem. Soc.* **1991**, *113*, 4364. d) D. Dubois, K. M. Kadish, S. Flanagan, L. J. Wilson. *J. Am. Chem. Soc.* **1991**, *113*, 7773. e) Q. Xie, E. Perez-Cordero, L. Echegoyen. *J. Am. Chem. Soc.* **1992**, *114*, 3978.

[25] For a review of fullerene electrochemistry, see: L. Echegoyen, L. E. Echegoyen. *Acc. Chem Res.* **1998**, *31*, 593.

[26] M. C. Scharber, D. Mühlbacher, M. Koppe, P. Denk,  C. Waldauf, A. J. Heeger, C. J. Brabec. *Adv. Mater.* **2006**, *18*, 789.

[27] For a review on metallopolymers see: P. Nguyen, P. Gómez-Elipe, I. Manners. *Chem. Rev.* **1999**, *99*, 1515.

[28] H. Wang, M. A. Winnik, I. Manners. *Macromolecules* **2007**, *40*, 3784.

[29] A. P. Soto, I. Manners. *Macromolecules* **2009**, *42*, 40.

[30] R. Resendes, A. Berenbaum, G. Stojevic, F. Jäkle, A. Bartole, F. Zamanian, G. Dubois, C. Hersom, K. Balmain, I. Manners. *Adv. Mater.* **2000**, *12*, 327.

[31] A. Sundararaman, M. Victor, R. Varughese, F. Jäkle. *J. Am. Chem. Soc.* **2005**, *127*, 13748.

[32] a) S. S. H. Mao, T. D. Tilley. *Macromolecules* **1997**, *30*, 5566. b) L. L. Schafer, J. R. Nitschke, S. S. H. Mao, F.-Q. Liu, G. Harder, M. Haufe, T. D. Tilley. *Chem. Eur. J.* **2002**, *8*, 74.

[33] P. J. Fagan, W. A. Nugent, J. C. Calabrese. *J. Am. Chem. Soc.* **1994**, *116*, 1880.

[34] J. R. Nitschke, S. Zürcher, T. D. Tilley. *J. Am. Chem. Soc.* **2000**, *122*, 10345.

[35] Y. Morisaki, Y. Aiki, Y. Chujo. *Macromolecules* **2003**, *36*, 2594.

[36] A. D. Miller, J. F. Tannaci, S. A. Johnson, H. Lee, J. L. McBee, T. D. Tilley. *J. Am. Chem. Soc.* **2009**, *131*, 4917.

[37] Y. Zhou, C. Zhong, L. Xiao, Y. Liu, H. Zhang. *J. Inorg. Organomet. Polym.* **2009**, *19*, 328.

[38] R. Yoshida, T. Takahashi, T. Yamaguchi, H. Ichijo. *J. Am. Chem. Soc.* **1996**, *118*, 5134.

[39] H. Kang, R. Liu, H. Sun, J. Zhen, Q. Li, Y. Huang. *J. Phys. Chem. B.* **2012**, *116*, 55.

[40] K. Sonogashira, S. Kataoka, S. Takahashi, N. Hagihara. *J. Organomet. Chem.* **1978**, *160*, 319.

[41] a) H. B. Fyfe, M. Miekuz, D. Zargarian, N. J. Taylor, T. B Marder. *J. Chem. Soc., Chem. Commun.* **1991**, 188. b) S. Takahashi, Y. Takai, H. Morimoto, K. Sonogashira. *J. Chem. Soc., Chem. Commun.* **1984**, 3. c) S. Guha, C. C. Frazier, K. Kang, S. E. Finberg. *Optics Lett.* **1989**, *14*, 952.

[42] a) F. Guo, Y.-G. Kim, J. R. Reynolds, K. S. Schanze. *Chem. Commun.* **2006**, 1887. b) K. S. Schanze, E. E. Silverman, X. Zhao. *J. Phys. Chem. B* **2005**, *109*, 18451.

[43] a) M. Peyrone. *Eur. J. Org. Chem.* **1844**, *51*, 1. b) B. Rosenberg, L. Van Camp, T. Krigas. *Nature* **1965**, *205*, 698. c) B. Rosenberg, L. Van Camp, J. E. Trosko, V. H Mansour. *Nature* **1969**, *222*, 385.

[44] a) S. J. Berners-Price. *Angew. Chem. Int. Ed.* **2011**, *50*, 804.

[45] J. Ni, X. Zhang, Y.-H. Wu, L.-Y. Zhang, Z.-N. Chen. *Chem. Eur. J.* **2011**, *17*, 1171.

[46] a) R. Favez, R. Roulet, A. A. Pinkerton, D. Schwarzenbach. *Inorg. Chem.* **1980**, *19*, 1356. b) K. Sonogashira, Y. Fujikura, T. Yatake, N. Toyoshima, S. Takahashi, N. Hagihara. *J. Organomet. Chem.* **1978**, *145*, 101. c) S. Kotani, K. Shiina, K. Sonogashira. *J. Organomet. Chem.* **1992**, *429*, 403.

[47] a) A. K. La Groia, A. Ricci, M. Bassetti, D. Masi, C. Bianchini, C. Lo Sterzo. *J. Organomet. Chem.* **2003**, *683*, 406. b) N. Chawdhury, A. Köhler, R. H. Friend, M. Younus, N. J. Long, P. R. Raithby, J. Lewis. *Macromolecules* **1998**, *31*, 722. c) W.-Y. Wong, C.-L. Ho. *Acc. Chem. Res.* **2010**,

*43*, 1246. d) S. Takahashi, M. Kariya, T. Yatake, K. Sonogashira, N. Hagihara. *Macromolecules* **1978**, *11*, 1063.

[48] a) S. Kotani, K. Shiina, K. Sonogashira. *Appl. Organomet. Chem.* **1991**, *5*, 417. b) T. Matsumoto, S. Kotani, K. Shiina, K. Sonogashira. *Appl. Organomet. Chem.* **1993**, *7*, 613.

[49] N. J. Long, A. J. P. White, D. J. Williams, M. Younus. *J. Organomet. Chem.* **2002**, *649*, 94.

[50] W.-Y. Wong, X.-Z. Wang, Z. He, K.-K. Chan, A. B. Djurišić, K.-Y. Cheung, C.-T. Yip, A. M.-C. Ng, Y. Y. Xi, C. S. K. Mak, W.-K. Chan. *J. Am. Chem. Soc.* **2007**, *129*, 14372.

[51] P.-T. Wu, T. Bull, F. S. Kim, C. K. Luscombe, S. A. Jenekhe. *Macromolecules* **2009**, *42*, 671.

[52] T. A. Clem, D. F. J. Kavulak, E. J. Westling, J. M. J. Fréchet. *Chem. Mater.* **2010**, *22*, 1977.

[53] A. E. Douglas, G. Herzberg. *Can. J. Research* **1940**, *18A*, 12, 179.

[54] O. A. Mosher, R. P. Frosch. *J. Chem. Phys.* **1970**, *52*, 5781.

[55] G. Verhaegen, W. G. Richards, C. M. Moser. *J. Chem. Phys.* **1967**, *46*, 160.

[56] The bulk modulus of c-BN is 400 GPA; M. Grimsditch, E. S. Zouboulis. *J. Appl. Phys.* **1994**, *76*, 832.

[57] The bulk modulus of diamond is 442 GPa: M. L. Cohen. *Phys. Rev. B.* **1985**, *32*, 7988.

[58] a) N. V. Novikov, T. D. Osetinskaya, A. A. Shul'zhenko, A. P. Podoba, A. N. Sokolov, I. A. Petmsha, *Dopov. Akad. Nauk. Ukr. RSR, Ser. A Fiz. Mat. Tekh. Nauki USSR* **1983**, 72. b) Young, Hugh D, *University Physics*, 7th Ed., Addison Wesley, **1992**, Table 15-5.

[59] a) R. H. Wentorf. *J. Chem. Phys.* **1957**, *26*, 956. b) L. H. Dreger, V. V. Dadape, J. L. Margrave. *J. Phys. Chem.* **1962**, *66*, 1556.

[60] S. Rudolph. *American Ceramic Society Bulletin* **2000**, *79*, 50.

[61] a) M. Engler, C. Lesniak, R. Damasch, B. Ruisinger, J. Eichler. "Hexagonal Boron Nitride (h-BN) - Applications from Metallurgy to Cosmetics". *Proceedings from the ACM of the German Ceramic Society*, **2007**, No. 12, E49, Dresden. b) R. S. Pease. *Nature* **1950**, *165*, 722.

[62] R. H. Wentorf. *J. Chem. Phys.* **1961**, *34*, 809.

[63] For full design and operation of the "Belt" apparatus, see: H. T. Hall. *Rev. Sci. Instr.* **1960**, *31*, 125.

[64] a) F. P. Bundy, R. H. Wentorf. *J. Chem. Phys.* **1963**, *38*, 1144. b) Z. Pan, H. Sun, Y. Zhang, C. Chen. *Phys. Rev. Lett.* **2009**, *102*, 055503.

[65] H. J. Milledge, E. Nave, F. H. Weller. *Nature* **1959**, 715.

[66] T. E. O'Connor. *J. Am. Chem. Soc.* **1962**, *84*, 1753.

[67] S. Yazu, H. Sumiya, J. Degawa. *European Patent 0,220,462*, **1986**.

[68] S. Shanfield, R. Wolfson. *J. Vac. Sci. Technol. A* **1983**, *1*, 323.

[69] P. Lin, C. Deshpandey, H. J. Doerr, R. F. Bunshah, K. L. Chopra, V. Vankar. *Thin Solid Films* **1987**, *153*, 487.

[70] S. Weissmantel, G. Reisse, B. Keiper, S. Schulze. *Diamond and Related Materials* **1999**, *8*, 377.

[71] C. E. Bamberger, G. M. Begun. *J. Am. Ceram. Soc.* **1986**, *69*, C95.

[72] For a comprehensive review on common synthesis and characterization techniques, see: P. B. Mirkarimi, K. F. McCarty, D. L. Medlin. *Materials Science and Engineering* **1997**, *R21*, 47.

[73] C. K. Narula, R. Schaeffer, R. T. Paine. *J. Am. Chem. Soc.* **1987**, *109*, 5556.

[74] C. K. Narula, R. Schaeffer, A. Datye, R. T. Paine. *Inorg. Chem.* **1989**, *28*, 4053.

[75] a) G. L. Wood, R. T. Paine. *Chem. Mater.* **2006**, *18*, 4716. b) E. A. Pruss, G. L. Wood, W. J. Kroenke, R. T. Paine. *Chem. Mater.* **2000**, *12*, 19.

[76] D.-P. Kim, K.-T. Moon, J.-G. Kho, J. Economy, C. Gervais, F. Babonneau. *Polym. Adv. Technol.* **1999**, *10*, 702.

[77] D. R. Strongin, J. K. Mowlem, M. W. Ruckman, M. Strongin. *Appl. Phys. Lett.* **1992**, *60*, 2561.

[78] F. H. Stephens, V. Pons, R. T. Baker. *Dalton. Trans.* **2007**, 2613.

[79] a) R. D. Suenram, L. R. Thorne. *Chem. Phys. Lett.* **1981**, *78*, 157. b) L. R. Thorne, R. D. Suenram, F. J. Lovas. *J. Chem. Phys.* **1983**, *78*, 167.

[80] D. A. Dixon and M. Gutowski. *J. Phys. Chem. A* **2005**, *109*, 5129.

[81] A. P. M. Robertson, R. Suter, L. Chabanne, G. R. Whittell, I. Manners. *Inorg. Chem.* **2011**, *50*, 12680.

[82] A. W. Ehlers, E. J. Baerends, F. M. Bickelhaupt, U. Radius. *Chem. Eur. J.* **1998**, *4*, 210.

[83] K. W. Böddeker, S. G. Shore, R. K. Bunting. *J. Am. Chem. Soc.* **1966**, *88*, 4396.

[84] a) H. Dorn, R. A. Singh, J. A. Massey, J. M. Nelson, C. A. Jaska, A. J. Lough, I. Manners. *J. Am. Chem. Soc.* **2000**, *122*, 6669. b) J.-M. Denis, H. Forintos, H. Szelke, L. Toupet, T.-N. Pham, P.-J. Madec, A.-C. Gaumont. *Chem. Commun.* **2003**, 54.

[85] J. R. Vance, A. P. M. Robertson, K. Lee, I. Manners. *Chem. Eur. J.* **2011**, *17*, 4099.

[86] C. A. Jaska, I. Manners. *J. Am. Chem. Soc.* **2004**, *126*, 1334.

[87] V. Pons, R. T. Baker, N. K. Szymczak, D. J. Heldebrant, J. C. Linehan, M. H. Matus, D. J. Grant, D. A. Dixon. *Chem. Commun.* **2008**, 6597.

[88] a) P. M. Kuznesof, D. F. Shriver, F. E. Stafford. *J. Am. Chem. Soc.* **1968**, *90*, 2557. b) C. T. Kwon, H. A. McGee Jr. *Inorg. Chem.* **1970**. *9*, 2458. c) E. R. Lory, R. F. Porter. *J. Am. Chem. Soc.* **1973**, *95*, 1766.

[89] X. Chen, J-C. Zhao, S.G. Shore. *J. Am. Chem. Soc.* **2010**. *132*, 10658.

[90] J. Li, S. M. Kathmann, G. K. Schenter, M. Gutowski. *J. Phys. Chem. C* **2007**, *111*, 3294.

[91] F. H. Stephens, R. T. Baker, M. H. Matus, D. J. Grant, D. A. Dixon. *Angew. Chem. Int. Ed.* **2007**, *46*, 746.

[92] P. Paetzold. *Angew. Chem. Int. Ed. Engl.* **1967**, *6*, 572.

[93] a) P. Paetzold, C. von Plotho, G. Schmid, R. Boese, B. Schrader, D. Bougeard, U. Pfeiffer, R. Gleiter, W. Schäfer. *Chem. Ber.* **1984**, *117*, 1089. b) P. Paetzold, C. von Plotho, E. Niecke, R. Rüger. *Chem. Ber.* **1983**, *116*, 1678.

[94] E. Bulach, G. E. Herberich, I. Manners, H. Mayer, P. Paetzold. *Angew. Chem. Int. Ed. Engl.* **1988**, *27*, 958.

[95] E. Rivard, W. A. Merrill, J. C. Fettinger, R. Wolf, G. H. Spikes, P. P. Power. *Inorg. Chem.* **2007**, *46*, 2971.

[96]  E. R. Lory, R. F. Porter. *J. Am. Chem. Soc.* **1973**, *95*, 1766.

[97] J. L. Gay-Lussac, J. L. Thenard. *Mem. Phys. Chim. Soc. d'Arcueil* **1809**, *2*, 210.

[98] A. Solovyev, Q. Chu, S. J. Geib, L. Fensterbank, M. Malacria, E. Lacôte, D. P. Curran. *J. Am. Chem. Soc.* **2010**, *132*, 15072.

[99] J. D. Dill, P. v. R. Schleyer, J. A. Pople. *J. Am. Chem. Soc.* **1975**, *97*, 3402.

[100] Y. Wang, B. Quillian, P. Wei, C. S. Wannere, Y. Xie, R. B. King, H. F. Schaefer, P. v. R. Schleyer, G. H. Robinson. *J. Am. Chem. Soc.* **2007**, *129*, 12412.

[101] a) P. Bissinger, H. Braunschweig, K. Kraft, T. Kupfer. *Angew. Chem. Int. Ed.* **2011**, *50*, 4704. b) R. Kinjo, B. Donnadieu, M. A. Celik, G. Frenking, G. Bertrand. *Science* **2011**, *333*, 610. c) S. J. Bonyhandy, D. Collins, G. Frenking, N. Holzmann, C. Jones, A. Stasch. *Nature Chem.* **2010**, *2*, 865. d) S. Yao, Y. Xiong, M. Driess. *Chem. Eur. J.* **2010**, *16*, 1281. e) O. Back, G.Kuchenbeiser, B. Donnadieu, G. Bertrand. *Angew. Chem.* **2009**, *48*, 5530. f) A. Sidiropoulos, C. Jones, A. Stasch, S. Klein, G. Frenking. *Angew. Chem. Int. Ed.* **2009**, *48*, 9701. g) R. Kinjo, B. Donnadieu, G. Bertrand. *Angew. Chem. Int. Ed.* **2010**, *49*, 5930.

[102] Y. Wang, Y. Xie, P. Wei, R. B. King, H. F. Schaefer, P. v. R. Schleyer, G. H. Robinson. *Science* **2008**, *321*, 1069.

[103] a) S. M. I Al-Rafia, A. C. Malcolm, R. McDonald, M. J. Ferguson, E. Rivard. *Chem. Commun.* **2012**, *48*, 1308. b) K. C. Thimer, S. M. I. Al-Rafia, M. J. Ferguson, R. McDonald, E. Rivard. *Chem. Commun.* **2009**, 7119. c) S. M. I. Al-Rafia, A. C. Malcolm, S. K. Liew, M. J. Ferguson, E. Rivard. *J. Am. Chem. Soc.* **2011**, *133*, 777.

[104] G. R. Smith and W. A. Guillory, *J. Chem. Phys.* **1972**, *56*, 1423.

[105] S. M. I. Al-Rafia, A. C. Malcolm, R. McDonald, M. J. Ferguson, E. Rivard. *Angew. Chem. Int. Ed.* **2011**, *50*, 8354.

[106] S. M. I. Al-Rafia; unpublished results within our research group.

[107] a) A. Adolf, U. Vogel, M. Zabel, A. Y. Timoshkin, M. Scheer. *Eur. J. Inorg. Chem.* **2008**, 3482. b) K.-C. Schwan, A. Y. Timoshkin, M. Zabel, M. Scheer. *Chem. Eur. J.* **2006**, *12*, 4900. c) U. Vogel, A. Y. Timoshkin, M. Scheer. *Angew. Chem. Int. Ed.* **2001**, *40*, 4409.

# Chapter 2

# Platinum containing polymers for use in polymer-based photovoltaic applications

**Chapter 2**

**Platinum containing polymers for use in polymer-based photovoltaic applications**

## 2.1 Introduction

Metallopolymer synthesis has been a growing field of interest for light-emitting (luminescence) and solar cell applications [1] with device performance often linked to the light-induced charge transfer that often occurs between metal atoms and ligands in their coordination sphere. The use of electron rich metal atoms as active components in photovoltaic cells has been in practice for many years in the form of dye-sensitized solar cells (DSSCs) [2]. The primary function of the electron rich metal (typically Ru or Pt) is to create a low energy pathway for electrons to enter excited states, encouraging formation of optically broad and intense metal-to-ligand charge transfer (MLCT) absorptions, such that excited state electrons can be siphoned from the dye-metal complex onto cathodic substrates (conventionally $TiO_2$). The purpose of Ru and Pt is to provide a wealth of electrons to excite, and to stabilize short lived, high spin states via the heavy atom effect [3]. While these metals are common in DSSCs, research has shifted focus towards cost-effective metals like cobalt, which can attain photovoltaic conversion efficiencies (PCEs) of 12% in the form of photoactive organometallic complexes [4]. Another growing avenue of potentially cost-effective photovoltaic research is that of polymer-based solar cells (PBSCs). The key advantages attributable to PBSCs are derived from the mechanical and physical properties that come hand-in-hand with polymers: such as flexibility, solution processability, and in some cases low fabrication cost per device. The primary drawback of PBSCs is their generally low PCE values [5] in comparison with those achieved by bulk crystalline silicon or multi-heterojunction (MHJ) based cells [6]. The gold standard PBSC material in terms of high device performance to cost ratios is poly(3-hexylthiophene), which has commonly reported PCEs of between 2 - 4% [7], and highly tunable conductance based on polymer doping and functional group variation [8]. While the highest current PCE for polymer based solar cells is 9.8% [9], the cost-performace ratio of PBSCs has yet to match

silicon based solar cells, nor has the technology reached the point of grid parity. Platinum-acetylide polymers were some of the first metallopolymers to be synthesized, and to date are the most well studied Pt containing polymers, with numerous examples reported in the literature [10a]. These materials have PCEs between 0.3 and 1.5%, a value that falls short of current less costly polymers, and fails to meet the cost-effectiveness necessary for grid parity. However Pt-containing polymers are thermally stable and allow for the stabilization of high-spin excited states, increasing the breadth of available excited states, broadening the optical band-gap absorption of the polymer. The goal of this work is to meet the high molar absorptivities of DSSCs which aids in maximizing the absorption of light per mole of monomer, with the mechanical properties of PBSCs by incorporating platinum into the polymer backbone of a polythiophene derivative. In this work, Pt-thienyl complexes were synthesized and functionalized such that aryl bromide (Ar-Br) cross-coupling or homo-coupling methods could be used to obtain polymeric materials. The general scheme for these reaction pathways is given in Scheme 2.1.1.
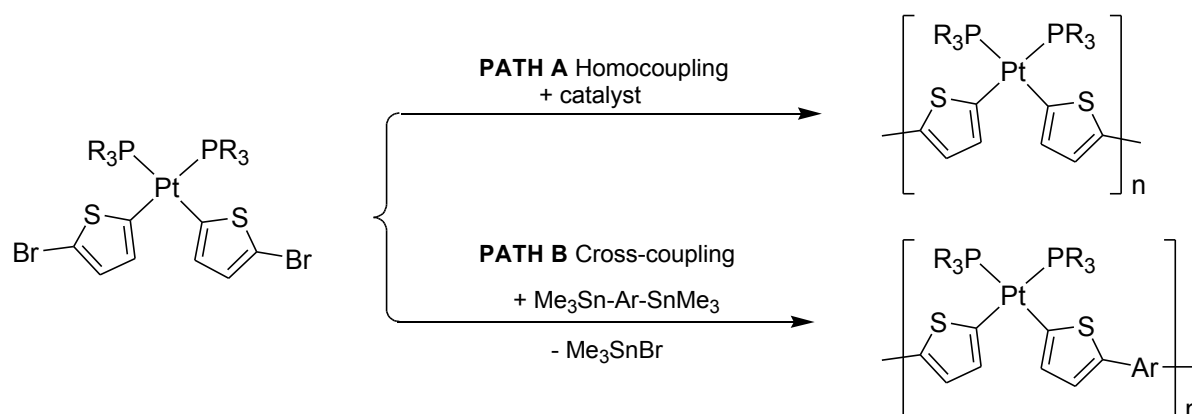


**Scheme 2.1.1**: Proposed general scheme for the polymerization of thienyl-Br functionalized Pt complexes.

## 2.2 Results and Discussion

The synthesis of the proposed monomer $[(Bu_3P)_2Pt(SC_4H_2Br)_2]$ (**3**) is shown in Scheme 2.2.1. The purpose of coordinating phosphine-ligands to the Pt centre is two-fold: literature precendence has shown the P-Pt bonds in Pt(II) complexes of the general form $(R_3P)_2PtX_2$ (X =

anionic ligands) are thermally stable in the presence of air and moisture, and the one-bond coupling

between $^{31}$P and $^{195}$Pt allows for the *in-situ* analysis of reaction products by $^{31}$P NMR spectroscopy.

In addition, the bonding of a thienyl group directly to Pt has been shown to increase the degree of

conjugation and yield intense MLCT bands, and broader absorption profiles [10b]. However, prior

to this study, there has been no reported attempts to incorporate platinum thienyl residues within a

polymeric array.
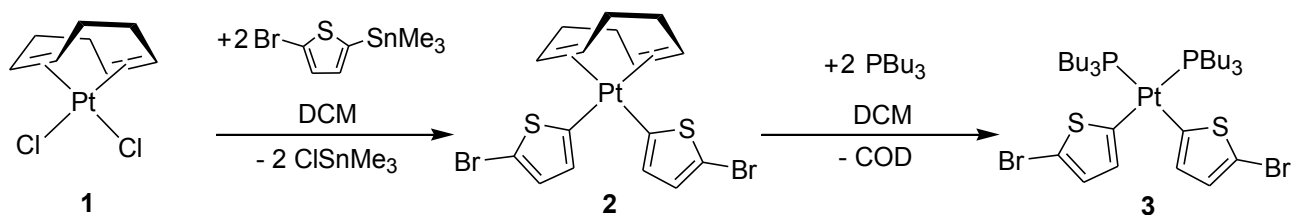


**Scheme 2.2.1**: Synthetic route towards the bromothienyl precursor [(Bu$_3$P)$_2$Pt(SC$_4$H$_2$Br)$_2$] (**3**).

Sonogashira has shown that it is possible to synthesize bis(thienyl) Pt(II) complexes that

were similar to **3** [10b], however the coordinated thienyl groups did not contain reactive sites

required for polymerization. However, by installing a bromine substituent at the 5-position of the

thienyl rings in **3**, it was hoped that metal-catalyzed aryl-Br cross-coupling could be used to prepare

Pt-containing polymers by condensation polymerization of the monomer (Path A, Scheme 2.1.1), or

co-polymerization with another monomer (Path B). The synthesis of the desired monomer was

accomplished by the reaction of 2-trimethylstannyl-5-bromothiophene with Pt(COD)Cl$_2$ (COD =

1,5-cyclooctadiene) to give complex **2** (Figure 2.2.1), followed by displacement of COD with two

equivalents of tributylphosphine to give the target complex (Bu$_3$P)$_2$Pt(BrC$_4$H$_2$S)$_2$ (**3**) in high yield

(95%) as a pale yellow solid. Compound **3** was identified using $^1$H, $^{31}$P and $^{13}$C{$^1$H} NMR

spectroscopy, combustion analysis, and single crystal X-ray diffraction (Figure 2.2.2).

Compound **3** was found to adopt a *cis*-conformation in the solid state, while $^{31}$P NMR

spectroscopy showed a singlet at -3.7 ppm in CDCl$_3$ with diagnostic flanking $^{195}$Pt satellites ($^1J_{P-Pt}$ =

2057 Hz). The presence of mutually coupled doublet resonances at 6.82 and 6.32 ppm in the $^1$H NMR spectrum ($^3J_{H-H}$ = 2.8 Hz) was consistent with direct attachment of thienyl rings to a Pt centre. While **3** was found to be *cis* in the solid state (Figure 2.2.2), it was discovered that solvent-dependant *cis-trans* isomerization of the complex could occur. For example, when dissolved in CDCl$_3$, **3** showed a singlet at -3.7 ppm ($^1J_{P-Pt}$ = 2057 Hz) in the $^{31}$P spectrum, however when the same complex was dissolved in C$_6$D$_6$, a singlet at 2.7 ppm with much wider spaced Pt satellites ($^1J_{P-Pt}$ = 2543 Hz) was observed, corresponding to the arrangement of the PBu$_3$ ligands in the *trans* conformation. When **3** is dissolved in toluene, both isomers are present in a 60:40 *trans:cis* ratio. Interestingly, *cis-trans* isomerization could also be thermally induced by heating a sample of **3** in CDCl$_3$ to 60 ºC; as shown in Figure 2.2.3, a mixture of isomers is obtained (40% *trans*).
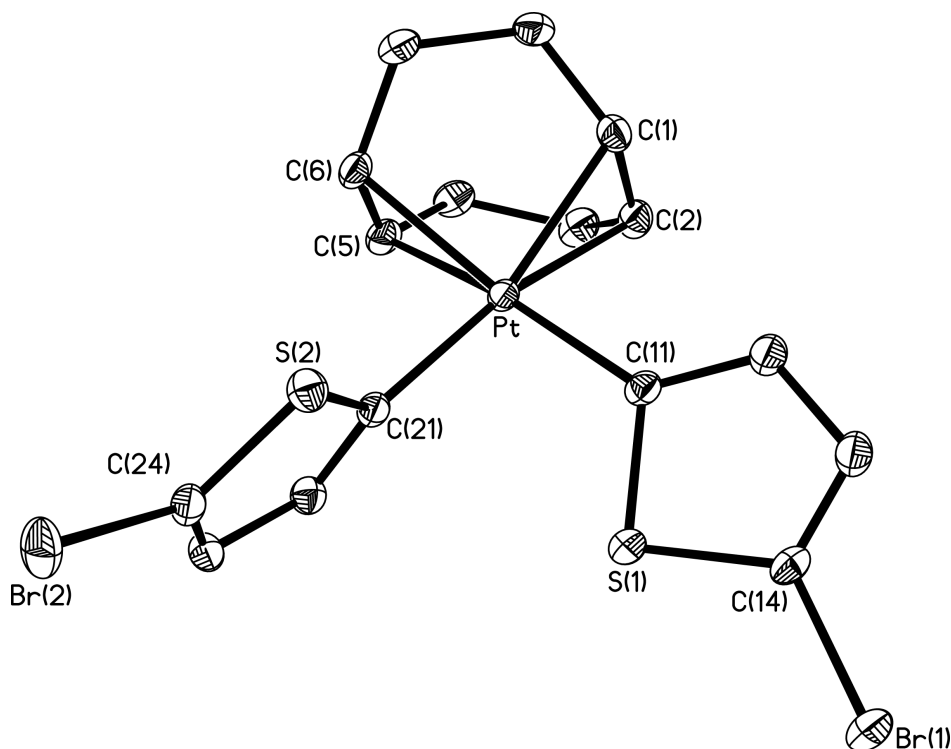


**Figure 2.2.1:** Thermal ellipsoid plot (30% probability) of (COD)Pt(SC$_4$H$_2$Br)$_2$ (**2**). Carbon-bound hydrogen atoms have been omitted for clarity. Selected bond lengths [Å] and angles [º]: Pt-C(1) 2.254(4), Pt-C(2) 2.231(4), Pt-C(6) 2.238(3), Pt-C(5) 2.256(4), Pt-C(21) 2.018(3), Pt-C(11) 2.018(4), C(21)-Pt-C(11) 90.32(14), S(2)-C(24)-Br(2) 121.1(2), S(2)-C(14)-Br(1) 126.8(3).
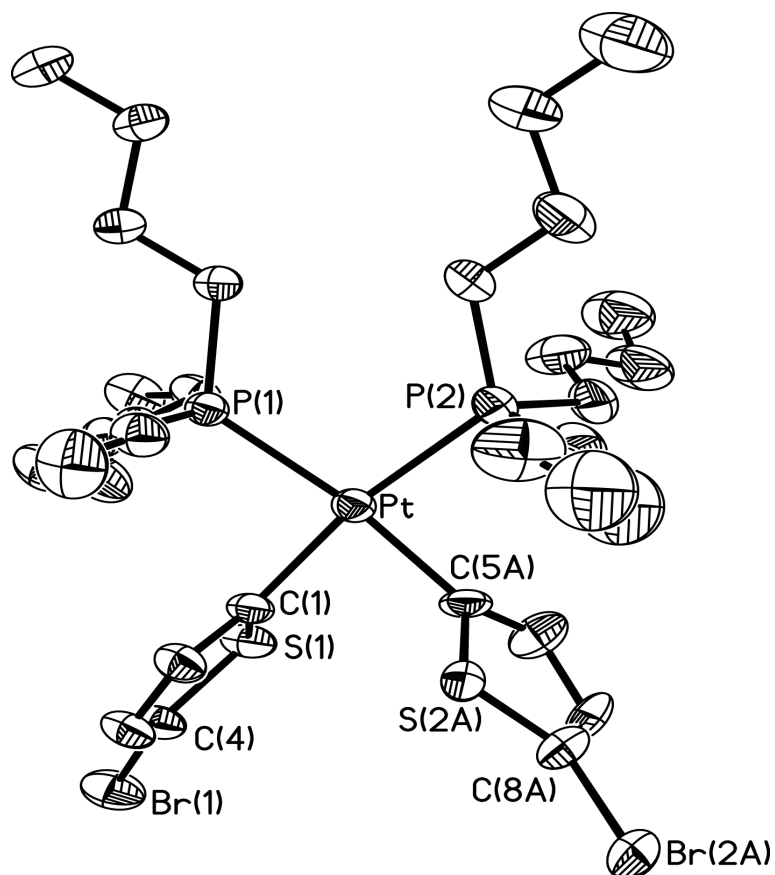
**Figure 2.2.2**: Thermal ellipsoid plot (30% probability) of $(Bu_3P)_2Pt(SC_4H_2Br)_2$ (**3**). Carbon-bound hydrogen atoms and hexane solvate have been omitted for clarity. Selected bond lengths [Å] and angles [°]: P(1)-Pt 2.3159(14), P(2)-Pt 2.3286(16), Pt-C(1) 2.059(5), Pt-C(5A) 1.987(13), C(4)-Br(1) 1.890(6), C(C8A)-Br(2A) 1.885(16), P(1)-Pt-P(2) 103.92(6), C(1)-Pt-C(5A) 86.3(11), S(1)-C(4)-Br(1) 121.3(3), S(2A)-C(8A)-Br(2A) 124.5(13).
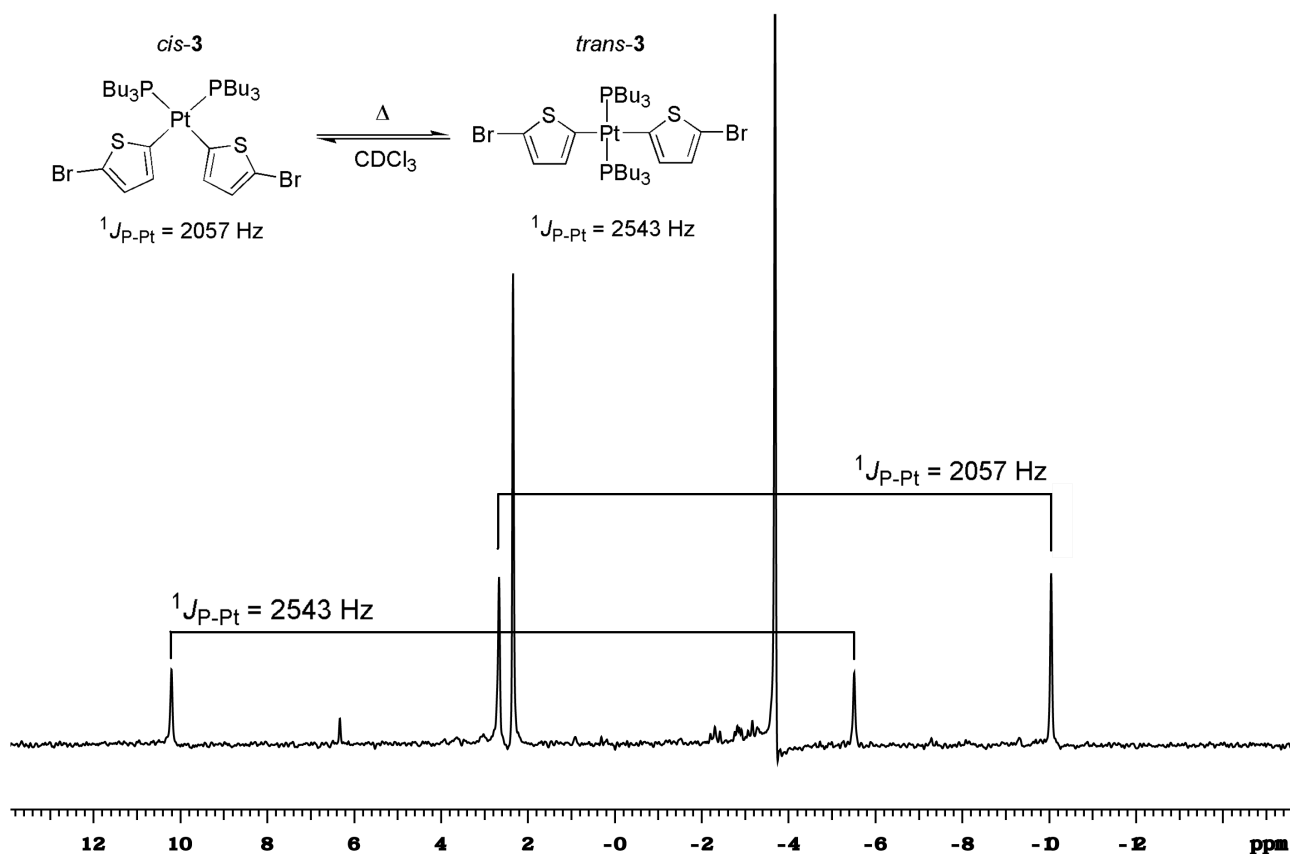
**Figure 2.2.3**: $^{31}P\{^1H\}$ NMR spectrum of **3** at 60 °C in CDCl$_3$ showing the presence of both *cis*-**3** and *trans*-**3** in solution.
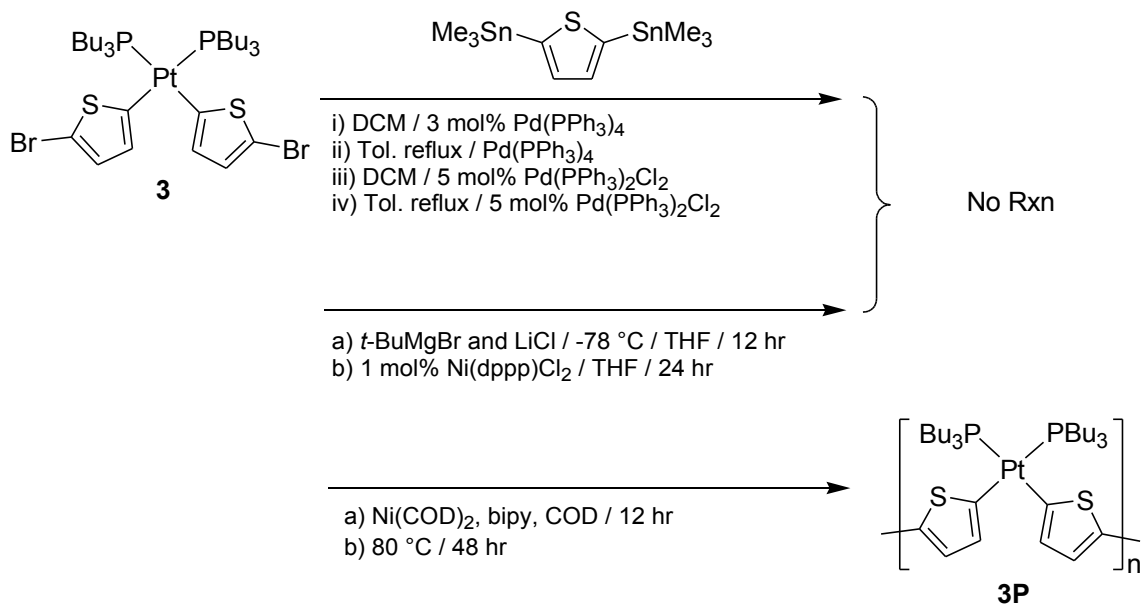


**Scheme 2.2.2**: Attempted polymerization of the bis(thienyl) platinum complex **3**.

In order to convert **3** into polymers, Stille, Grignard Metathesis (Kumada), and Yamamoto coupling were investigated (Scheme 2.2.2). Attempts to polymerize **3** with 2,5-bis(trimethylstannyl)thiophene (Stille cross-coupling) in the presence of Pd catalysts showed no signs of reaction regardless of catalyst loading. Refluxing **3** in toluene with 3 mol% of $Pd(PPh_3)_4$ or 5 mol% of $(PPh_3)_2PdCl_2$ in the presence of the same substrates resulted only in the recovery of starting material with residual free $PBu_3$ (4%), implying ligand exchange between substrate and catalyst may be occurring. Grignard Metathesis polymerization (Kumada coupling) was attempted by reacting **3** with one equivalent of $t$BuMgCl at -78 ºC in the presence of catalytic $Ni(dppp)Cl_2$ [dppp = bis(diphenylphosphino)propane]; this chemistry yielded a mixture of products containing unreacted **3** (87%), free $PBu_3$ (2%) and several other unidentified products by $^{31}P$ NMR (10.0 ppm, 1%; 2.3 ppm, 7%; 5.7 ppm, 1%). GPC analysis of this crude mixture revealed no high molecular weight species ($M_w$ > 1000 g/mol). These results suggest the dppp ligand from the Ni catalyst participated in phosphine exchange at the Pt centre, releasing free $PBu_3$ and creating new products with Pt-bound dppp ligands.

Yamamoto coupling was performed by dissolving **3** in a solution containing one equivalent of $Ni(COD)_2$ (COD = 1,5 - cyclooctadiene), 2,2'-bipyridine, and COD, followed by heating to 80 ºC for 48 hours (bottom reaction in Scheme 2.2.2). The $^1H$ NMR spectrum showed peaks corresponding to unreacted **3** however significantly broadened, while the $^{31}P$ spectrum showed a singlet at -3.7 ppm corresponding to **3**, and several unidentified peaks between 4.2 and -9.6 ppm (Figure 2.2.4). Analysis of the crude reaction mixture by GPC revealed the presence of polymeric material with an average molecular weight ($M_w$) of 38 000 g/mol (polydispersity index (PDI) = 2.71), however repeated syntheses yielded oligomeric to polymeric products with molecular weights in the range of 3500 - 38 000 g/mol. UV-visible spectral analysis of **3** showed an absorption at 263 nm corresponding to charge transfer from Pt to the thienyl rings, while the orange coloured polymer (**3P**) exhibited a new broad absorption band at 370 nm ($\varepsilon$ = ~2000 L mol$^{-1}$ cm$^{-1}$)

corresponding to a π-π* transition of the polymeric material. This assignment is supported by observations made by Sonogashira and co-workers [10b], who noted that the π-π* band shifted upon moving from the unbrominated analogue of **3**, bis(2-thienyl)Pt(PBu$_3$)$_2$, to the dithienyl variant, bis(2-bithienyl)Pt(PBu$_3$)$_2$, due to an increase in conjugation length when two thienyl rings are joined, leading to a lowering of the π-π* energy gap. The π-π* bands with their corresponding molar absorptivity coefficients (ε) are given in Table 2.2.1. The range of π-π* absorptions can be attributed to the lack of homogeneity in the polymeric material, as evidenced by the broad range of molecular weight and polydispersity indeces (1.87 - 4.49). The presence of monomeric **3** in the resulting polymer was unavoidable as both the monomer and crude materials were both extensively soluble in all organic solvents. Unexpectedly no correlation could be drawn between molecular weight and the molar absorptivity or π-π* band position. It was expected that higher molecular weights would tend towards longer conjugation lengths, which would be observed in a red-shifted π-π* transition, however this was not the case. The effect of the different impurities is currently unknown, as pure polymeric materials could not be obtained by precipitation from cold hexanes or methanol, and the presence of unreacted **3** in unknown quantities would skew the ε values obtained for the MLCT band. The distribution (and composition) of the byproducts observed by ^{31}P NMR were also inconsistent from one experiment to the next, potentially the result of the presence of low mass oligomers. Compounding the difficulty of characterising these polymeric materials, it was previously established that the isomer form of the monomer (*cis* or *trans*) is dependant on both temperature and solvent; it is therefore unknown whether the polymer is isomerically regular or randomized.
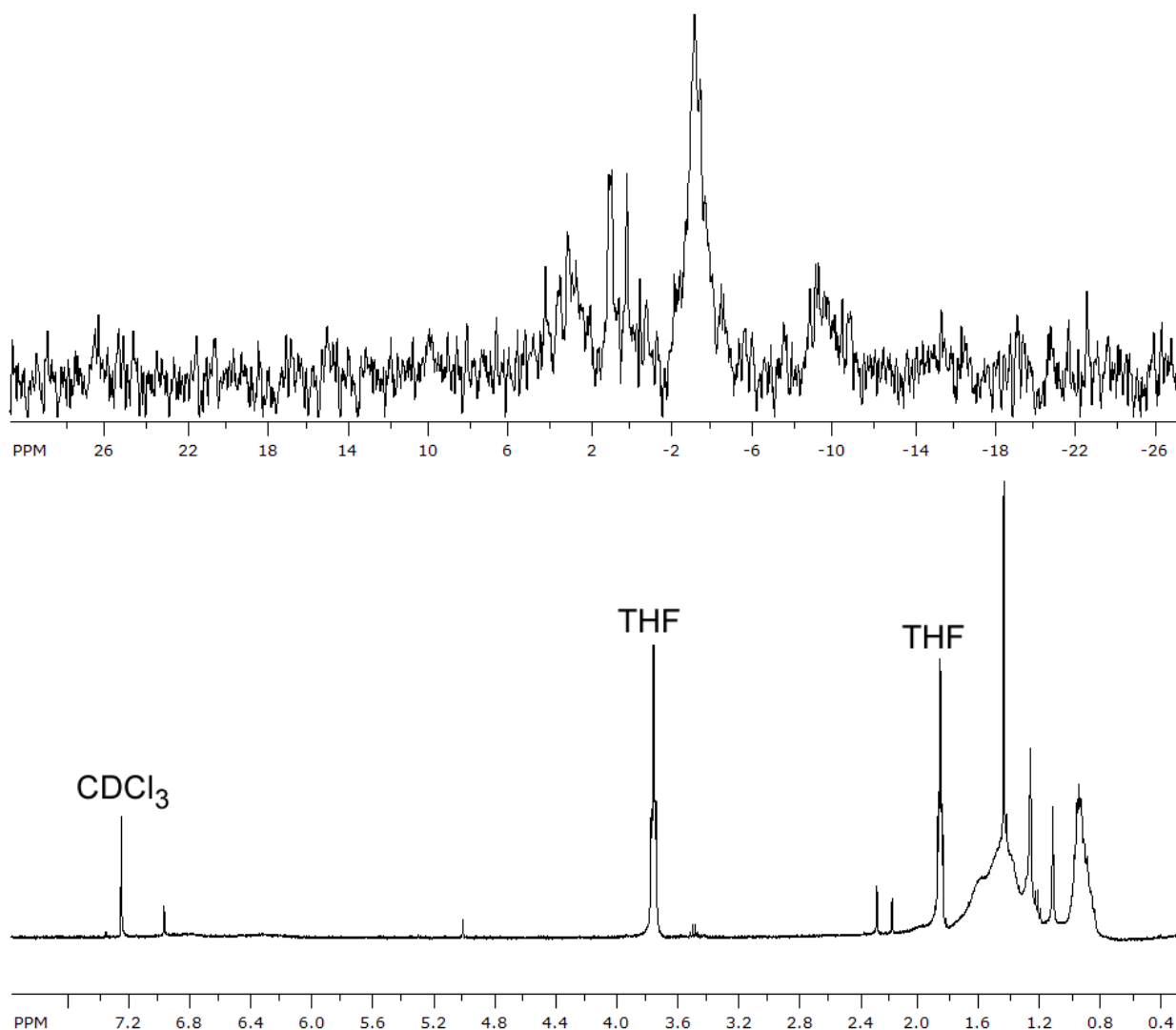
**Figure 2.2.4**: Representative $^{31}P\{^1H\}$ (CDCl$_3$, top) and $^1H$ (CDCl$_3$, bottom) NMR spectra of **3** after Yamamoto coupling, forming **3P**. NB: the complex $^{31}P$ peak structure makes it difficult to identify products or assess polymer purity.

**Table 2.2.1**: Electronic spectra and GPC data for **3** and **3P**

| Entry | MLCT (nm) | $\varepsilon_{MLCT}$ (L mol$^{-1}$ cm$^{-1}$) | $\pi$-$\pi$* (nm) | $\varepsilon_{\pi\text{-}\pi*}$ (L mol$^{-1}$ cm$^{-1}$) | $M_w$ (g/mol) | PDI ($M_w/M_n$) |
|---|---|---|---|---|---|---|
| **3** | 263 | 3317 | - | - | - | - |
| Trial 1 | 263 | 12050 | 370 | 1947 | 38000 | 2.71 |
| Trial 2 | 236 | 9237 | 431 | 5688 | 13500 | 4.49 |
| Trial 3 | 246 | 4647 | 328 | 1969 | 3500 | 1.87 |
| Trial 4 | 264 | 7018 | 422 | 4322 | 23800 | 3.98 |

To ensure the relative geometry of the conjugated thiophene units at Pt remains unchanged during the polymerization, the monodentate PBu$_3$ ligands on Pt were replaced with the bidentate phosphine ligands, bis(diphenylphosphino)ethane (dppe) and bis(diphenylphosphino)propane (dppp), in order to affix a *cis* conformation. The synthesis of the chelate complexes LPt(SC$_4$H$_2$Br)$_2$ (L = dppe, **4**; dppp, **5**) followed the same overall procedure used for the synthesis of **3** (Scheme 2.2.3). Specifically, **2** was reacted with one equivalent of either dppe or dppp to generate **4** (79% yield) and **5** (95% yield) as yellow and orange solids, respectively. Pt(dppe)(SC$_4$H$_2$Br)$_2$ (**4**) showed a singlet at 42.5 ppm in the $^{31}$P NMR spectrum ($^1J_{P-Pt}$ = 2072 Hz), while Pt(dppp)(SC$_4$H$_2$Br)$_2$ (**5**) exhibited a $^{31}$P NMR resonance at -3.3 ppm ($^1J_{P-Pt}$ = 1984 Hz) (Figure 2.2.7). Neither **4** or **5** showed any signs of solvent or temperature dependant isomerism, as is expected for d$^8$ square planar Pt complexes stabilized by bidentate ligands. Both compounds showed high thermal stability with melting points of 237 ºC (**4**, turns brown at 210 ºC) and 245 - 247 ºC (**5**). Crystals of **4** and **5** of suitable quality for X-ray diffraction were grown from diffusion of diethyl ether into saturated CH$_2$Cl$_2$ solutions (Figures 2.2.5 and 2.2.6).

Compound **4** had Pt-C$_{thienyl}$ bond lengths of 2.044(3) and 2.067(3) Å, while the corresponding lengths in **5** were 2.053(3) and 2.048(3) Å, which are the same within experimental error, and similar to those found for **3**. The Pt-P bond lengths for **4** [2.2771(10) and 2.2898(9) Å] were found to be slightly shorter than those found for **5** [2.3010(8) and 2.3107(8) Å], which may be attributed to the reduced strain of the Pt-P-C$_{alkyl}$ bond angles in the 5-membered ring formed by chelation of dppe in **4**, relative to the those found in the 6-membered ring formed in **5**. The P-Pt-P angle was 85.75(3)° in **4**, and 88.82(12)° in **5**, which are close to the 90° angle expected for d$^8$ square planar complexes. In contrast, **3** exhibited a P-Pt-P bond angle of 103.92(6)°, significantly larger than expected for square planar complexes, because of the added steric bulk (and inter-ligand repulsion) between the two *cis* PBu$_3$ groups.
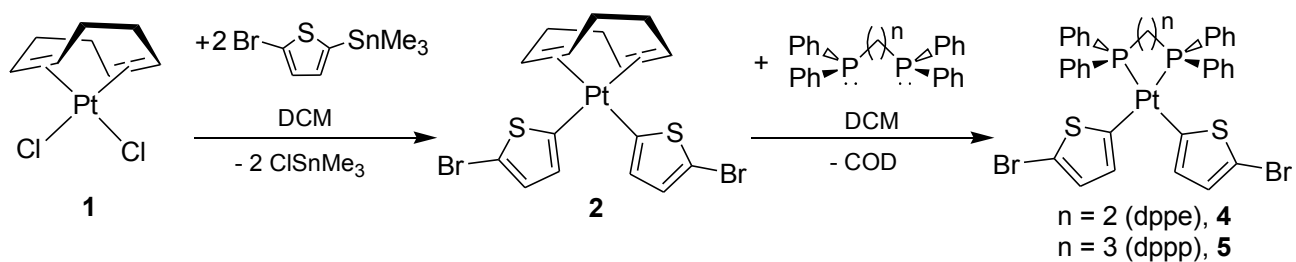
**Scheme 2.2.3**: Preparation of the *cis*-confined Pt thienyl complexes **4** and **5**.
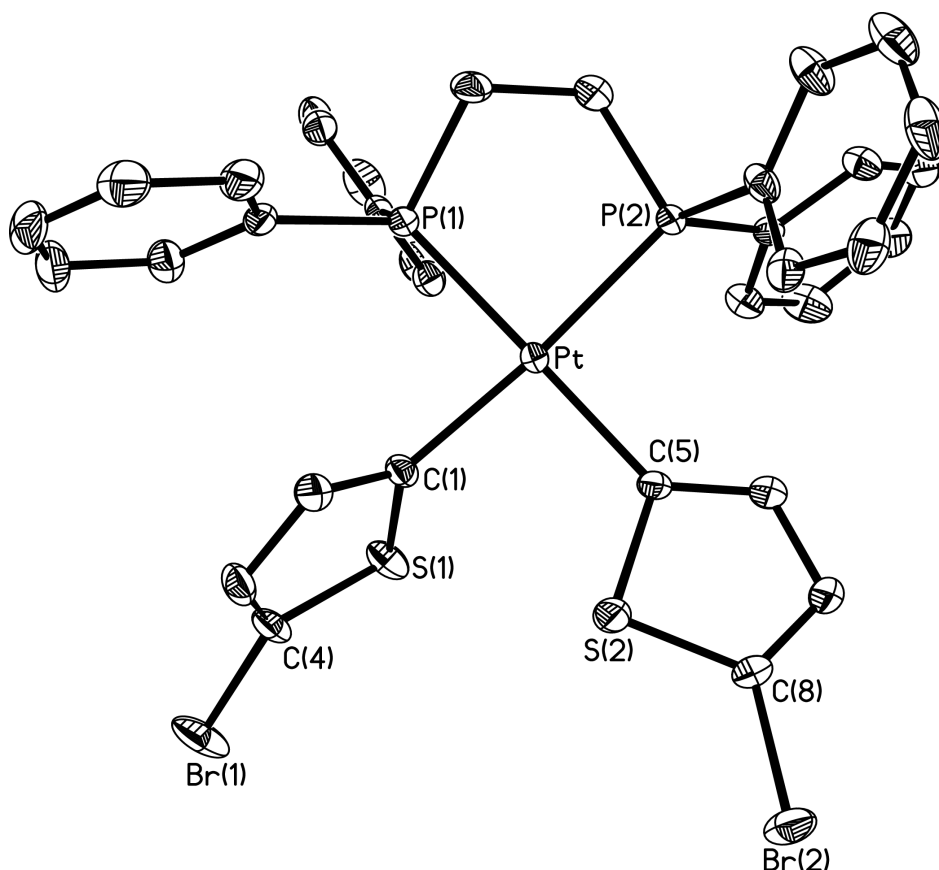


**Figure 2.2.5**: Thermal ellipsoid plot (30% probability) of (dppe)Pt(SC$_4$H$_2$Br)$_2$ (**4**). Carbon-bound hydrogen atoms have been omitted for clarity. Selected bond lengths [Å] and angles [°]: P(1)-Pt 2.2771(10), P(2)-Pt 2.2898(9), Pt-C(1) 2.044(3), Pt-C(5) 2.067(3), C(4)-Br(1) 1.879(4), C(8)-Br(2) 1.879(4), P(1)-Pt-P(2) 85.75(3), C(1)-Pt-C(5) 89.80(14), S(1)-C(4)-Br(1) 121.7(3), S(2)-C(8)-Br(2) 126.9(3).
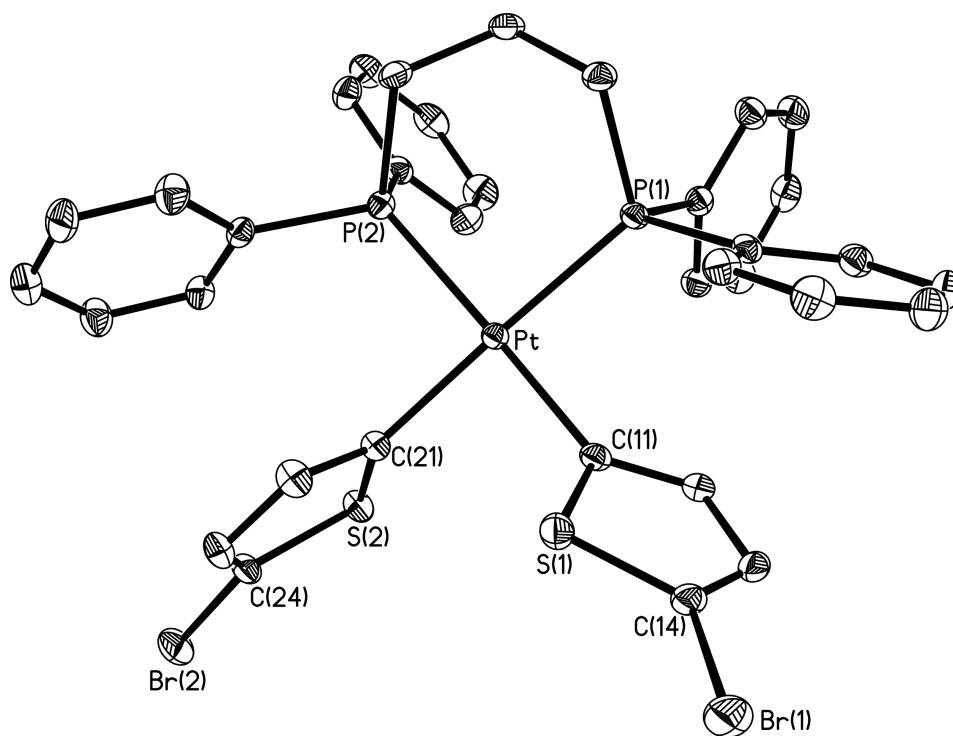
**Figure 2.2.6**: Thermal ellipsoid plot (30% probability) of (dppp)Pt(SC$_4$H$_2$Br)$_2$ (**5**). Carbon-bound hydrogen atoms have been omitted for clarity. Selected bond lengths [Å] and angles [°]: P(1)-Pt 2.3010(8), P(2)-Pt 2.3107(8), Pt-C(21) 2.053(3), Pt-C(11) 2.048(3), C(14)-Br(1) 1.888(3), C(24)-Br(2) 1.885(3), P(1)-Pt-P(2) 91.91(3), C(21)-Pt-C(11) 88.82(12), S(1)-C(14)-Br(1) 120.9(2), S(2)-C(24)-Br(2) 121.1(2).
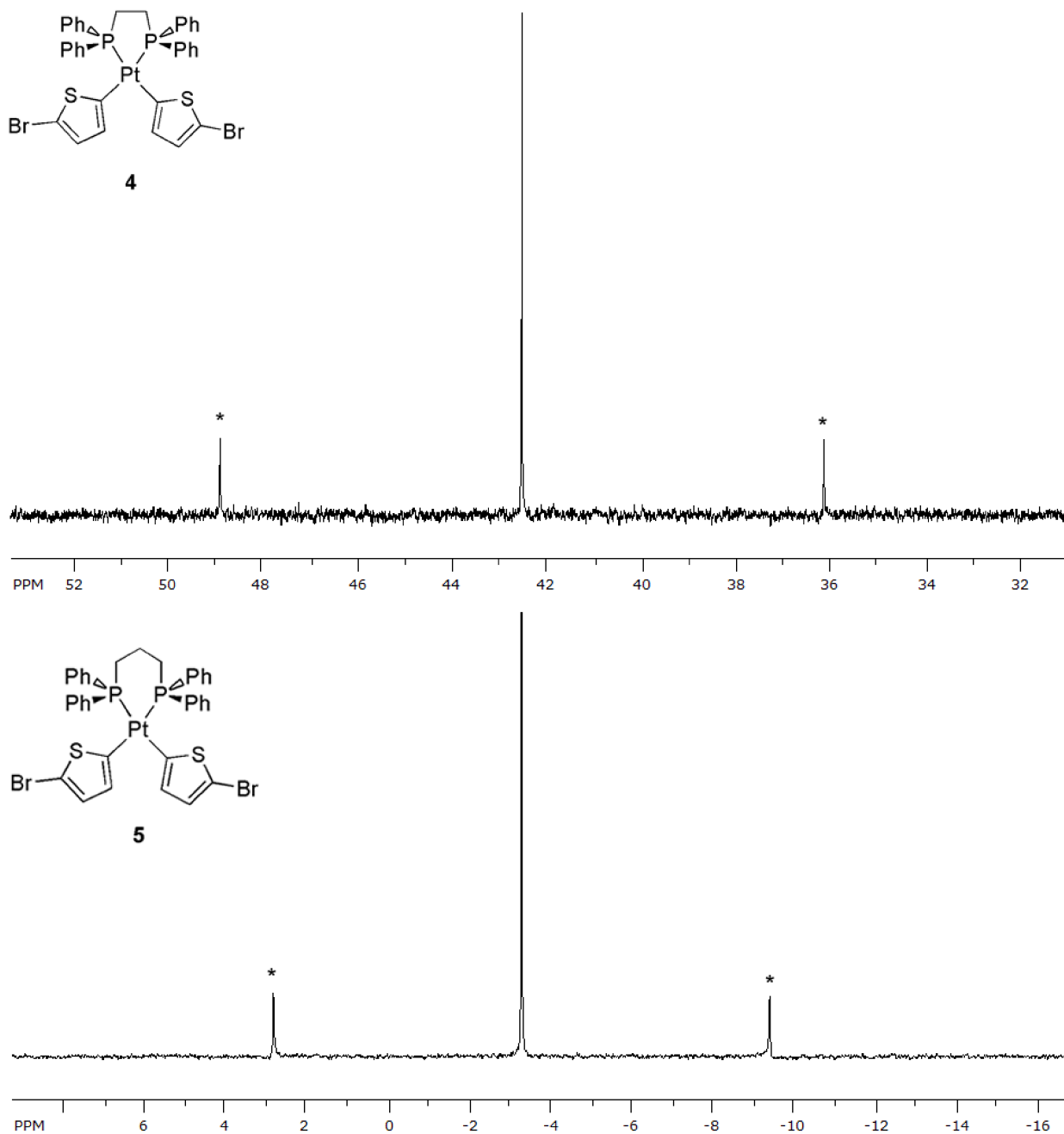
**Figure 2.2.7**: $^{31}P\{^1H\}$ NMR spectra of **4** (top) and **5** (bottom) with diagnostic $^{195}Pt$ satellites marked with (*).

To elucidate the necessary reaction conditions required for synthesizing platinum-thienyl polymers, we shifted our focus towards simplified cross-coupling procedures wherein **5** was coupled with monofunctional thienyl or acetylide units to afford controlled C-C bond formation involving a single Pt complex (Scheme 2.2.4). Compound **5** was chosen for this model study due to

its enhanced thermal stability, thus mitigating the degree at which the dppp ligand is released from the Pt centre. The presence of a bidentate ligand will also supress the degree to which ligand dissociation will occur due to the entropic benefit of the chelate effect. When **5** was combined with two equivalents of 2-trimethylstannylthiophene under Stille coupling conditions with 2 mol% Pd$_2$(dba)$_3$ in polar, arene and ethereal solvents, no evidence of C-C bond formation was observed; likewise no reaction was observed under microwave irradiation. When **5** was reacted with two equivalents of 2-trimethylstannylthiophene in the presence of catalytic Pd(PPh$_3$)$_4$ in ethereal solvents, starting material was recovered (90% by ^{31}P NMR), along with several minor unidentified products. When a substoichiometric amount of Pd(PPh$_3$)$_4$ (5 mol%) was reacted with **5** in the absence of 2-trimethylstannylthiophene and heated, a similar of product mixture was detected by ^{31}P NMR spectroscopy, implying some sort of phosphine exchange between the Pt and Pd centres had occurred.
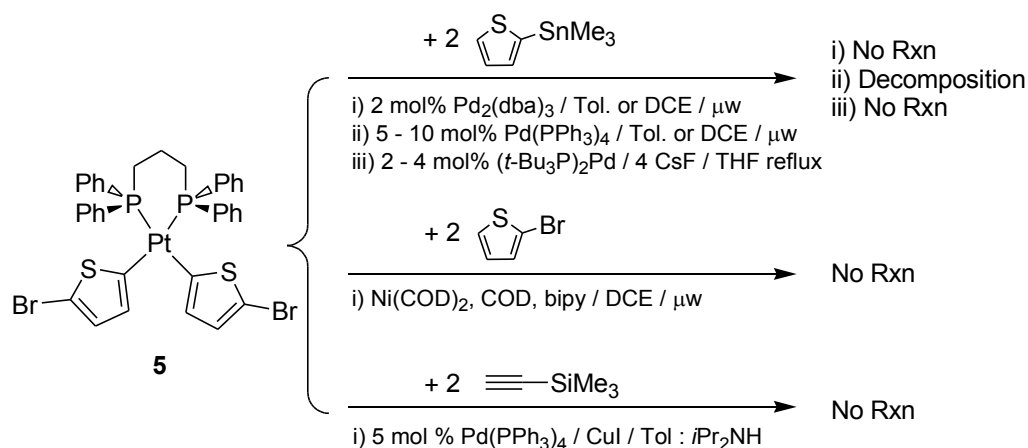


**Scheme 2.2.4**: Attempted C-C bond formation between **5** and 2-bis(trimethylstannyl)thiophene, 2-bromothiophene and trimethylsilylacetylene

This result was initially perplexing as the use of chelating phosphines was intended, in part, to reduce the amount of phosphine exchange and possible catalyst deactivation, however similar procedures in the literature [11] have shown Pd(PPh$_3$)$_4$ releases small amounts of free PPh$_3$ into

solution, which coordinate to square planar Pt complexes forming pentacoordinate complexes or displace inner shell ligands, inducing undesirable reactivity. The solution presented by Fréchet and co-workers to form platinum-containing polymer was to use a Pd catalyst stabilized by bulky tris(*tert*-butyl)phosphine ligands ($t$Bu$_3$P), in order to avoid coordination of PPh$_3$ to the Pt centre. Upon using ($t$Bu$_3$P)$_2$Pd in place of Pd(PPh$_3$)$_4$, polymerization of their cyclometalated square planar Pt complexes was achieved, with no undesired reactivity. Utilizing the same catalytic conditions as Fréchet and co-workers, we reacted **5** with 2-trimethylstannylthiophene in the presence of 2 mol% ($t$Bu$_3$P)$_2$Pd and 4 mole equivalents of CsF in refluxing THF. However in our system no sign of cross-coupling was observed despite repeating the reactions with various catalyst loadings (2 - 4 mol%) and when microwave-assisted heating of the mixtures was attempted in 1,2-dichloroethane. It is unclear at this time why **5** remains unreactive to Stille Cross-coupling when ($t$Bu$_3$P)$_2$Pd is used as a catalyst.

Attempts to react **5** with 2-bromothiophene via Yamamoto coupling [12] was done by heating at 40 ºC with stoichiometric Ni(COD)$_2$ in the presence of the stabilizing co-ligands bipy and COD. Work up of the reaction mixture yielded only starting material. It should be noted that an expected side product, bithiophene, formed from the Ni assisted cross-coupling of 2-bromothiophene, was never observed in any of the test reactions. Sonogashira cross-coupling was attempted by reacting **5** with two equivalents of trimethylsilylacetylene in the presence of catalytic Pd(PPh$_3$)$_4$ and CuI, again resulting in the recovery of only the Pt starting material. Overall it was surprising to observe that the reactivity of the monomer was inhibited to such an extent by substitution of two monodentate PBu$_3$ ligands for bidentate dppp. Exchanging PBu$_3$ for dppp has induced a resistance to most of the conventional aryl C-C bond forming coupling reactions, which stands in contrast to most of the literature, that demonstrates how effectively thienylbromides have been coupled using the reaction conditions described above [13].

This disparate behaviour in reactivity may be attributed to the nature of the substrate and the

catalyst employed. We used coordinatively saturated $Pd(PPh_3)_4$ as a cross-coupling catalyst, which dissociates $PPh_3$ ligands to become catalytically active, however the presence of free $PPh_3$ in solution has been attributed to Pt monomer degradation as described previously [11]. We proved this decomposition by reacting **5** with one equivalent of $Pd(PPh_3)_4$ at 70 °C in toluene which had a $^{31}P$ NMR spectrum that showed a complex mixture of products with no signs of **5** nor $Pd(PPh_3)_4$. Due to the proven effectiveness of $Pd(PPh_3)_4$ in the literature for Ar-Br homocoupling [13], it was decided that a coordinatively unsaturated, Pd(0) catalyst which cannot release free phosphine be ideal. However, when the coordinatively unsaturated catalyst $(tBu_3P)_2Pd$ was combined stoichiometrically with **5**, no reactivity was observed, which stands in opposition to the previous deduction. This may be due in part to the decreased lability of the $tBu_3P$ ligands on Pd. The lack of degradation of **5** in the presence of $(tBu_3P)_2Pd$ implies free $tBu_3P$ is not bonding to Pt to form pentacoordinate species or inducing Pt ligand displacement.

We then looked at the possible ways in which **5** can react with $Pd(PPh_3)_4$. The possibility of forming $(Ph_3P)_2Pt(SC_4H_2Br)_2$ was ruled out by independantly synthesizing it by reacting two equivalents of $PPh_3$ with **2** to yield the desired complex (the $^{31}P$ NMR spectrum exhibited a singlet at 17.9 ppm ($^1J_{P-Pt}$ = 2095 Hz)). This value did not match any of the observed products in the reaction between **5** and $Pd(PPh_3)_4$. It was confirmed that free dppp will readily react with the $Pd(PPh_3)_4$ catalyst, as $Pd(PPh_3)_4$ reacted with two equivalents of dppp to give $Pd(dppp)_2$ [14] and free $PPh_3$ quantitatively. We then combined one equivalent of $Pd(PPh_3)_4$ with **5**, and heated the mixture for 6 hours at 70 °C in $CDCl_3$. The $^{31}P$ NMR spectrum showed no signals corresponding to **5**, but the presence of $Pd(dppp)_2$ (5% at 4.5 ppm) was confirmed [14], as well as residual $Pd(PPh_3)_4$ (10%), $Pd(PPh_3)_3$ (10%), and free $PPh_3$ (10%) [15]. The presence of a new peak at -5.6 ppm (40%, $^1J_{P-Pt}$ = 3406 Hz) did not match any known dppp or $PPh_3$ complexes of Pt. In addition, two unidentified products at 28.9 (5%) and 24.1 (5%) ppm were also observed (Scheme 2.2.5). The complexes $Pt(PPh_3)_4$, $Pt(PPh_3)_3$, and $Pt(dppp)_2$ were not detected by NMR, which is important to

note, as formation of these products could only form following reductive elimination of bithiophene from **5**. The new major product had a similar $^{31}$P resonance to **5** (-3.3 ppm), which suggests that this product still contains Pt-bound dppp.
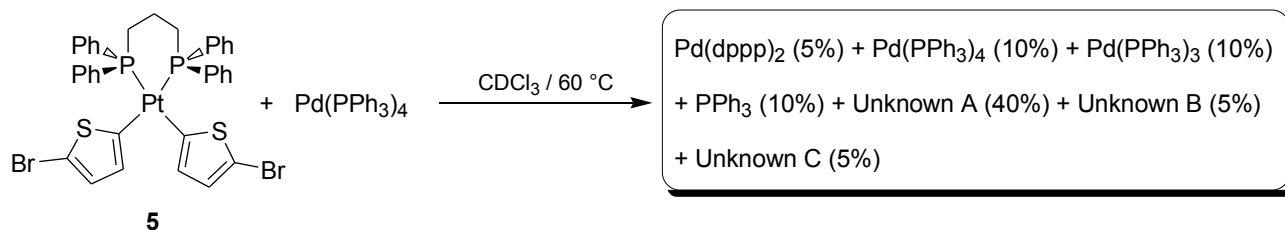


**Scheme 2.2.5**: Stoichiometric reaction between **5** and the cross-coupling catalyst Pd(PPh$_3$)$_4$, which yielded a complex mixture of products.

From the abovementioned observations. We postulate a few possible reaction pathways to explain why the cross-coupling reactions with **5** did not proceed as expected. In a proposed first step for the reaction of **5** with Pd(PPh$_3$)$_4$ (Scheme 2.2.6), oxidative addition of aryl-Br to the Pd(0) centre leads to the formation of the intermediate **6a**. This bimetallic intermediate contains two transition metals in the +2 oxidation state in d$^8$ square planar coordination environments. Due to the stability of the Pt(II) centre by the chelating phosphine, dppp, and the presence of labile PPh$_3$ ligands at Pd$^{2+}$, it is reasonable that deactivation pathways would involve Pd centres. After initial oxidative addition to Pd, reductive elimination can occur at the same metal centre, regenerating the catalyst and the monomer (i.e., the non-productive pathway). The next deactivation pathway involves isomerization of **6a** by isomerization to the less-hindered *trans* conformation (**7**) which may undergo transmetallation upon dissociation of one PPh$_3$ ligand, however this pathway is also unobserved (Scheme 2.2.6, Path A). Previous work has shown reductive elimination at Pt and Pd centres with chelating phosphines depends on several factors including concentration of strong donors in solution, and even minor changes to the molecular structure and electron withdrawing / donating substituents on the stabilizing ligands [16]. Thus making it difficult to accurately predict

the chemical behaviour of such species in solution.

The inhibition of the transmetallation step of Stille coupling was also considered as a possible stopping point for the reactivity of **5**. If **6a** is formed and further reacts with free dppp to displace the *cis* arranged PPh3 ligands on Pd, then dissociation of dppp to reveal an open coordination site at Pd will be significantly inhibited (Scheme 2.2.6, Path B). This dissociation step is a requirement for square planar Pt or Pd complexes to undergo transmetallation. The Pd complex Pd(dppp)2 is not reported to be catalytically active, however a two-coordinate Pd(dppp) intermediate has been invoked as the proposed active species in the Pd-catalyzed phenoxycarbonylation of alkynes [14b], where the reaction conditions involve combination of an alkyne, CO, and Zn in the presence of equimolar equivalents of Pd(OAc)2 and dppp.
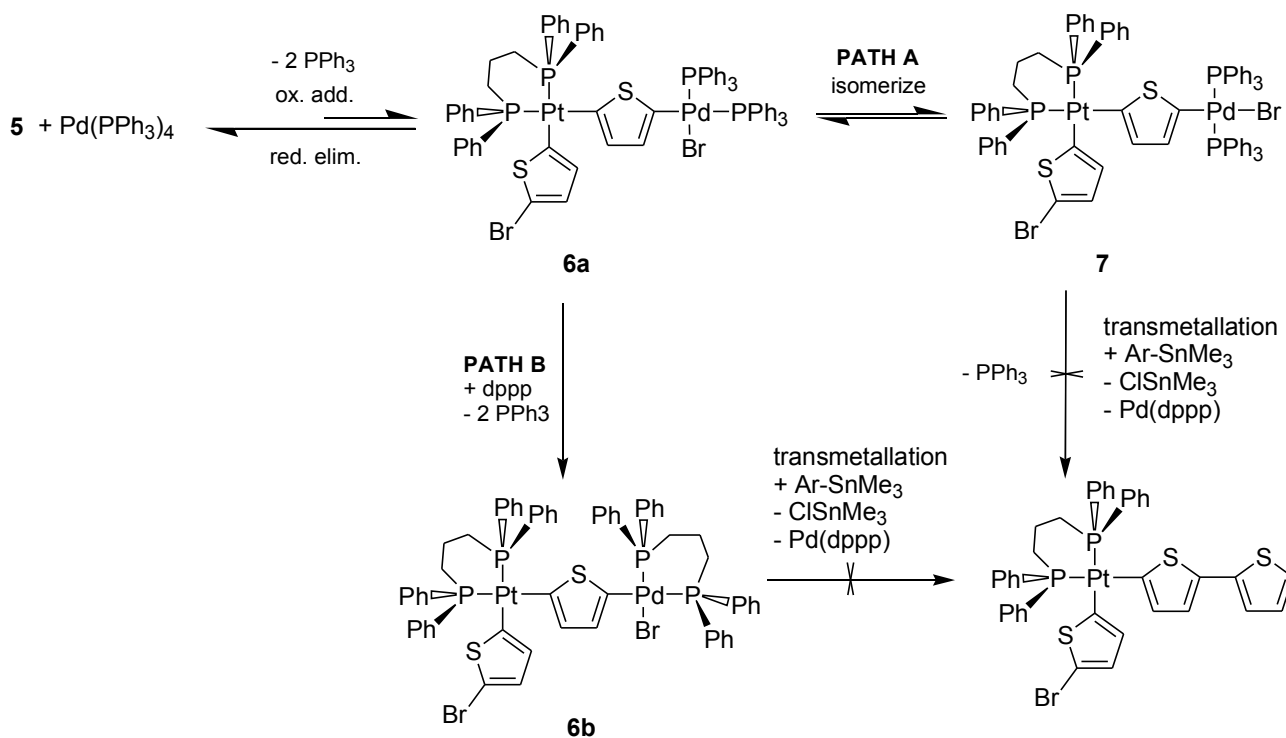


**Scheme 2.2.6**: Proposed mechanism for the first step of Pd(PPh3)4 cross-coupling of **5**, forming a bimetallic intermediate.

Predecent for the formation of such stable bimetallic complexes was set by Sonogashira and co-workers, who synthesized the diplatinum complex, Cl(PBu3)2Pt(μ-C4H2S)Pt(PBu3)2Cl (**8**) [10],

which we were able to further characterize via X-ray crystallography (Figure 2.2.8) using the synthetic pathway used to form **8** is listed in Scheme 2.2.7. The PBu$_3$ ligands on each Pt centre in **8** were found to be resting in the trans configuration in the solid state, and no solvent dependant isomerization was observed. The Pt-C bonds of **8** were 2.004(9) and 2.025(9) Å, which are the same within error as in the PBu$_3$-bound Pt complex, **3**. The Pt-P bond lengths were found to be 2.318(2), 2.308(2), 2.288(3), and 2.298(2) Å which are all close in value to or the same within error as the Pt-P bond lengths of 2.3159(14) and 2.3286(16) Å found in **3**. The P-Pt-P and Cl-Pt-C bond angles involving Pt(1B) were 174.45(9) and 178.8(3)° respectively; while the related angles involving Pt(2B) were 178.67(11) and 177.2(3)°, thus reflecting the presence of square planar geometries at both Pt-centres. The relative geometries of the planes formed by the chelating atoms to each Pt centre were co-planar, with the plane formed by the bridging thienyl ring resting orthogonal to them. This type of compound is preceded by similar examples in the literature as Lee and co-workers found that Pd(0) complexes of the form Me$_3$P-Pd$^{(0)}$-NHC (NHC = N-heterocyclic carbene) led to stable products upon oxidative addition of two equivalents with 2,5'-dibromobithiophene to form *trans*-(Me$_3$P)(NHC)BrPd$^{(II)}$-(C$_4$H$_2$S)$_2$-Pd$^{(II)}$Br(NHC)(PMe$_3$) [14]. Given that *trans*-(Me$_3$P)(NHC)BrPd$^{(II)}$-(C$_4$H$_2$S)$_2$-Pd$^{(II)}$Br(NHC)(PMe$_3$) was reported as the major product in 77% yield, it is unlikely that this complex has any further catalytic activity in the cross-coupling of aryl bromides, suggesting that these dinuclear complexes are resting states in organometallic oxidative addition chemistry.
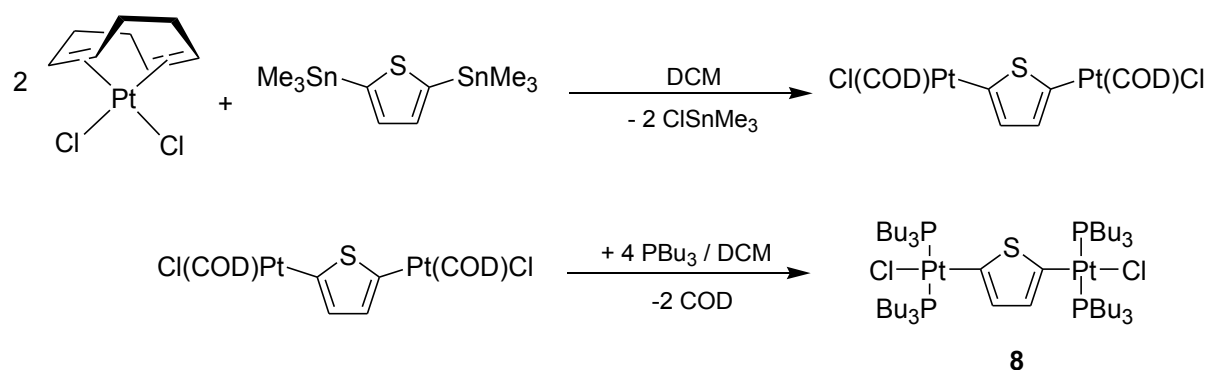
**Scheme 2.2.7**: Synthetic route for Cl(PBu$_3$)$_2$Pt(μ-C$_4$H$_2$S)Pt(PBu$_3$)$_2$Cl (**8**)
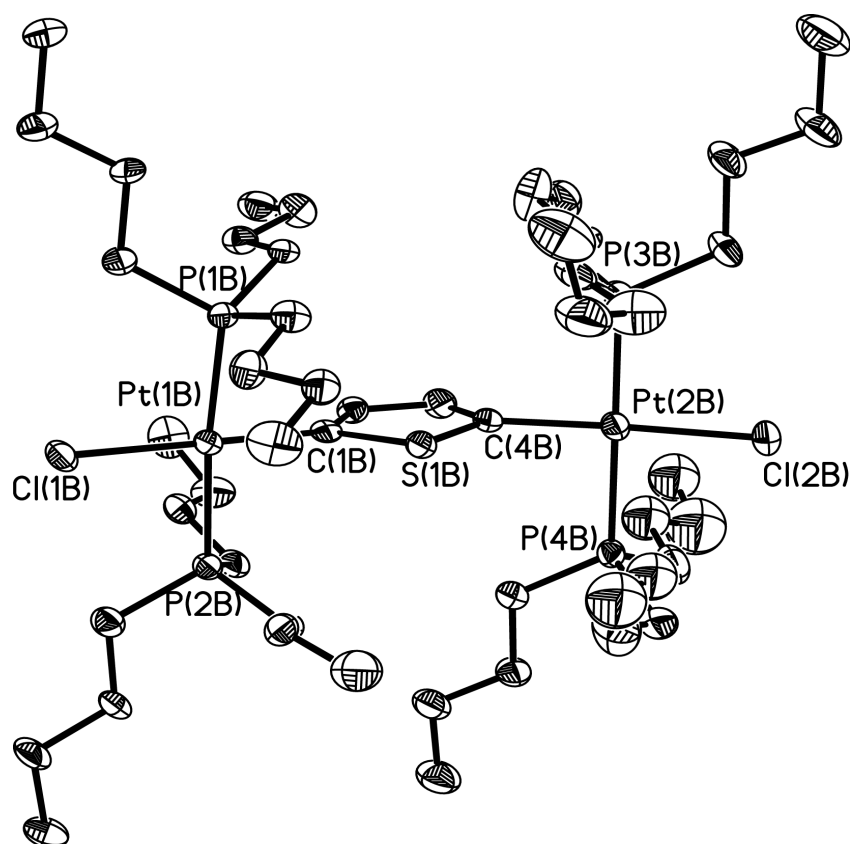


**Figure 2.2.8**: Thermal ellipsoid plot (30% probability) of Cl(Bu$_3$P)$_2$Pt(C$_4$H$_2$S)Pt(PBu$_3$)$_2$Cl (**8**). The second crystallographically independant molecule, hydrogen atoms and hexane solvate have been omitted for clarity. Selected bond lengths [Å] and angles [°]: Pt(1B)-C(1B) 2.004(9), Pt(1B)-P(1B) 2.318(2), Pt(1B)-P(2B) 2.308(2), Pt(1B)-Cl(1B) 2.380(2), Pt(2B)-C(4B) 2.025(9), Pt(2B)-P(3B) 2.288(3), Pt(2B)-P(4B) 2.298(2), Pt(2B)-Cl(2B) 2.386(3), Cl(1B)-Pt(1B)-C(1B) 178.8(3), P(1B)-Pt(1B)-P(2B)174.45(9), Cl(1B)-Pt(1B)-P(1B) 91.86(9), Cl(1B)-Pt(1B)P(2B) 92.62(8), Cl(2B)-Pt(2B)-C(4B) 177.2(3), P(3B)-Pt(2B)-P(4B) 178.67(11), Cl(2B)-Pt(2B)-P(3B) 93.00(10), Cl(2B)-Pt(2B)-P(4B) 87.30(9), P(2B)-Pt(1B)-C(1B)-S(1B) torsion angle 99.1(4), P(3B)-Pt(2B)-C(4B)-S(1B) torsion angle 93.4(5).

One possible method for overcoming this lack of reactivity, and to ensure the stability of the Pt monomer while encouraging the reductive elimination of the Pd-catalyst, is to utilize a sterically bulky phosphine ligand on Pt. Such a sterically encumbering ligand would encourage the formation of *trans* geometries at Pt, which when oxidatively added to the Pd(0) catalyst may prevent the formation of a *trans* geometry at Pd, promoting reductive elimination from the *cis* geometry to yield either the original Pt-complex or homocoupled products. Work done in our group has led to the synthesis of the sterically bulky tris(3,5-diisopropylphenyl)phosphine ligand, which when reacted with 0.5 equivalents of **2**, gives the Pt complex **9** (Scheme 2.2.8). Preliminary NMR data (Figure 2.2.9) and X-ray diffraction studies of **9** have shown that complex **9** resides exclusively in the *trans* conformation, with both thienyl substituents being co-planar. This co-planarity may be important in extending the conjugation length of any synthesized oligomers or polymers derived from **9**. Furthermore, a detailed study of this sterically encumbered monomer in Pd catalyzed cross-coupling chemistry is an area currently under investigation in our group.
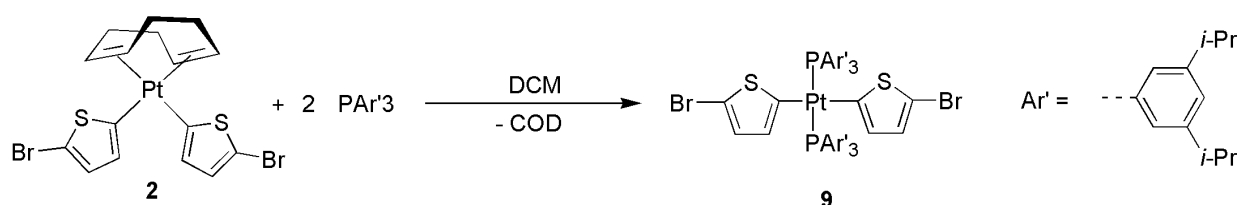


**Scheme 2.2.8**: Synthesis of dithienyl-Pt(II) complex stabilized by 2 tris(3,5-diisopropylphenyl)phosphine ligands.
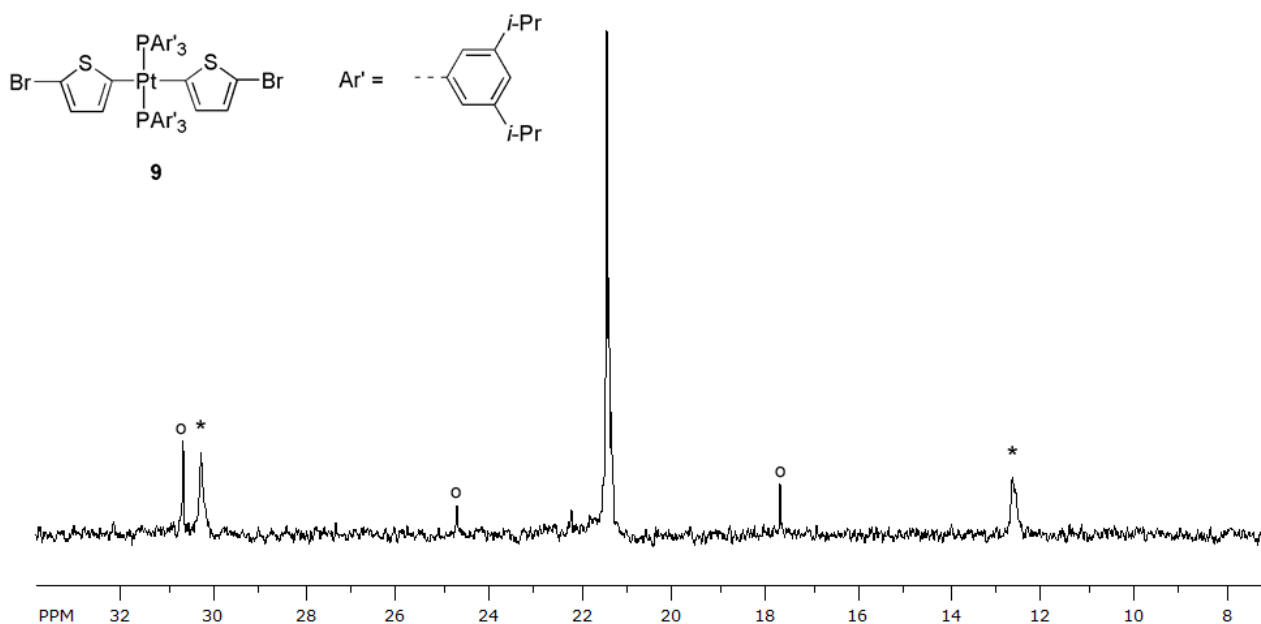
**Figure 2.2.9**: $^{31}P\{^1H\}$ NMR of the initial synthesis of **9** (*trans*), showing small amounts of impurity (o). The diagnostic flanking $^{195}Pt$ satellites are noted with (*).

## 2.3 Conclusions

In summary, a series of bromothienyl-functionalized platinum complexes have been synthesized and fully characterized, while initial attempts at polymerization were met with some success. The heretofore unknown polymerization of a Pt monomer with direct thienyl linkages was achieved with Yamamoto coupling, using $PBu_3$ ancilliary ligands on the Pt centre, however the coordination geometry of the Pt centres in the polymeric material is unknown due to an inability to form pure materials. Polymer purity and synthetic reproducibility were suspect due to the presence of starting material and the temperature and solvent dependant isomerism of the monomer. Attempts to polymerize platinum-bis(thienyl) complexes affixed in the *cis* conformation with bidentate phosphines were unsuccessful with either no observed reactivity under typical cross-coupling methods, or decomposition of the monomer itself. Future work in this area will involve an in-depth study of the effect of steric bulk at the Pt centre, as well as determining the total Pt content and catalyst loadings necessary for polymerization.

## 2.4 Experimental Section

**General.** All reactions were performed using standard Schlenk line techniques under an atmosphere of nitrogen or in an inert atmosphere glove box (Innovative Technology, Inc.). Solvents were dried using Grubbs-type solvent purification system manufactured by Innovative Technology, Inc., degassed (freeze-pump-thaw method) and stored under an atmosphere of nitrogen prior to use. Synthesis of *trans*-(Bu$_3$P)$_2$PtCl$_2,$ Compounds **2 - 5** were adapted from literature procedures [10b,17]. Compound **8** was synthesized using a modified procedure based on literature procedures, however no crystal structure has yet been published [10b]. $^1$H and $^{31}$P NMR spectra were collected on a Varian iNova-400 spectrometer, and $^{13}$C{$^1$H} NMR spectra were collected on a Varian VNMRS-500 cold probe spectrometer. Samples were referenced externally to SiMe$_4$ [$^1$H, $^1$H{$^{11}$B}, $^{13}$C{$^1$H}] and H$_3$PO$_4$ ($^{31}$P). Elemental analyses were performed by the Analytical and Instrumentation Laboratory at the University of Alberta. Infrared spectra were recorded on a Nicolet IR100 FTIR spectrometer as Nujol mulls between NaCl plates. Melting points were measured in sealed glass capillaries under nitrogen using a MelTemp melting point apparatus and are uncorrected.

**X-ray Crystallography.** Crystals suitable for X-ray diffraction studies were removed from a vial (in glove box) and immediately coated with thin layer of hydrocarbon oil (Paratone-N). A suitable crystal was then mounted on glass fiber, and quickly placed in a low temperature stream of nitrogen on the X-ray diffractometer [18]. All data were collected using a Bruker APEX II CCD detector/D8 diffractometer using Mo Kα or Cu Kα radiation, with the crystals cooled to -100 °C. The data were corrected for absorption through Gaussian integration from the indexing of the crystal faces [19]. Crystal structures were solved using direct (**3, 4:** SHELXS-97 [20]) or Patterson (**2, 5**: DIRDIF [21]) methods, and refined using SHELXS-97. The assignment of hydrogen atoms positions were based on the sp$^2$ or sp$^3$ hybridization geometries of their attached carbon atoms, and were give thermal parameters 20% greater than those of their parent atoms.

69

**Synthetic Procedures**

**Synthesis of *trans*-(Bu₃P)₂PtCl₂:** 0.477 g (1.01 mmol) of bis(benzonitrile) platinum dichloride was suspended in 40 mL of toluene. While stirring, 0.51 mL (2.04 mmol) of PBu₃ was added via syringe at room temperature. The mixture was stirred for 12 hours to yield a clear yellow solution, and the volatiles were removed under vacuum to yield a pale yellow solid. The product was purified by recrystallization from 3:1 hexanes:THF at -35 °C to give *trans*-(PBu₃)₂PtCl₂ as colourless prisms (0.57g, 85%). The *cis* isomer can be isolated by dissolving the solid in chloroform or dichloromethane, and the *trans* isomer can be isolated by dissolving the solid in benzene.

$^1$H NMR (400 MHz, CDCl₃): δ = 1.99 (m, 12H, -C$H_2$CH₂CH₂CH₃), 1.54 (m, 12H, -CH₂C$H_2$CH₂CH₃), 1.43 (m, 12H, -CH₂CH₂C$H_2$CH₃), 0.94 (t, 18H, $^3J_{HH}$ = 7.2 Hz, -CH₂CH₂CH₂C$H_3$). $^{13}$C{$^1$H} NMR (100 MHz, CDCl₃): δ = 26.1 (PBu₃), 23.8 (PBu₃), 23.6 (PBu₃), 13.3 (PBu₃). $^{31}$P{$^1$H} (161.8 MHz, CDCl₃ (*cis*)): δ = 1.0 (*cis*, $^{195}$Pt satellites: $^1J_{P\text{-}Pt}$ = 3517 Hz). $^{31}$P{$^1$H} (161.8 MHz. C₆D₆ (*trans*)): -4.4 (*trans*, $^{195}$Pt satellites: $^1J_{P\text{-}Pt}$ = 2386 Hz).


**Reaction of *trans*-(Bu₃P)₂PtCl₂ with 2,5-bis(trimethylstannyl)thiophene:** In a Schlenk flask flushed with nitrogen, Pt(PBu₃)₂Cl₂ (92.1 mg, 0.225 mmol) and 2,5-bis(trimethylstannyl)thiophene (56.0 mg, 0.222 mmol) were dissolved in 2 mL of DCM to yield a clear pale yellow solution. To this solution was added (PPh₃)₂PdCl₂ (4 mg , 0.006 mmol, 2 mol%). The solution was allowed to stir overnight to yield a dark brown mixture. Volatiles were removed *in vacuo* to yield the brown mixture of solid products. $^1$H NMR (CDCl₃) of this compound showed very broad peaks between 2.0 and 0.65 ppm, however $^{31}$P{$^1$H} NMR showed six new phosphorus environments with no discernible $^{195}$Pt satellites, at 7.8, 7.4, 6.4, 2,4, 2.0 and 0.5 ppm. GPC analysis showed an average molecular weight of 100 kDa, however reproduction of this result was unsuccessful.

**Synthesis of 2-bromo-5-trimethylstannylthiophene:** In a Schlenk flask 2-bromothiophene (5.48 g, 33.6 mmol) was dissolved in 100 mL of THF. The solution was cooled to -78 °C, and 2.0 M lithium diisopropylamide (LDA) (16.8 mL, 33.6 mmol) was added dropwise via syringe under a flow of nitrogen. The solution turned from colourless to orange after the addition of LDA was complete, and finally to a deep red after 1 hr at -78 °C. Trimethyltin chloride (35.0 mL, 35.0 mmol, 1.0 M solution in hexanes) was then added dropwise. Upon complete addition of the $ClSnMe_3$, the solution turned from deep red to pale clear yellow. The solution was stirred for 1 hr at -78 °C and then raised to room temperature for an additional 4 hours. 100 mL of water was then added, and the product was extracted with 3 x 50 mL portions of diethyl ether. The organic fraction was dried with $MgSO_4$, filtered, and the volatiles were removed under high vacuum to yield the product (orange liquid) in 96% yield (10.5 g).

$^1$H NMR (400 MHz, $CDCl_3$): δ = 7.14 (d, 2H, $^3J_{HH}$ = 3.2 Hz, $BrC_4H_2SSnMe_3$), 6.96 (d, 2H, $^3J_{HH}$ = 3.2 Hz, $BrC_4H_2SSnMe_3$), 0.38 (9H, $-Sn(CH_3)_3$, $^3J_{\text{H-119Sn}}$ = 58.0 Hz; $^3J_{\text{H-117Sn}}$ = 55.6 Hz). $^{13}C\{^1H\}$ NMR (100.5 MHz, $CDCl_3$): δ = 140.0 (Ar$C$), 135.2 (Ar$C$), 130.6 (Ar$C$), 116.1 (Ar$C$), -8.0 ($-Sn(CH_3)_3$). HR-MS Calcd. $M^{+\bullet}$(*m/z* 325.88); Found: $M^{+\bullet}$(*m/z* 325.87).


**Synthesis of *cis*-bis(5-bromothienyl)(1,5-cyclooctadiene) platinum (II) *cis*-(BrC₄H₂S)₂Pt(COD) (2):** In a Schlenk flask under nitrogen, 2-bromo-5-trimethylstannylthiophene (112.5 mg, 0.34 mmol) and *cis*-$Cl_2Pt(COD)$ (64.5 mg, 0.17 mmol) were dissolved in 5 mL of dichloromethane, and stirred for 6 hours at room temperatre to yield a clear dark yellow solution. The volatiles were then removed in vacuo to yield **2** as a pale yellow solid (0.102 g, 96%). Crystals of **2** suitable for X-ray crystallography were grown from a saturated solution of THF:hexanes at -35 °C (orange plates).

$^1$H NMR (400 MHz, $CDCl_3$): δ = 6.98 (d, 2H, $^3J_{HH}$ = 3.6 Hz, Br[CC$H$CHCS]Pt), 6.50 (d, 2H, $^3J_{HH}$ = 3.6 Hz, Br[CCHC$H$CS]Pt, $^{195}$Pt satellites: $^3J_{\text{H-Pt}}$ = 49.6 Hz), 5.47 (br s, 4H, η²-(-CHCH-)-Pt, $^{195}$Pt satellites: $^2J_{\text{H-Pt}}$ = 42.0 Hz), 2.62 (br s, 8H, [-C$H_2$C$H_2$-]). $^{13}C\{^1H\}$ NMR (125 MHz, $CDCl_3$): δ =

147.4 (Ar$C$), 131.5 (Ar$C$), 130.1 (Ar$C$), 112.5 (Ar$C$), 105.1 (COD $C$H), 30.1 (COD $C$H$_2$). Mp (°C) 173 - 175 (decomposed, turned black). Anal. Calcd. for $C_{18}H_{22}Br_2PtS_2$: C, 32.89; H, 3.37; S, 9.76. Found: C, 33.56; H, 3.05; S, 9.84.

**Synthesis of _cis_-di(5-bromothienyl)bis(tri-n-butylphosphine) platinum (II) (BrC$_4$H$_2$S)$_2$Pt(PBu$_3$)$_2$ (3):** To a slurry of _cis_-(BrC$_4$H$_2$S)$_2$Pt(COD) (61.4 mg, 0.098 mmol) in 6 mL of hexanes was added two equivalents of PBu$_3$ (50 µL, 0.20 mmol). After stirring for 3 hours at room temperature, the initially yellow suspension became a clear yellow solution. The volatiles were removed in vacuo to yield **3** as a pale yellow solid (101 mg, 95%). Crystals of **3** suitable for X-ray crystallography were obtained by cooling a saturated hexanes solution to -35 °C (pale yellow prisms).

$^1$H NMR (400 MHz, CDCl$_3$): δ = 6.82 (d, 2H, $^3J_{HH}$ = 2.8 Hz, Pt-(BrC$_4$$H$$_2$S)), 6.32 (d, 2H, $^3J_{HH}$ = 2.8 Hz, Pt-(BrC$_4$$H$$_2$S)), 1.58 (m, 12H, -C$H$$_2$CH$_2$CH$_2$CH$_3$), 1.45 (br m, 12H, -CH$_2$C$H$$_2$CH$_2$CH$_3$), 1.40 (m, 12H, -CH$_2$CH$_2$C$H$$_2$CH$_3$), 0.94 (t, 18H, $^3J_{HH}$ = 7.2 Hz, -CH$_2$CH$_2$CH$_2$C$H$$_3$). $^{13}$C{$^1$H} NMR (128 MHz, CDCl$_3$): δ = 137.3 (Ar$C$), 133.8 (Ar$C$), 128.7 (Ar$C$), 128.4 (Ar$C$), 26.5 (P$Bu_3$), 24.4 (P$Bu_3$), 13.9 (P$Bu_3$), 13.8 (P$Bu_3$). $^{31}$P{$^1$H} NMR (161.8 MHz, CDCl$_3$): δ = -3.7 (_cis_, $^{195}$Pt sattelites: $^1J_{P-Pt}$ = 2057 Hz). Anal. Calcd. for $C_{32}H_{58}Br_2P_2PtS_2$: C, 41.61; H, 6.33; S, 6.94. Found: C, 41.81; H, 6.43; S, 6.46. Mp (°C): 85 - 86 (melts).

**Thermal Isomerization of (BrC$_4$H$_2$S)$_2$Pt(PBu$_3$)$_2$ (3):** 5 mg of (SC$_4$H$_2$Br)$_2$Pt(PBu$_3$)$_2$ was dissolved in 0.5 mL of CDCl$_3$ in a J. Young NMR tube under an atmosphere of nitrogen. The sample was checked _in-situ_ by $^{31}$P{$^1$H} NMR to verify the presence of the _cis_-isomer of the compound. The sample was then heated at 60°C for 24 hours. The NMR spectrum of the heated sample showed the two isomers in solution (approximately 40% _trans_).

$^{31}$P{$^1$H} NMR (161.8 MHz, CDCl$_3$): δ = -3.7 (_cis_, $^{195}$Pt satellites: $^1J_{P-Pt}$ = 2057 Hz), 2.7 (_trans_, $^{195}$Pt

satellites: $^1J_{\text{P-Pt}} = 2543$ Hz).

**Polymerization of (BrC₄H₂S)₂Pt(PBu₃)₂ (3):** a) Palladium assisted cross-coupling: 104.3 mg (0.112 mmol) of **3** and 4 mg (0.003 mmol, 3 mol%) of $Pd(PPh_3)_4$ were dissolved in 2 mL of $CH_2Cl_2$ to yield a clear yellow solution. After stirring for 12 hours at room temperature, the solution turned dark orange. Volatiles were removed in vacuo to yield an orange solid. $^1$H and $^{31}$P NMR of this compound showed only starting material and residual free $PPh_3$. Repeating the synthesis in toluene at reflux afforded no additional reactivity. Repeating the reaction with 5 mol% $(PPh_3)_2PdCl_2$ in $CH_2Cl_2$ and toluene (reflux) also affords no reactivity

b) Grignard metathesis polymerization: 183.0 mg (0.198 mmol) of **3** and 8.4 mg (0.199 mmol) of LiCl were dissolved in 3 mL of THF and cooled to -78 °C. To this solution was added 198 μL (0.198 mmol) of 1.0 M $t$BuMgCl. The solution turned opaque yellow as the reaction mixture was allowed to warm to room temperature. The turbid mixutre was left to stir for 12 hours, at which point a 1 mL THF solution containing 1.0 mg (0.002 mmol, 1 mol%) of $Ni(dppp)Cl_2$ was added followed by stirring for 24 hours. The resulting mixture was a pale peach colour. In-situ $^{31}$P{$^1$H} NMR showed free $PBu_3$ (-31 ppm) and starting material, along with other unidentified products. GPC analysis showed that no polymeric ($M_w$ >1000 g/mol) compounds were present in the crude mixture.

c) Yamamoto cross-coupling: A 1 mL toluene solution of 30.3 mg (0.11 mmol) of $Ni(COD)_2$, 17.2 mg (0.11 mmol) of 2,2'-bipyridine, and 13.5 μL (0.11 mmol) of 1,5-cyclooctadiene (COD) was added to a 2 mL toluene solution containing 102 mg (0.11 mmol) of **3**. The resulting solution was deep blue, and left to stir for 12 hours at room temperature to yield a dark orange-brown solution. The mixture was then heated to 80 °C for 48 hours. Volatiles were removed in vacuo, and the resulting sticky orange residue was dissolved in 3 mL of THF, filtered and dried under vacuum again to yield a sticky orange crude solid. $^1$H NMR (CDCl₃) showed broadened peaks similar to that of the starting material. The $^{31}$P{$^1$H} NMR spectrum showed broadened peaks for the starting

material at -3.7 ppm; unidentified peaks at 4.2 and -9.6 ppm were also present. GPC analysis showed the resulting material to have $M_w$ = 38 000 Da; repeated syntheses yielded materials with molecular weights ranging from $M_w$ = 3500 - 38 000 Da. The product peaks found in the $^{31}$P NMR spectra were inconsistent from one experiment to the next.

**Synthesis of cis-bis(5-bromothienyl)diphenylphosphinoethane platinum (II), (BrC$_4$H$_2$S)$_2$Pt(dppe) (4):** *cis*-(BrC$_4$H$_2$S)$_2$Pt(COD) (**2**) (41.6 mg 0.07 mmol) was dissolved in 5 mL of CH$_2$Cl$_2$ to yield a clear yellow solution. A solution of bis(diphenylphosphino)ethane (26.0 mg, 0.07 mmol) in 5 mL CH$_2$Cl$_2$ was added to the solution of **3** and left to stir for 12 hours at room temperature. The resulting solution was clear yellow. Volatiles were removed in vacuo to yield **4** as a yellow solid in (48.4 mg, 79%). Crystals of **4** suitable for X-ray crystallography were obtained by slow diffusion of diethyl ether into a saturated CH$_2$Cl$_2$ solution (orange prisms).

$^1$H NMR (400 MHz, CDCl$_3$): δ = 7.62 - 7.40 (m, 20H, (C$_6$H$_5$)$_2$P), 6.70 (d, 1H, $^3J_{HH}$ = 1.2 Hz, CHC*H*CBr), 6.69 (d, 1H, $^3J_{HH}$ = 1.2 Hz, CHC*H*CBr), 6.17 (t, 2H, $^3J_{HH}$ = 1.2 Hz, C*H*CHCBr, $^{195}$Pt satellites: $^3J_{H-Pt}$ = 44.0 Hz), 2.37 (br, 4H, Ph$_2$PC*H$_2$*C*H$_2$*PPh$_2$). $^{31}$P{$^1$H} NMR (CDCl$_3$, 161.8 MHz): δ = 42.5 (*cis*, Ph$_2$*P*CH$_2$CH$_2$*P*Ph$_2$ , $^{195}$Pt satellites: $^1J_{P-Pt}$ = 2072 Hz). $^{13}$C{$^1$H} NMR (128 MHz, CDCl$_3$): δ = 133.6 (Ar*C*), 133.5 (Ar*C*), 131.2 (Ar*C*), 129.9 (Ar*C*), 128.9 (Ar*C*), 128.8 (Ar*C*), 128.7 (Ar*C*), 128.6 (Ar*C*), 28.0 (-P*C*H$_2$*C*H$_2$P-). Anal. Calcd. for C$_{34}$H$_{28}$P$_2$Br$_2$PtS$_2$: C, 44.51; H, 3.08; S, 6.99. Found: C, 43.99; H, 3.01; S, 6.89. Mp (°C) 210 - 211 (turns brown), 237 - 238 (melts).

**Synthesis of cis-bis(5-bromothienyl)diphenylphosphinopropane platinum (II), (BrC$_4$H$_2$S)$_2$Pt(dppp) (5):** Complex **2** (135.2 mg, 0.21 mmol) was dissolved in 5 mL of CH$_2$Cl$_2$ to yield a clear yellow solution. A solution of bis(diphenylphosphino)propane (84.2 mg, 0.21 mmol) in 5 mL CH$_2$Cl$_2$ was added and the reaction was stirred for 12 hours at room temperature. The

resulting solution was clear orange. The volatiles were removed from the resulting orange solution to yield **5** as an orange powder (189.0 mg, 95%). Crystals of **5** suitable for X-ray crystallography were obtained by slow diffusion of ether into a saturated DCM solution (orange prisms).

$^1$H NMR (CDCl$_3$, 400 MHz): δ 7.55-7.29 (m, 20H, (Ar$H$)$_2$P), 6.46 (d, $^3J_{HH}$ = 1.6 Hz, 2H, BrC$_2H$C$_2$HS), 5.93 (br, 2H, BrC$_2$HC$_2H$S, $^{195}$Pt satellites: $^3J_{H-Pt}$ = 43.2 Hz), 2.58 (br, 4H, $H_2$CCH$_2$C$H_2$), 1.88 (m, 2H, H$_2$CC$H_2$CH$_2$). $^{31}$P{$^1$H} NMR (CDCl$_3$, 161.8 MHz): δ -3.3 (Ph$_2$PCH$_2$CH$_2$CH$_2$PPh$_2$, $^{195}$Pt satellites: $^1J_{P-Pt}$ = 1984 Hz). $^{13}$C{$^1$H} NMR (128 MHz, CDCl$_3$): δ = 133.3 (ArC), 131.2 (ArC), 130.6 (ArC), 130.4 (ArC), 129.7 (ArC), 128.7 (ArC), 128.3 (ArC), 127.7 (ArC), 28.0 (-P$C$H$_2$CH$_2$CH$_2$P-), 19.1 (-PCH$_2$$C$H$_2$CH$_2$P-). Anal. Calcd. for C$_{35}$H$_{30}$P$_2$S$_2$PtBr$_2$: C, 45.03; H, 3.45; S, 6.87. Found: C, 45.24; H, 3.27; S, 6.89. Mp (°C) 245-247 (melts).

**Attempted cross-coupling of (BrC$_4$H$_2$S)$_2$Pt(dppp) (5):** a) Stille cross-coupling with 2-trimethylstannylthiophene: In a Schlenk flask flushed with nitrogen, **5** (27.4 mg, 0.03 mmol) and 2-trimethylstannylthiophene (10.3 μL, 0.06 mmol) were dissolved in 5 mL of toluene to yield a clear yellow solution. To this solution, Pd(PPh$_3$)$_4$ (3.4 mg, 1 mol%) was added and the solution was refluxed for 12 hours. The resulting mixture was yellow-green with the formation of a black precipitate. Volatiles were removed under vacuum to yield a dark yellow solid. $^{31}$P{$^1$H} NMR of this product showed starting material and trace amounts of free PPh$_3$. Repeating this reaction in THF yielded several unidentifiable peaks in the $^{31}$P{$^1$H} NMR spectrum, however 90% (by integration) of starting material remained unreacted.

b) Microwave-assisted Stille cross-coupling: In a sealed microwave reactor vial was dissolved 60 mg (0.063 mmol, 1 mol%) of **5**, 23.0 μL (0.12 mmol) of 2-trimethylstannylthiophene, and 7.4 mg of Pd(PPh$_3$)$_4$ in 3 mL of 1,2-dichloroethane. The microwave vial was placed in the reactor for 1 hr at 80 °C (avg. power was 17 W) to yield a clear yellow solution. Only starting material was present by *in situ* $^{31}$P{$^1$H} NMR. The vial was placed back into the reactor and heated to 90 °C for 8 hours

(avg. power was 30W) to yield a dark orange solution with black precipitate. Only **5** was present in the $^{31}P\{^1H\}$ NMR spectrum. The reaction was repeated with the following catalyst and co-ligand combinations to yield only **5** by $^{31}P\{^1H\}$ NMR: 2 mol% $Pd_2(dba)_3$, 5 mol% $Pd(PPh_3)_4$; 8 mol% $AsPh_3$; 10 mol% $Pd(PPh_3)_4$, 15 mol% $AsPh_3$; 2 mol% $Pd_2(dba)_3$, 4 mol% $Pd(P(tBu)_3)_2$, 4 mol. eq. CsF; 2 mol% $Pd(P(tBu)_3)_2$, 4 mol. eq. CsF.

c) Microwave-assisted Yamamoto cross-coupling: In a sealed microwave reactor vial, **5** (66.8 mg, 0.071 mmol), 2-bromothiophene (23.1 mg, 0.142 mmol), $Ni(COD)_2$ (19.5 mg, 0.07 mmol), COD (8.6 μL, 0.071 mmol) and 2,2'-bipyridine (11.1 mg, 0.071 mmol) were dissolved in 3 mL of 1,2-dichloroethane. The yellow-green solution was heated at 40 °C in a microwave reactor for 8 hours to yield a dark brown solution. Only **5** was present by $^1H$ and $^{31}P\{^1H\}$ NMR, showing no signs of reaction.

d) Sonogashira cross-coupling: In a Schlenk flask flushed with nitrogen, **5** (68.6 mg, 0.073 mmol), trimethylsilylacetylene (21 μL, 0.15 mmol), CuI (0.7 mg, 0.073 mmol) and $Pd(PPh_3)_4$ (4.2 mg, 0.073 mmol) were dissolved in 10 mL of toluene:diisopropylamine (7:3 ratio) to yield a clear yellow solution. The solution was heated at 70°C for 12 hours to yield a cloudy yellow mixture. The volatiles were removed *in vacuo* to yield to an orange solid. $^1H$ and $^{31}P\{^1H\}$ NMR showed only the presence **5**, showing no signs of reaction.


**Synthesis of Cl(PBu_3)_2Pt(μ-C_4H_2S)Pt(PBu_3)_2Cl (8):** At room temperature, a solution of $Pt(COD)Cl_2$ (192.5 mg, 0.51 mmol) in 7 mL $CH_2Cl_2$ was added to a 8 mL solution of 2,5-bis(trimethylstannyl)thiophene (105.4 mg, 0.25 mmol) in $CH_2Cl_2$. The clear yellow solution was stirred for 12 hours to yield a yellow slurry, indicating the formation of the intermediate product 2,5-bis(ClPt(COD))_2(C_4H_2S). To the stirring slurry was added 256 μL (1.03 mmol) of $PBu_3$. The complete addition of the phosphine caused the solution to immediately turn deep clear yellow. The volatiles were removed *in vacuo* and the product was extracted in 10 mL of hexanes. The volatiles

were removed from the mother liqour to yield a pale yellow solid (87%, 302 mg). Crystals of **8** suitable for X-ray crystallography were obtained by cooling a saturated THF:hexane solution to -35°C (pale yellow prisms). This compound had been synthesized previously in the literature [10b], however this is a modified version of the synthesis, and no crystal structure has yet been published.

$^{1}$H NMR (400 MHz, CDCl$_3$): δ = 6.90 (s, 2H, -[CC*H*C*H*S]-, $^{195}$Pt satellites: $^{3}J_{\text{H-Pt}}$ = 23.5 Hz), 1.66 (br, 24H, P(C*H*$_2$CH$_2$CH$_2$CH$_3$)$_3$), 1.52 (br m, 24H, $^{3}J_{\text{HH}}$ = 3.6 Hz, P(CH$_2$C*H*$_2$CH$_2$CH$_3$)$_3$), 1.42 (sextet, 24H, $^{3}J_{\text{HH}}$ = 7.6 Hz, P(CH$_2$CH$_2$C*H*$_2$CH$_3$)$_3$), 0.93 (t, 36H, $^{3}J_{\text{HH}}$ = 7.6 Hz, P(CH$_2$CH$_2$CH$_2$C*H*$_3$)$_3$). $^{13}$C{$^{1}$H} NMR (100 MHz, CDCl$_3$): δ = 125.1 (*C*CHCHC*S*), 114.3 (C*C*HCHCS), 26.0 (P*Bu*$_3$), 24.3 (P*Bu*$_3$), 20.3 (P*Bu*$_3$), 13.9 (P*Bu*$_3$). $^{31}$P{$^{1}$H} NMR (161.8 MHz, CDCl$_3$): δ = -6.4 (*P*Bu$_3$, $^{195}$Pt satellites: $^{1}J_{\text{P-Pt}}$ = 2649 Hz). Anal. Calcd. for C$_{52}$H$_{110}$P$_2$Cl$_2$SPt: C, 46.18; H, 8.20; S, 2.37. Found: C, 45.22; H, 8.15; S, 2.33. Mp (°C): 100 - 101 (melts).

## 2.5 Crystallographic Tables

**Table 2.5.1.** Crystallographic Data for Compounds **2** and **3**.

| | 2 | 3 | 4 |
|---|---|---|---|
| empirical formula | $C_{16}H_{16}Br_2PtS_2$ | $C_{32}H_{58}Br_2P_2PtS_2$ | $C_{34}H_{28}Br_2P_2PtS_2$ |
| fw | 627.32 | 923.75 | 917.53 |
| cryst. dimens. (mm) | $0.21 \times 0.17 \times 0.17$ | $0.57 \times 0.36 \times 0.06$ | $0.31 \times 0.25 \times 0.17$ |
| cryst. syst. | triclinic | triclinic | orthorhombic |
| space group | $P$ (No. 2) | $P$ (No. 2) | $P2_12_12_1$ |
| unit cell | | | |
| $a$ (Å) | 9.2337 (5) | 9.4079 (12) | 10.2910 (5) |
| $b$ (Å) | 9.9857 (6) | 10.2731 (13) | 17.6215 (8) |
| $c$ (Å) | 10.1881 (6) | 21.475 (3) | 17.6371 (8) |
| $\alpha$ (°) | 74.7445 (6) | 94.4793 (16) | |
| $\beta$ (°) | 68.8269 (6) | 98.2316 (16) | |
| $\gamma$ (°) | 81.1783 (6) | 109.5480 (14) | |
| V (Å$^3$) | 843.33 (8) | 1918.0 (4) | 3198.4 (3) |
| Z | 2 | 2 | 4 |
| $\rho_{calcd}$ (g cm$^{-3}$) | 2.470 | 1.600 | 1.905 |
| $\mu$ (mm$^{-1}$) | 13.29 | 5.953 | 7.140 |
| T (K) | 173(1) | 173(1) | 173(1) |
| $2\theta_{max}$ (°) | 55.14 | 53.18 | 55.00 |
| total data | 7604 | 15665 | 28422 |
| unique data ($R_{int}$) | 3862 (0.0123) | 7976 (0.0270) | 7313 (0.0326) |
| observed data a [$I > 2\sigma(I)$] | 3596 | 6326 | 6904 |
| params. | 190 | 379 | 370 |
| R$_1$ [$I > 2\sigma(I)$][a] | 0.0192 | 0.0383 | 0.0207 |
| wR$_2$ [all data][a] | 0.0505 | 0.0982 | 0.0467 |
| difference map $\Delta\rho$ (e Å$^{-3}$) | 1.216 / –0.786 | 1.309 / –1.252 | 0.922 / –1.099 |

[a] $R_1 = \Sigma||F_o| - |F_c|| / \Sigma|F_o|$; $wR_2 = [\Sigma w(F_o{}^2 - F_c{}^2)^2 / \Sigma w(F_o{}^4)]^{1/2}$

**Table 2.5.2.** Crystallographic Data for Compounds **5** and **8.**

| | 5 | 8 |
|---|---|---|
| empirical formula | $C_{35}H_{30}Br_2P_2PtS_2$ | $C_{58}H_{124}Cl_2P_4Pt_2S$ |
| fw | 931.56 | 1438.59 |
| cryst. dimens. (mm) | $0.58 \times 0.13 \times 0.08$ | $0.42 \times 0.38 \times 0.24$ |
| cryst. syst. | triclinic | monoclinic |
| space group | $P\bar{1}$ | $P2_1$ |
| unit cell | | |
| $a$ (Å) | 9.1235 (5) | 12.1410 (11) |
| $b$ (Å) | 12.9043 (8) | 45.923 (4) |
| $c$ (Å) | 15.0858 (9) | 12.6005 (11) |
| $\alpha$ (°) | 97.7213 (7) | |
| $\beta$ (°) | 104.1687 (7) | 91.5479 (14) |
| $\gamma$ (°) | 102.1434 (7) | |
| $V$ (Å³) | 1650.85 (17) | 7022.9 (11) |
| Z | 2 | 4 |
| $\rho_{calcd}$ (g cm⁻³) | 1.874 | 1.361 |
| $\mu$ (mm⁻¹) | 6.918 | 4.208 |
| T (K) | 173(1) | 173(1) |
| $2\theta_{max}$ (°) | 55.22 | 55.40 |
| total data | 14714 | 62454 |
| unique data ($R_{int}$) | 7550 (0.0261) | 32301 |
| observed data a [I > 2σ(I)] | 6835 | 30123 |
| params. | 379 | 1063 |
| $R_1$ [I > 2σ(I)]ᵃ | 0.0247 | 0.0520 |
| $wR_2$ [all data]ᵃ | 0.0593 | 0.1221 |
| difference map $\Delta\rho$ (e Å⁻³) | 1.225 / –0.860 | 2.965 / –2.053 |

ᵃ $R_1 = \Sigma ||F_o| - |F_c|| / \Sigma |F_o|$; $wR_2 = [\Sigma w(F_o{}^2 - F_c{}^2)^2 / \Sigma w(F_o{}^4)]^{1/2}$

## 2.6 References

[1] a) For a relevant review of metallopolymer chemistry: J.-C. Eloi, L. Chabanne, G. R. Whittell, I. Manners. *Materials Today* **2008,** *11*, 28. b) S. A. Sapp, C. M. Elliot, C. Contado, S. Caramori, C. A. Bignozzi. *J. Am. Chem. Soc.* **2002**, *124*, 11215. c) J. J. Nelson, T. J. Amick, C. M. Elliott. *J. Phys. Chem. C* **2008**, *112*, 18255. d) R. J. Forster, J. G. Vos. *Macromolecules* **1990**, *23*, 4372. e) S. S. H. Mao, T. D. Tilley. *Macromolecules* **1997**, 30, 5566.

[2] a) H. Tributsch. *Photochem. Photobio.* **1972**, *16*, 261. b) B. O'Regan, M. Gratzel. *Nature* **1991**, *353*, 737. c) A. Nattestad, A. J. Mozer, M. K. R., Fischer, Y.-B. Cheng, A. Mishra, P. Bauerle, U. Bach. *Nature Materials* **2010**, *9*, 31. d) F. Gao, Y. Wang, J. Zhang, D. Shi, M. Wang, R. Humphry-Baker, P. Wang, S. M. Zakeeruddin, M. Gratzel. *Chem. Commun.* **2008**, 2635. e) X. Xin, M. Scheiner, M. Ye, Z. Lin. *Langmuir* **2011**, *27*, 14594. f) P. G. Bomben, K. C. D. Robson, P. Sedach, C. P. Berlinguette. *Inorg. Chem.* **2009**, *48*, 9631. g) P. G. Bomben, T. J. Gordon, E. Schott, C. P. Berlinguette. *Angew. Chem. Int. Ed.* **2011**, *50*, 10682.

[3] B. Wardle. *Principles and Applications of Photochemistry.* John Wiley and Sons, Ltd., United Kingdom, 2009, pp. 66.

[4] A. Yella, H.-W. Lee, H. N. Tsao, C. Yi, A. K. Chandiran, Md.K. Nazeeruddin, E. W.-G. Diau, C.-Y. Yeh, S. M. Zakeeruddin, M. Gratzel. *Science* **2011**, *334*, 629.

[5] a) G. Dennler, M. C., Scharber, C. J. Brabec. *Adv. Mater.* **2009**, *21*, 1323. b) L.-M. Chen, Z. Hong, G. Li, Y. Yang. *Adv. Mater.* **2009**, *21*, 1434. c) Q. Chen, B. J. Worfolk, T. C. Hauger, U. Al-Atar, K. D. Harris, J. M. Buriak. *ACS Appl. Mater. Interfaces* **2011**, *21*, 3962. d) B. J. Worfolk, D. A. Rider, A. L. Elias, M. Thomas, K. D. Harris, J. M. Buriak. *Adv. Funct. Mater.* **2011**, *21*, 1816. e) M. Thomas, B. J. Worfolk, D. A. Rider, M. T. Taschuk, J. M. Buriak. *ACS Appl. Mater. Interfaces* **2011**, *3*, 1887.

[6] For a comprehensive historical comparison of solar cell PCEs, see: S. Price, R. Margolis. *2008 Solar Technologies Market Report: January 2010.* Technical report for National Renewable Energy

Laboratory. January 2010. NREL Report TP-6A2-46025; DOE/GO-102010-2867.

[7] a) Y. H. Kim, C. Sachse, M. L. Machala, C. May, L. Muller-Meskamp, K. Leo. *Adv. Funct. Mater.* **2011**, *21*, 1076. b) S. Pfuetzner, J. Meiss, A. Petrich, M. Riede, K. Leo. *Appl. Phys. Lett.* **2009**, *94*, 3303.

[8] a) F. Zhang, M. Johansson, M. R. Andersson, J. C. Hummelen, O. Inganäs. *Adv. Mater.* **2002**, *14*, 662. b) X. Crispin, F. Jakobsson, A. Crispin, P. Grim, P. Andersson, A. Volodin, C. Van Haesendonck, M. Van Der Auweraer, W. Salaneck, M. Berggren. *Chem. Mater.* **2006**, *18*, 4354. c) J. Huang, P. F. Miller, J. S. Wilson, A. J. de Mello, J. C. de Mello, D. D. C. Bradley. *Adv. Funct. Mater.* **2005**, *15*, 290. d) J. Ouyang, C. W. Chu, F. C. Chen, Q. Xu, Y. Yang. *Adv. Funct. Mater.* **2005**, *15* , 203. e) P. A. Levermore, L. Chen, X. Wang, R. Das, D. D. C. Bradley. *Adv. Mater.* **2007**, *19*, 2379. f) Y. H. Ha, N. Nikolov, S. K. Pollack, J. Mastrangelo, B. D. Martin, R. Shashidhar. *Adv. Funct. Mater.* **2004**, *14*, 615.

[9] For the most recent PBSC efficiency record, see the press release: S. Rhor. *Heliatek achieves new world record for organic solar cells with certified 9.8% cell efficiency.* Technical report for Heliatek organic based photovoltaics. Dresden, Germany. December 2011.

[10] a) N. Chawdhury, A. Kohler, R. Friend, M. Younus, N. Long, P. Raithby, J. Lewis. *Macromolecules* **1998**, *31*, 722. b) S. Kotani, K. Shiina, K. Sonogashira. *J. Organomet. Chem.* **1992**, *429*, 403.

[11] T. A. Clem, D. F. J. Kavulak, E. J. Westling, J. M. J. Fréchet. *Chem Mater.* **2010,** *22*, 1977.

[12] a) K. Onimura, M. Matsushima, K. Yamabuki, T. Oishi. *Polymer Journal* **2010**, *42*, 290. b) T. Yamamoto, S. Wakabayashi, K. Osakada. *J. Organomet. Chem.* **1992**, *428*, 223. c) T.-Z. Liu, Y. Chen. *Polymer 2005*, **46**, 10383. d) N. C. Yang, D. H. Suh. *Polymer* **2001**, *42*, 7987. e) J. Schmidt, M. Werner, A. Thomas. *Macromolecules* **2009**, *42*, 4426.

[13] a) M. Takahashi, K. Masui, H. Sekiguchi, N, Kobayashi, A. Mori, M. Funahashi, N. Tamaoki. *J. Am. Chem. Soc.* **2006**, *128*, 10930. b) J. Hassan, L. Lavenot, C. Gozzi, M. Lemaire. *Tetrahedron*

*Lett.* **1999**, *40*, 857.

[14] a) J.-H. Lee, H.-T. Jeon, Y.-J. Kim, K.-E. Lee, Y. O. Jang, S. W. Lee. *Eur. J. Inorg. Chem.* **2011**, 1750. b) H. Kuniyasu, T. Yoshizawa, N. Kambe. *Tetrahedron Lett.* **2010**, *51*, 6818.

[15] D. M. Norton, E. A. Mitchell, N. R. Botros, P. G. Jessop, M. C. Baird. *J. Org. Chem.* **2009**, *74*, 6674.

[16] a) R. A. Stockland, Jr., A. M. Levine, M. T. Giovine, I. A. Guzei, J. C. Cannistra. *Organometallics* **2004**, *23*, 647. b) S. Shekhar, J. F. Hartwig. *J. Am. Chem. Soc.* **2004**, *126*, 13016. c) A. Yahav-Levi, I. Goldberg, A. Vigalok. *J. Am. Chem. Soc.* **2006**, *128*, 8710.

[17] B.T. Heaton, A. Pidcock. *J. Organometal. Chem.* **1968**, *14*, 235.

[18] H. Hope, *Prog. Inorg. Chem.* **1995**, *41*, 1.

[19] R. H. Blessing. *Acta Cryst.* **1995**, *A51*, 33.

[20] Schneider, T. R., Sheldrick, G. M. *Acta Crystallogr.* **2002**, *D58*, 1772.

[21] P.T. Beurskens, G. Beurskens, R. de Gelder, J. M. M. Smits, S. Garcia-Granda, R. O. Gould. (**2008**). The *DIRDIF-2008* program system. Crystallography Laboratory, Radboud University Nijmegen, The Netherlands.

# Chapter 3

# Isolation of inorganic ethene (H$_2$BNH$_2$): en route to boron nitride

## Chapter 3

## Isolation of inorganic ethene (H$_2$BNH$_2$): en route to boron nitride

### 3.1 Introduction

Ammonia borane and amine borane derivatives have been used as chemical sources of hydrogen [1,2] and precursors for boron nitride (BN) [3]. Air stable at room temperature in the solid state, ammonia borane (AB or H$_3$N•BH$_3$) contains 19.4% hydrogen by weight [1] and was widely regarded as a highly promising hydrogen storage material. H$_3$N•BH$_3$ is considered isoelectronic, isostructural and isolobal with ethane (H$_3$C-CH$_3$), while borazine [(HBNH)$_3$] has the same relationship with its hydrocarbon counterpart, benzene. The key difference between ethane, benzene and their inorganic B-N analogues is the B-N bonds in the latter species are quite polar, allowing for a wider range of bonding through dipole interactions, and reactivity from the presence of protic and hydridic hydrogen atoms. While the parent inorganic ethene and acetylenes have been isolated at -196 ºC [4,5], they remain elusive at room temperature due to their volatility and ability to spontaneously self-polymerize. McGee and co-workers first reported the isolation of inorganic ethene (H$_2$NBH$_2$) by condensation at 4 K [4], while inorganic acetylene (HBNH) was first observed by Porter and co-workers [5], but was later characterized in detail by Andrews, et al. using matrix isolation techniques [6].

Moreover, molecular boron nitride (BN), an inorganic analogue of C$_2$, is of great interest. Ceramic boron nitride [(BN)$_x$] is a synthetic material that is isostructural with diamond in its cubic form [7] and is similarly as hard with nearly unparalleled thermal stability, making it ideal for mechanical and electronic applications such as heat sinks and electronic insulators [8]. Current synthetic methods for boron nitride require reaction temperatures of >1500 ºC and pressures up to 5 GPa, and often require very specialized equipment [9,10]; in rare circumstances, lower temperature methods have been used [11]. Therefore, it would be of great value to synthesize chemical precursors that may aid in the synthesis of boron nitride under mild reaction conditions (e.g., < 200

°C). The parent inorganic ethene, $H_2BNH_2$, is a suitable precursor to molecular BN, by removal of two equivalents of $H_2$. The work presented herein describes the trapping of the parent inorganic ethene using a donor-acceptor approach, and our attempts to convert these adducts into a complex of BN via dehydrogenation chemistry (Scheme 3.1.1).
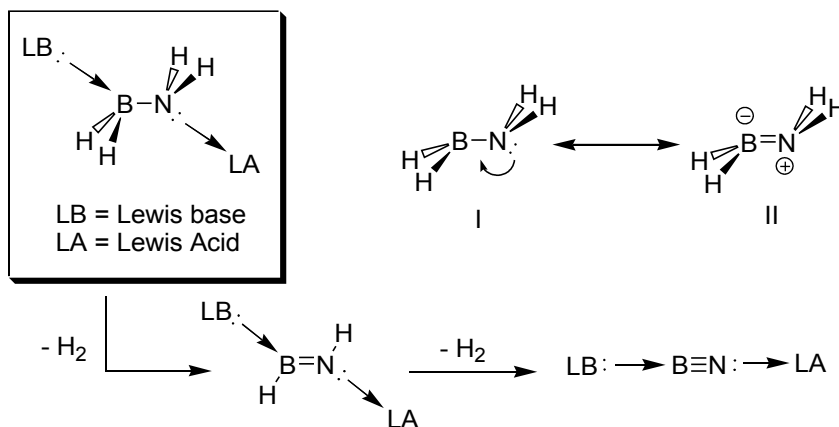


**Scheme 3.1.1**: Dehydrogenation of $H_2BNH_2$, the canonical resonance forms (**I** and **II**) are shown.

Research in our group has focused on the trapping of unstable or reactive closed-shell molecules or molecular fragments using a donor-acceptor stabilization protocol. Previously, we have reported the isolation of adducts of molecular $GeH_2$ [12,13], $SnH_2$ [13], and $SiH_2$ [14], as well the mixed heavy group 14 element ethylene congeners $H_2Ge=SiH_2$ and $H_2Sn=SiH_2$ [15]. In theory, this general donor-acceptor approach could be used to access a stable complex of BN, given the anticipated Lewis acidic and basic properties of the B and N atoms, respectively. The goal of this work was to initially isolate inorganic ethene ($H_2N-BH_2$) in the form of a donor-acceptor adduct at room temperature, and then induce two successive hydrogen elimination events to produce a stable adduct of coordinated BN (Scheme 3.1.1). In this work an inorganic analogue of ethene was successfully isolated using our donor-acceptor method, and preliminary dehydrocoupling chemistry has been investigated.

**3.2 Results and Discussion**

One of the key issues with synthesizing $H_2BNH_2$ is that it readily oligomerizes to form cycloborazanes $(H_2BNH_2)_n$ (n = 2 - 5) [16]. $H_2BNH_2$ was first trapped cryochemically by pyrolysis of borazine with subsequent trapping of the products at 4 K. It was reported that $H_2NBH_2$ began to polymerize at temperatures as low as -155 ºC [4]. Our method for trapping $H_2BNH_2$ allows for the formation of a room temperature, stable bottleable compound whereby the reactivity and bonding characteristics of the coordinated $H_2BNH_2$ unit can be examined more readily (Scheme 3.2.1). The synthetic pathway described herein makes use of the nucleophilic olefin $IPrCH_2$ ($IPrCH_2$ = $(HCNDipp)_2C=CH_2$; Dipp = $2,6-iPr_2C_6H_3$) which has been shown previously to act as a Lewis base, in similar fashion as N-heterocyclic carbenes (NHCs) like IPr [IPr = $(HCNDipp)_2C$:] [17]. Stable adducts of $H_2BNH_2$ were isolated via the ring-opening of cyclic aminodiboranes by strong nucleophilic electron donors. The cyclic μ-aminodiborane ($H_2NB_2H_5$, **1**) was generated *in-situ* by reaction of anhydrous ammonia borane ($H_3N•BH_3$) and $H_3B•THF$ for 72 hours in a 5:1 hexanes:THF solvent mixture. Addition of $IPrCH_2$ to a solution of **1** caused the adduct $IPrCH_2•H_2BNH_2•BH_3$ (**2**) to precipitate from solution as a white powder in a moderate isolated yield of 64%. The formation of the product was confirmed by NMR ($^1H$, $^{11}B$, $^1H\{^{11}B\}$, GCOSY) and IR spectroscopy.
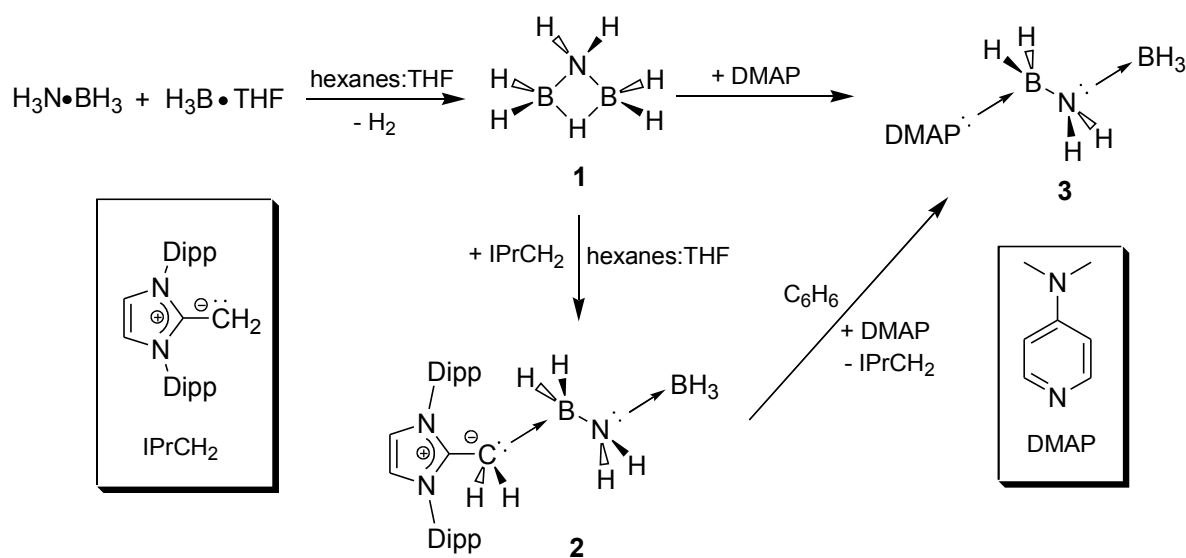
**Scheme 3.2.1**: Synthesis of $H_2BNH_2$ bis-adducts **2** and **3**.

The presence of $IPrCH_2$ in the adduct was confirmed by $^1H$ NMR, while a triplet and a quartet resonance were observed in the proton-coupled $^{11}B$ NMR spectrum (triplet, $\delta = -14.7$, $^1J_{B-H} = 94.5$ Hz; quartet, $\delta = -21.9$, $^1J_{B-H} = 86.9$ Hz), which could be assigned to the internal $-BH_2-$ and terminal $-BH_3$ groups respectively (by $^1H\{^{11}B\}$ NMR decoupled at the $^{11}B$ resonances $-14.7$ and $-21.9$ ppm). Linkage of the nucleophilic $-CH_2$ group of $IPrCH_2$ to the $-BH_2-$ unit of the inorganic chain was proven by $^1H\{^{11}B\}$ aoGCOSY NMR. The resonance corresponding to boron-bound hydrogen atoms of the $-BH_2-$ at 1.40 ppm showed off-diagonal coupling to the resonance at 1.88 ppm belonging to the terminal $-CH_2$ group of the nucleophilic olefin. The resonance corresponding to the central $-NH_2-$ unit could not be identified due to coincidence with the doublets corresponding to an isopropyl group on the $IPrCH_2$ donor, however an N-H stretching band at 3340 cm$^{-1}$ could be located by IR spectroscopy. The adduct demonstrated indefinite stability in the solid state under $N_2$, and was stable in non-polar solvents up to 100 °C (benzene, toluene). Limited stability of **2** was noted in chlorinated solvents (dichloromethane, 1,2-dichloroethane, chloroform), however this species rapidly decomposed in THF (decomposition half-life of 24 hours). The decomposition product showed a resolved pentet in the $^{11}B$ NMR spectrum ($\delta = -40.6$ ppm, $^1J_{B-H} = 81.3$ Hz)

corresponding to a $BH_4^-$ anion, and a highly shifted downfield singlet at 8.18 ppm in the $^1H$ NMR spectrum ($CDCl_3$) corresponding to the unsaturated backbone of the [$IPrCH_3^+$] cation [18]. $IPrCH_2•H_2BNH_2•BH_3$ could not be crystallized in a form suitable for X-ray crystallography using arene or ethereal solvents (THF, hexanes, ether or toluene) and crystals of **2** grown from saturated $CH_2Cl_2$ and $ClCH_2CH_2Cl$ solutions exhibited significant twinning, thus preventing the terminal B atom of the inorganic chain, $-BH_2NH_2BH_3$, from being refined anisotropically.

It was found that very specific σ-donors were required to prepare adducts of the general form $LB•H_2BNH_2•BH_3$ (LB = Lewis base) from the ring opening of **1**. For example, the addition of the N-heterocyclic carbene, IPr, resulted in the formation of the adduct $IPr-BH_3$ [19] (64%, δ = -35 ppm, quartet in $^{11}B$ NMR, $^1J_{B-H}$ = 86.3 Hz), and an unknown product (36%, δ = -17.5 ppm, br s in $^{11}B$ NMR). Similarly, when the strong σ-donor tricyclohexylphosphine ($PCy_3$) was added to 1, the known phosphine-borane adduct, $Cy_3P-BH_3$ was formed in a 90% yield (by integration of peaks, δ = 22.9 ppm, 1:1:1:1 quartet by $^{31}P\{^1H\}$ NMR, $^1J_{P-B}$ = 64 Hz; doublet by $^{11}B\{^1H\}$ NMR: -46.3 ppm, $^1J_{B-P}$ = 63 Hz), with 10% of an unknown product, tentatively assigned to $Cy_3P•H_2BNH_2•BH_3$ [$^{11}B$ NMR: δ = -25.0 (br) and -21.5 (q, $^1J_{B-P}$ =111 Hz); $^{31}P\{^1H\}$ NMR: 6.9 ppm, (br)].

In order to investigate if the terminal $BH_3$ unit in the amino-borane adducts $LB•H_2BNH_2•BH_3$, could be displaced by other Lewis acids, $IPrCH_2•H_2BNH_2•BH_3$ was reacted with one equivalent of $B(C_6F_5)_3$ in a 10:1 toluene:THF mixture, with the hope that the terminal $BH_3$ group would be exchanged by the stronger Lewis acid $B(C_6F_5)_3$, to form $IPrCH_2•H_2BNH_2•B(C_6F_5)_3$. The reaction was monitored *in situ* for 3 hours. The presence of the methylimidazolium [$IPrCH_3^+$] cation was confirmed by $^{13}C\{^1H\}$ NMR, however the diagnostic unsaturated backbone protons of the imidazolium ring could not be identified due to the presence of numerous peaks from aryl resonances, where the backbone resonance should also appear. A doublet was present in the $^{11}B$ NMR spectrum (d, δ = -25.4 ppm, $^1J_{B-H}$ = 93.3 Hz) with accompanying $^{19}F$ NMR resonances that were in agreement with the literature values for the $HB(C_6F_5)_3^-$ anion [18]. These data suggest the

formation of [IPrCH$_3^+$][HB(C$_6$F$_5$)$_3^-$] as the major soluble product. A second unidentified product in

the $^{11}$B spectrum was located at -19 ppm as a broad singlet (10%). The borane adduct, H$_3$B•THF

was identified in the $^{11}$B spectrum (10%), implying this reaction involves intial displacement of the

terminal BH$_3$ with B(C$_6$F$_5$)$_3$, or competitive exchange of the two boranes. This is followed by

migration of H$^-$ to B(C$_6$F$_5$)$_3$ to form [HB(C$_6$F$_5$)$_3^-$] and H$^+$ transfer to IPrCH$_2$ to form [IPrCH$_3^+$],

extruding HNBH in the process (Scheme 3.2.2). This mechanism is similar to that proposed for the

decomposition of IPrCH$_2$•H$_2$BNH$_2$•BH$_3$ to [IPrCH$_3^+$][BH$_4^-$], where a concerted hyrdride / proton

shift occurs. A possible alternative decomposition route involves decomposition of **2** into [IPrCH$_3^+$]

[BH$_4^-$], followed by a hydride shift from [BH$_4^-$] to B(C$_6$F$_5$)$_3$, forming [HB(C$_6$F$_5$)$_3^-$]. The exact route

of decomposition is currently unknown. The chemical fate of any extruded HBNH is unknown, and

is a current area of investigation in our group. Due to the limited solubility of **2** in most organic

solvents, and its tendency to decompose in THF, attempts to dehydrogenate the H$_2$NBH$_2$ unit were

unsuccessful. Support for a proton transfer step occuring during decomposition comes from the

observed tendency of these nucleophilic olefins and carbenes to react readily with acidic protons to

form imidazolium salts [18d].
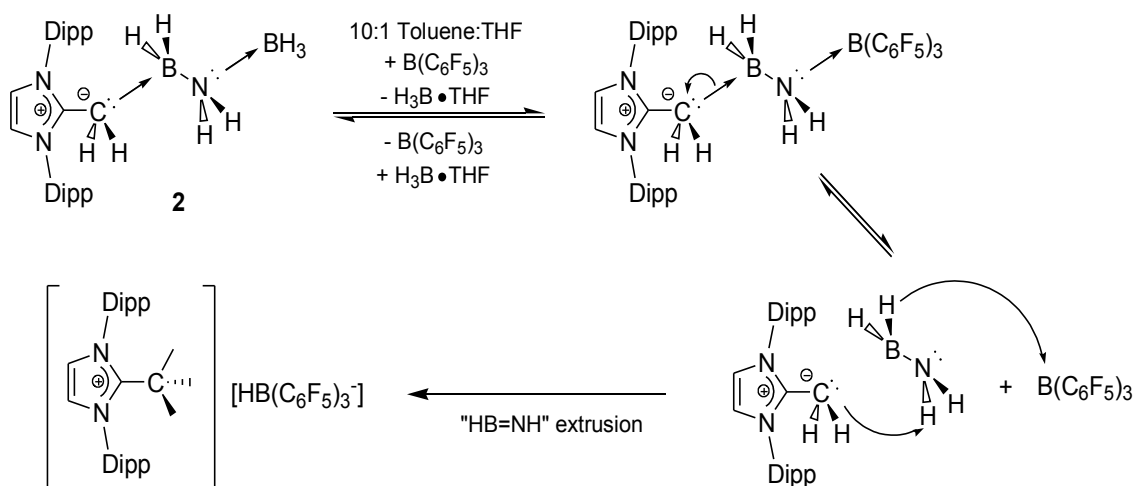


**Scheme 3.2.2**: Proposed proton-hydride shift leading to the decomposition of **2** into [IPrCH$_3^+$][HB(C$_6$F$_5$)$_3^-$].

In an attempt to avoid the decomposition path outlined in Scheme 3.2.2, p-dimethylaminopyridine (DMAP) was chosen to replace IPrCH$_2$ as a neutral Lewis base. We repeated the abovementioned synthetic procedure using DMAP in place of IPrCH$_2$ to yield the desired adduct, DMAP•H$_2$BNH$_2$•BH$_3$ (3) as a white solid in a high isolated yield of 75%. The structure of DMAP•H$_2$BNH$_2$•BH$_3$ (3) is presented in Figure 3.2.1, and has the expected geometry proposed in Scheme 3.1.1.
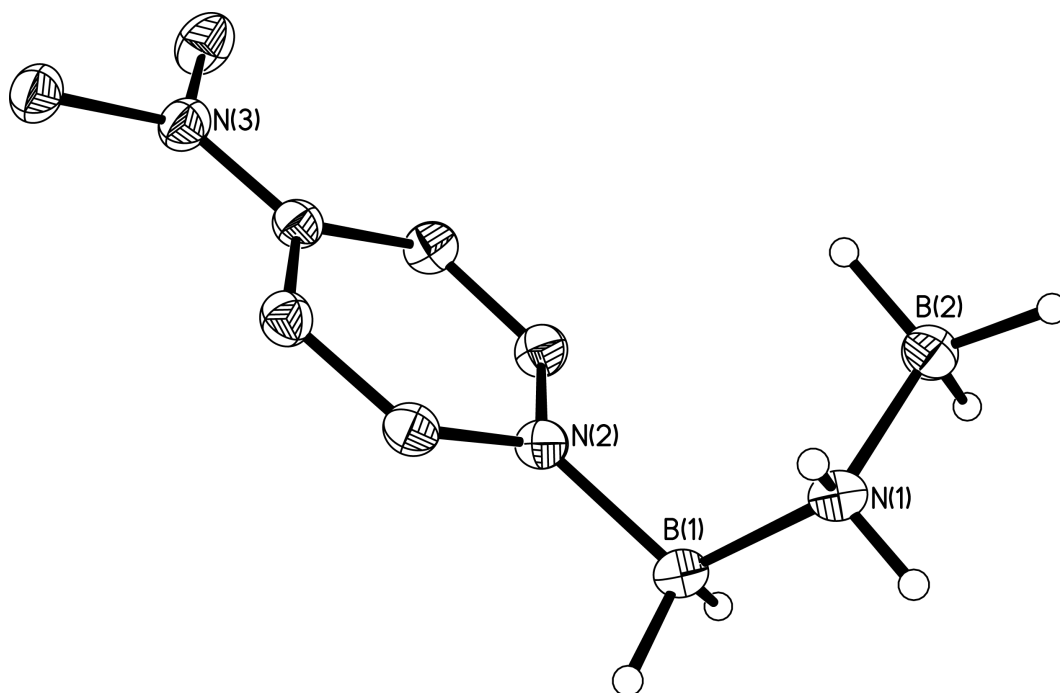


**Figure 3.2.1**: Thermal ellipsoid plot (30 % probability) of DMAP•H$_2$BNH$_2$•BH$_3$ (3), with carbon-bound hydrogen atoms and hexane solvate molecules have been omitted for clarity. The hydrogen atoms bound boron and nitrogen were located from the electron difference map. Selected bond lengths [Å] and angles [°]: B(1)-H 1.109(13) and 1.125(13), B(2)-H 1.102(15), 1.145(14) and 1.147(17), N(2)-B(1) 1.5728(15), B(1)-N(1) 1.5720(17), N(1)-B(2) 1.5939(16), N(2)-B(1)-N(1) 110.44(9), B(1)-N(1)-B(2) 118.68(9), N(2)-B(1)-N(1)-B(2) torsion angle 65.71(13).

The N$_{DMAP}$-BH$_2$-NH$_2$-BH$_3$ array rests in a gauche conformation about the B-N bond vector similar to that of H$_3$N•BH$_3$ [20], with an N$_{DMAP}$-B-N-B torsional angle of 65.71(13)°. The central H$_2$B-NH$_2$ bond distance was 1.5720(17) Å, which was the same within experimental error as the B-N bond of 1.58(2) Å in H$_3$N•BH$_3$ found by Crabtree and co-workers [20]. The B-N bond length

involving the terminally bound $BH_3$ group in **3** was 1.5939(16) Å, which is of similar value as in

Shore's inorganic butane analogue, $H_3NBH_2NH_2BH_3$, which had terminal B-N bond lengths of

1.600 and 1.588 Å [21]. The $^{11}B$ NMR spectrum conclusively proved the presence of $-BH_2-$ and

$-BH_3$ groups in **3** (triplet, $\delta$ = -3.7, $^1J_{B-H}$ = 99.5 Hz; quartet, $\delta$ = -21.8 ppm, $^1J_{B-H}$ = 91.9 Hz). Due to

the low number of resonances in the $^1H$ NMR spectrum of **3**, the central $-NH_2-$ unit was located in

the form of a broad singlet at 2.19 ppm. By doing selectively decoupled $^1H\{^{11}B\}$ NMR experiments,

the $BH_2$ and $BH_3$ were also assigned in the $^1H$ NMR spectrum. Tthe 3-bond coupling of the terminal

$-BH_3$ to the adjacent $-NH_2-$ was located as a triplet at 1.26 ppm ($^3J_{B-H}$ = 4.4 Hz), when decoupling

was carried out at the resonant $^{11}B$ frequency for the terminal $BH_3$ unit.
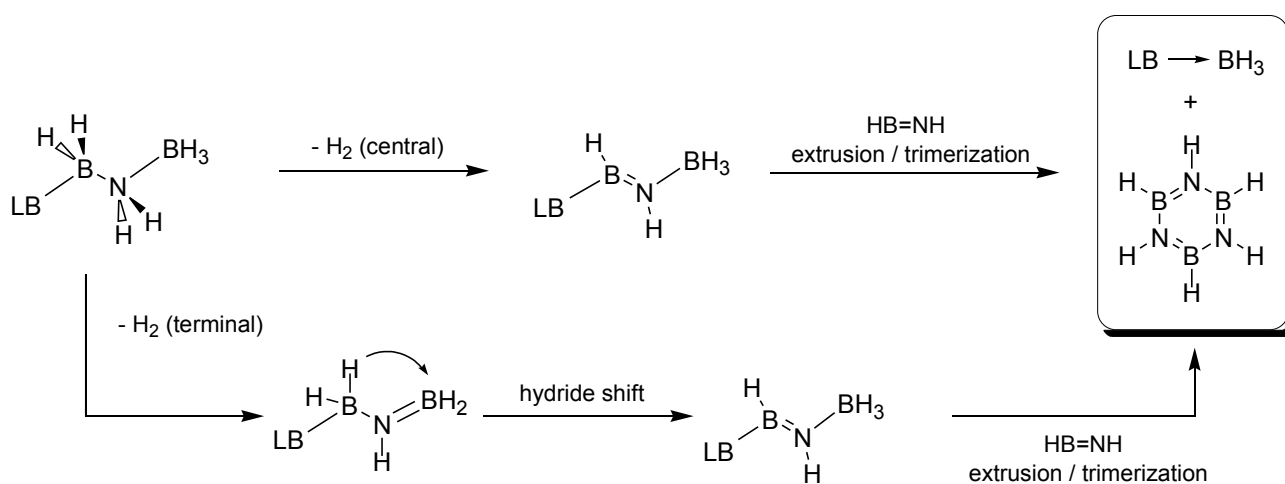


**Scheme 3.2.3**: Possible dehydrogenation reaction pathways for $H_2BNH_2$ adducts.

Of great intrest was the fact that the DMAP adduct (**3**) was completely stable at room

temperature in THF and chlorinated solvents. The thermal stability of **3** is significantly different

then that of $IPrCH_2•H_2BNH_2•BH_3$ (**2**), showing decomposition in refluxing $C_6D_6$ to form the known

adduct, DMAP-$BH_3$ ($^{11}B$ NMR: q, $\delta$ = -13.9 ppm, $^1J_{B-H}$ = 92.7 Hz) and borazine $(HBNH)_3$ ($^{11}B$

NMR: d, $\delta$ = 30.6 ppm, $^1J_{B-H}$ = 141.1 Hz) [22], implying thermal dehydrogenation had transpired,

followed by extrusion of HBNH and subsequent trimerization. By comparison, **2** was completely

stable in refluxing $C_6D_6$. No evidence for the formation of $[DMAPH^+][BH_4^-]$ was observed. It is

unkown if dehydrogenation of **3** occurs at the central $H_2BNH_2$ or terminal $H_2NBH_3$ units, thus two reaction pathways are again possible (Scheme 3.2.3). In order to displace $BH_3$ with a Lewis acid that could not undergo dehydrogenation, thus promoting the $H_2$ loss exclusively from the central $H_2BNH_2$ unit, compound **3** was reacted with $B(C_6F_5)_3$. When the two compounds were combined in toluene an intractable mixture of unknown products was obtained, as a complicated series of resonances were observed in both ^{11}B and ^{19}F NMR spectra. These results demonstrate that the B-H and N-H bonds of the adduct are quite reactive, so we decided to synthesize the N-methylated analogue ($DMAP•H_2BNMe_2•BH_3$) to supress the possible hydrogen elimination chemistry, and encourage the formation of the Lewis acid-exchanged product $DMAP•H_2BNMe_2•B(C_6F_5)_3$.

Synthesis of the adduct $DMAP•H_2BNMe_2•BH_3$ (**5**) was achieved through a similar ring-opening pathway as used to prepare the $H_2BNH_2$ adducts, but starting from the μ-dimethylaminodiborane (**4**). Compound **4** was prepared in 40% yield by the reaction of $Me_2NH•BH_3$ with one equivalent of $BH_3•THF$ after 3 days of heating at 60 °C. In order to facilitate the dehydrocoupling step of the reaction, $[Rh(COD)Cl]_2$ was used as a catalyst to first convert $Me_2NH•BH_3$ into the known dimer $[Me_2NBH_2]_2$ (^{11}B NMR: triplet, $\delta = 4.75$ ppm, $^1J_{B-H} = 112.8$ Hz) [23]. The *in situ* generated dimer $[Me_2NBH_2]_2$ was then reacted with one equivalent of $H_3B•THF$ at 60 °C for 8 hours to generate $NMe_2B_2H_5$ (**4**) in quantitative yield (Scheme 3.2.4). Addition of one equivalent of DMAP to **4** causes ring-opening and precipitation of the desired linear adduct, $DMAP•H_2BNMe_2•BH_3$ (**5**), as a pale yellow solid in 63 % yield. Using the same methodology, stable adducts involving $IPrCH_2$ and IPr donors were also prepared ($IPrCH_2•H_2BNMe_2•BH_3$ (**6**) and $IPr•H_2BNMe_2•BH_3$ (**7**)). The structures of adducts **5** - **7** are shown in Figures 3.2.2 - 3.2.4. The central $H_2BNMe_2$ units in **5** - **7** bear structural similarity to the parent $H_2BNH_2$ adduct **3**, with the L-$BH_2$-$NMe_2$-$BH_3$ chain resting in the gauche conformations for L = DMAP and $IPrCH_2$ (e.g. the $C_{IPrCH2}$-B-N-$B_{terminal}$ torsion angle was 51.3(6)°), while an anti-conformation was found within the IPr adduct (**7**) [$C_{IPr}$-B-N-$B_{terminal}$ torsion angle = 178.38(12)°]. This difference may in part be due to the

increased steric bulk of the IPr, relative to the IPrCH$_2$ and DMAP donors, which cause the H$_2$BNMe$_2$BH$_3$ chain to take on an alternate low energy conformation. In the case with IPrCH$_2$, the olefinic CH$_2$ carbon creates enough distance between -NMe$_2$- and the bulk of the ligand such that the gauche conformation is favoured. Due to the fact that the parent inorganic ethene could not be isolated with IPr using this method, our focus shifted solely to the IPrCH$_2$ and DMAP adducts of both the parent H$_2$BNH$_2$ and H$_2$BNMe$_2$, in order to form a basis for reasonable comparison.
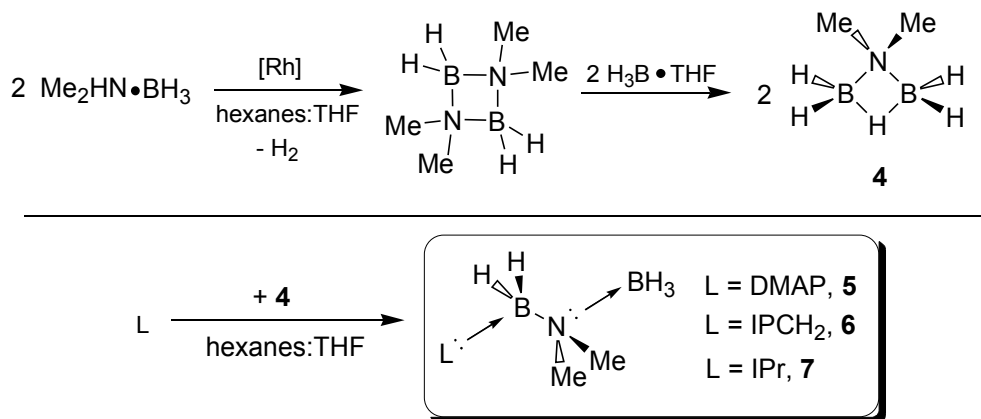


**Scheme 3.2.4**: Synthesis of μ-dimethylaminodiborane (**4**) and the H$_2$BNMe$_2$ adducts **5** - **7**.
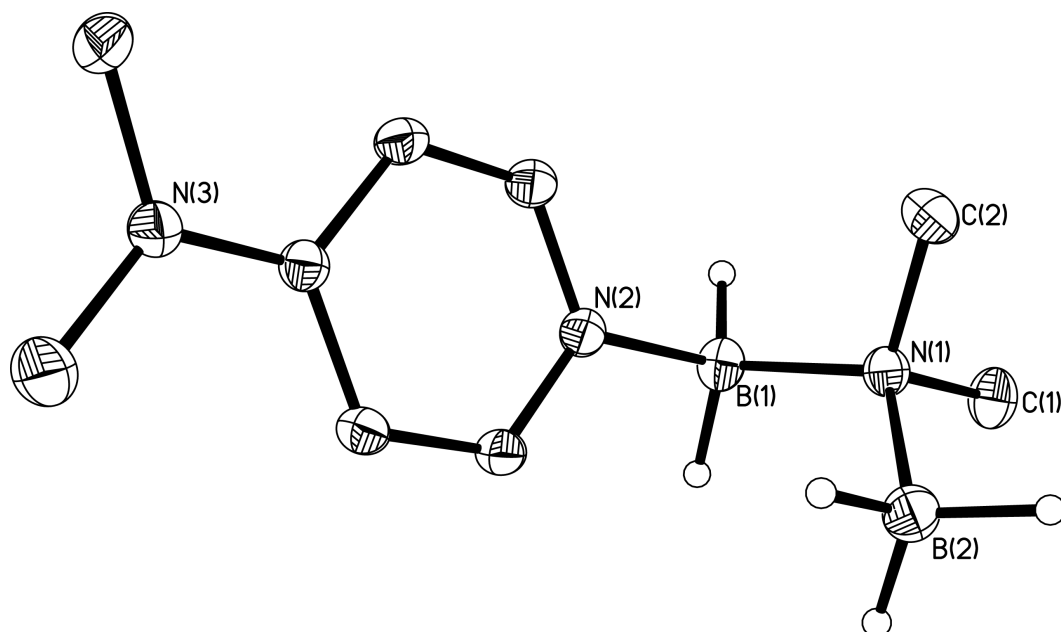
**Figure 3.2.2**: Thermal ellipsoid plot (30 % probability) of DMAP•H$_2$BNMe$_2$•BH$_3$ (**5**), with carbon-bound hydrogen atoms and dichloroethane solvate removed for clarity. The boron bound hydrogen atoms were located from the electron difference map. Selected bond lengths [Å] and angles [°]: B(1)-H 1.115(14) and 1.104(15), B(2)-H 1.130(15), 1.130(16), and 1.126(18), N(2)-B(1) 1.5722(19), B(1)-N(1) 1.5801(18), N(1)-C(1) 1.4835(16), N(1)-C(2) 1.4800(17), N(1)-B(2) 1.6020(19), N(2)-B(1)-N(1) 111.32(11), B(1)-N(1)-B(2) 114.53(11), N(2)-B(1)-N(1)-B(2) torsion angle 60.99(15).
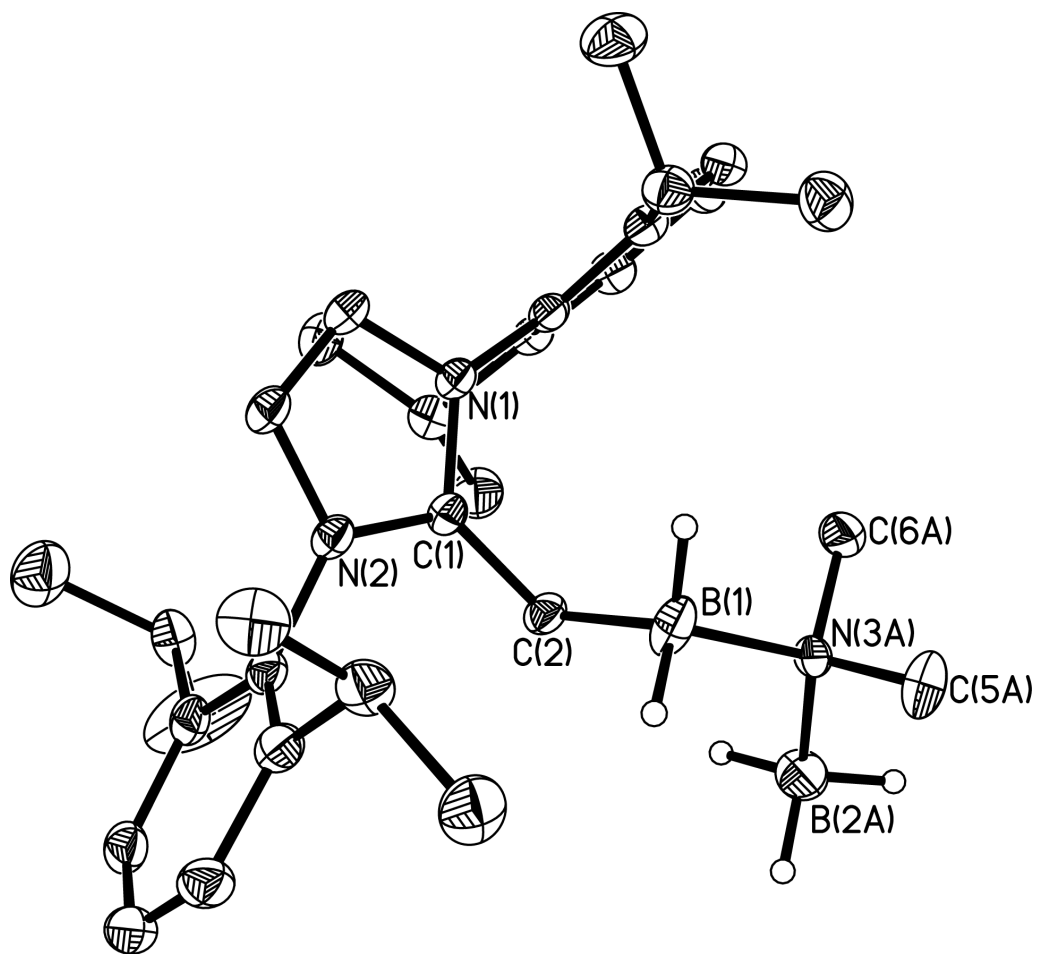
**Figure 3.2.3:** Thermal ellipsoid plot (30 % probability) of IPrCH$_2$•H$_2$BNMe$_2$•BH$_3$ (**6**), with carbon-bound hydrogen atoms omitted for clarity. The boron bound hydrogen atoms were located from the electron difference map. Selected bond lengths [Å] and angles [º]: C(2)-B(1) 1.660(3), B(1)-N(3A) 1.659(9), N(3A)-C(5A) 1.462(16), N(3A)-C(6A) 1.469(8), N(3A)-B(2A) 1.595(12), C(2)-B(1)-N(3A) 107.9(4), B(1)-N(3A)-B(2A) 116.3(7), C(2)-B(1)-N(3A)-B(2A) torsion angle 51.3(6).
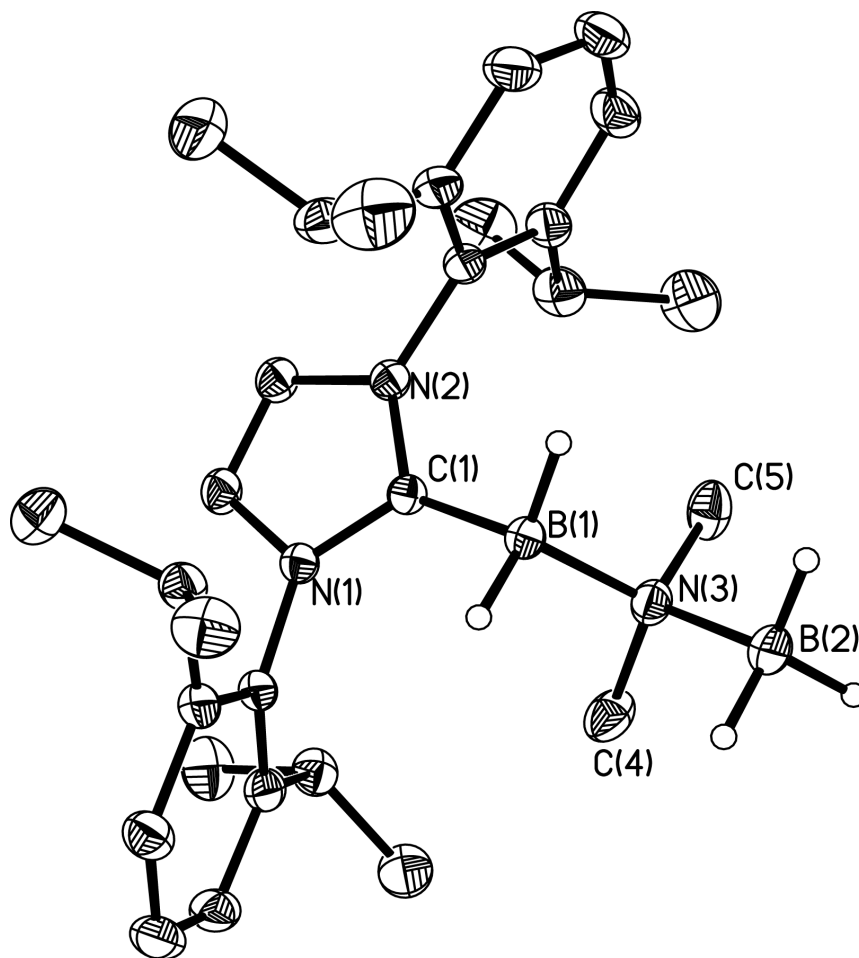
**Figure 3.2.4**: Thermal ellipsoid plot (30 % probability) of IPr•H$_2$BNMe$_2$•BH$_3$ (**7**), with carbon-bound hydrogen atoms omitted for clarity. The boron bound hydrogen atoms were located from the electron difference map. Selected bond lengths [Å] and angles [º]: B(1)-H 1.146(18) and 1.130(18), B(2)-H 1.12(2), 1.16(2), and 1.16(2), C(1)-B(1) 1.639(2), B(1)-N(3) 1.588(2), N(3)-C(4) 1.477(2), N(3)-C(5) 1.475(2), N(3)-B(2) 1.617(2), C(1)-B(1)-N(3) 114.39(12), B(1)-N(3)-B(2) 110.63(13), C(1)-B(1)-N(3)-B(2) torsion angle 178.38(12).

DMAP•H$_2$BNMe$_2$•BH$_3$ (**5**) and IPrCH$_2$•H$_2$BNMe$_2$•BH$_3$ (**6**) exhibited H$_2$B-NMe$_2$ bond lengths of 1.5801(18) Å and 1.659(9) Å, respectively. The terminal Me$_2$*N-B*H$_3$ [1.6020(19) Å] and H$_2$*N-BH$_3$ [1.5939(16) Å] bond lengths in **5** and **3** respectively, were the same within experimental error. While it was not evident from the structural comparison of **5** and **6**, it was confirmed that DMAP is a stronger Lewis base than IPrCH$_2$. This was confirmed by reacting one equivalent of DMAP with **2** and **6** to quantitatively yield **3** and **5**, with free IPrCH$_2$ (Scheme 3.2.5). The $^{11}$B NMR spectrum for the reaction of DMAP•H$_2$BNMe$_2$•BH$_3$ (**5**) with B(C$_6$F$_5$)$_3$ exhibited two doublets (-16.9 ppm, $^1J_{\text{B-H}} =$

166 Hz; -24.8 ppm, $^1J_{B\text{-}H}$ = 88 Hz) and a quartet (-14.7 ppm, $^1J_{B\text{-}H}$ = 142 Hz) with equal integration. The $^1$H NMR spectrum showed only one major unidentified DMAP environment (65%). These data when taken with the tendancy of B(C$_6$F$_5$)$_3$ to abstract a hydride from **2**, suggest the possible formation of [DMAP•HBNMe$_2$•BH$_3$$^+$][H(BC$_6$F$_5$)$_3$$^-$]. Investigation of the interaction of strong Lewis acids like B(C$_6$F$_5$)$_3$ with H$_2$BNR$_2$ adducts is an area of ongoing investigation in our group.



R = H, **2**
R = Me, **6**

R = H, **3**
R = Me, **5**
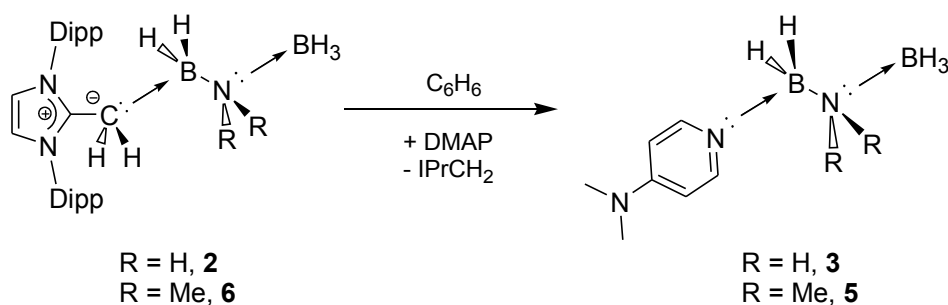
**Scheme 3.2.5**: Displacement of IPrCH$_2$ with DMAP to form **3** and **5**.

Theoretical studies (B3LYP / cc-pVDZ) were performed on DMAP•H$_2$BNH$_2$•BH$_3$, DMAP•H$_2$BNMe$_2$•BH$_3$, and the structurally truncated complexes ImMe$_2$CH$_2$•H$_2$BNH$_2$•BH$_3$ and ImMe$_2$CH$_2$•H$_2$BNMe$_2$•BH$_3$ [ImMe$_2$CH$_2$ = (HCNMe)$_2$C=CH$_2$]. All of the DFT calculations demonstrated polar and dative bonds for the donor-BH$_2$ (C$_{IPrCH2}$$^{\delta\text{-}}$-B$^{\delta+}$; N$_{DMAP}$$^{\delta\text{-}}$-B$^{\delta+}$) and internal and terminal B-N bonds (H$_2$N$^{\delta\text{-}}$-B$^{\delta+}$H$_3$; Me$_2$N$^{\delta\text{-}}$-B$^{\delta+}$H$_3$), confirming the validity of the bonding models for the adducts described herein; furthermore there was reasonable agreement between the X-ray structural data and the calculated bond lengths and angles (see Table 3.6.1). In a comparitive study using DMAP as the donor, the difference in bond interaction between the structurally similar parent H$_2$BNH$_2$ and H$_2$BNMe$_2$ was evident. The Wiberg bond index for H$_2$B-NH$_2$ in **3** (0.69) was slightly higher then that of H$_2$B-NMe$_2$ in **5** (0.61). It was observed based on the calculated bond indices that the DMAP interaction strength with BH$_2$ was effectively the same for H$_2$B-NH$_2$ (0.603) and H$_2$B-NMe$_2$ (0.605). The terminal NH$_2$-BH$_3$ interaction was found to be slightly greater in **3** (0.63) then that of NMe$_2$-BH$_3$ in **5** (0.57). This result can be rationalized by realizing that the pendant methyl

97

groups create a sterically encumbered site, slightly hindering the Me$_2$N: from approaching the BH$_3$ to achieve optimal orbital overlap, despite being more electron rich. Studies using ImMe$_2$CH$_2$ as a donor yielded similar results. The bond order based on Wiberg index of C$_{ImMe2CH2}$-B$_{NH2}$ (0.714) and C$_{ImMe2CH2}$-B$_{NMe2}$ (0.720) were approximtely the same, and the terminal N-BH$_3$ linkage was slightly weaker in ImMe$_2$CH$_2$•H$_2$BNMe$_2$•BH$_3$ (0.55) compared to ImMe$_2$CH$_2$•H$_2$BNH$_2$•BH$_3$ (0.60). Molecular orbital calculations showed the expected configuration for the BH$_2$-NH$_2$-BH$_3$ chains (and the methylated analogues), showing p-p overlap as the dominant bonding interaction (see Figures 3.6.1 - 3.6.4 for selected MOs). For ImMe$_2$CH$_2$•H$_2$BNH$_2$•BH$_3$ and DMAP•H$_2$BNH$_2$•BH$_3$, there existed a bonding interaction (HOMO-18 in Figure 3.6.1 and HOMO-19 in Figure 3.6.2) between the B-N-B atoms, where p-character orbitals on B-H and N-H bonds formed a π-symmetry bonding interaction across all 3 atoms. This positive overlap may contribute to the overall reason for why the gauche conformer is the dominant geometry, as opposed to anti, as intramolecular B-H•••H-N interactions are maximized.

Many dehydrocoupling reactions were performed on the H$_2$BNH$_2$ adducts described herein. It has been well established in the literature that Rh(I) complexes are very effective at inducing rapid dehydrocoupling of amine boranes [23]. The reaction of IPrCH$_2$•H$_2$BNH$_2$•BH$_3$ (**2**) with catalytic [Rh(COD)Cl]$_2$ in toluene yielded two major products by *in-situ* ^{11}B NMR spectroscopy; a doublet was present at 31 ppm ([1]$J_{B-H}$ = 141 Hz) corresponding to the formation of borazine (80%), and a broad singlet was seen at 18.9 ppm which was not identified (20%). The presence of borazine implied that loss of H$_2$ from H$_2$BNH$_2$ occured to yield HBNH followed by extrusion and trimerization to form borazine. In contrast to this, when DMAP•H$_2$BNH$_2$•BH$_3$ was reacted with catalytic [Rh(COD)Cl]$_2$ in THF, no reaction was evident by either *in-situ* ^{11}B or ^{1}H NMR, however an intractable black powder was present, typically attributed to precipitated Rh metal. The mother liqour of the reaction was decanted and dried under vaccum to recover 71% of initial DMAP•H$_2$BNH$_2$•BH$_3$ used; due to lack in solubility of the precipitate in any organic solvent, it is

unknown what, if any, new products remained in the insoluble precipitate. When taken with the lack of knowledge of the side products of the reaction, these results provide a challenge for understanding what, if any, dehydrocoupling events are taking place. This necessitated the need to seek other methods of dehydrogenating $H_2BNH_2$ adducts.

Recently Liu and co-workers reported that transition metal halides (MX and $MX_2$, M = Fe, Ni, Co, Cu; X = F, Cl, Br, and I) can catalytically dehydrocouple amine-boranes of the form $RH_2B \cdot NH_2R$ (R = alkyl) [24]. We therefore explored if similar transition metal halides could induce $H_2$ elimination from $DMAP \cdot H_2BNH_2 \cdot BH_3$ (**3**). When **3** was reacted with catalytic quantities of $NiBr_2 \cdot DME$ (DME = 1,2-dimethoxyethane) in THF, $^{11}B$ NMR spectroscopy showed that the reaction produced $DMAP-BH_3$ [25] and borazine in approximately 1:1 ratio. When CuBr was used instead, the starting material was consumed entirely, yielding $DMAP-BH_3$ and borazine in a 1:1 ratio (by $^{11}B$ NMR; an unidentified broad singlet at 5.5 ppm was observed in 5% yield by integration). Both pure CuBr and the adduct $CuBr \cdot SMe_2$ were tested as dehydrogenation catalysts, and both yielded near quantitative conversion of **3** to $DMAP-BH_3$ and borazine. This result, when taken with the results from the reaction of **2** with $[Rh(COD)Cl]_2$, imply that indeed our complexes of $H_2BNH_2$ are undergoing one dehydrocoupling event, followed by extrusion of the newly formed inorganic ethyne (HBNH) and trimerization to form borazine. The free DMAP and $BH_3$ subsequently coordinate to each other forming the air- and moisture-stable $DMAP-BH_3$ adduct. This result is promising as it provides and alternate synthetic route to borazine; it has been shown previously that borazine can be utilized as a precursor for the low-pressure synthesis of boron nitride [26], however it is difficult to synthesize pure borazine using existing methods [22]. The elimination of HBNH from the adduct (scheme 3.2.6) was likely due to the increased s-character of the resulting $sp^2$ bonding orbitals on N within the putative adduct $DMAP \cdot HB=NH \cdot BH_3$. This would cause a reduction in the σ-donating capability of the lone pair, resulting in a weaker donor-acceptor interaction involving $BH_3$. Therefore, a synthetic route for placing stronger Lewis acids at the

molecular terminus will be required to stabilize HBNH in the form of a donor-acceptor adduct.
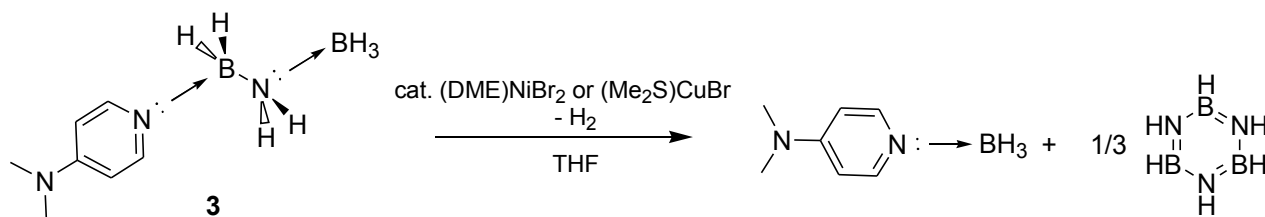


**Scheme 3.2.6**: Dehydrogenation of **3** with (DME)NiBr$_2$ and (Me$_2$S)CuBr. DME = 1,2 - dimethoxyethane.

We then attempted to add steric bulk the H$_2$BNH$_2$ centre, by synthesizing DMAP•H$_2$BNH$t$Bu•BH$_3$ (**9**). It was hypothesized that the $t$Bu group would increase the electron density on nitrogen via inductive effects making it a stronger donor and the larger size of the substituent would prevent oligomerization, allowing for the isolation of HBN$t$Bu in the form of a stable donor-acceptor adduct. Compound **9** was synthesized by ring-opening of $t$BuNHB$_2$H$_5$ (**8**) with DMAP (Scheme 3.2.7). Reacting one equivalent of $t$BuH$_2$N•BH$_3$ with H$_3$B•THF in 5:1 hexanes:THF at room temperature for three days yielded $t$BuNHB$_2$H$_5$ (**8**), which was confirmed by in situ $^{11}$B NMR spectroscopy (t of d, $^1J_{BH}$ = 30 Hz (B-H bridging) and 127 Hz (B-H terminal)). One equivalent of DMAP was then added to a solution of **8** to precipitate **9** as a white solid in an isolated yield of 73% (Scheme 3.2.5). The formation of DMAP•H$_2$BNH$t$Bu•BH$_3$ was confirmed by NMR spectroscopy and X-ray crystallography (Figure 3.2.7). Compound **9** exhibited a N$_{DMAP}$-BH$_2$ bond length of 1.583(2) Å, which is intermediate between the same bond length in **3** and **5** respectively. The central H$_2$B-NH($t$Bu) bond length was found to be 1.593(2) Å, which is slightly elongated compared to **3** and **5**, which may be due in part to the increased steric bulk of the $t$Bu group. The adduct also rests in the gauche conformation, similar to adducts **3**, **5** and **6**, with a N$_{DMAP}$-B-N-B$_{terminal}$ torsion angle of 76.66(18)°.

With the *tert*-butylated adduct **9** in hand, we decided to explore dehydrogenative chemistry to access the iminoborane adduct DMAP•HBN($t$Bu)•BH$_3$. Reaction of **9** with a catalytic amount of

Me$_2$S•CuBr in benzene resulted in the observation of DMAP-BH$_3$ and **8** in 15 and 21% yield respectively with 64% unreacted **9**, by integration of the $^{11}$B NMR spectrum, implying dehydrogenation had not proceeded in a manner similar to **5**. This stands in contrast to previous dehydrogenation experiments with Me$_2$S•CuBr, where rapid H$_2$ elmination was observed via the formation of borazine. We then reacted **9** with a catalytic amount of [Rh(COD)Cl]$_2$ in benzene (see Scheme 3.2.7). *In situ* $^{11}$B NMR analysis confirmed the formation of (HBN$t$Bu)$_3$ (**10**, 5%, d, -25.2 ppm, $^1J_{\text{B-H}}$ = 143 Hz), poly-$t$-butylborazylene (11%, br s, -30.1), (H$_2$BNH$t$Bu)$_3$ (**11**, 31%, t, -4.7 ppm, $^1J_{\text{B-H}}$ = 95 Hz) [27], DMAP-BH$_3$ (31%), and **8** (21%). The formation of large quantities of (H$_2$BNH$t$Bu)$_2$ is interesting as it implies that extrusion of H$_2$BNH$t$Bu is the primary reaction pathway, with only a small percentage of **9** undergoing dehydrogenation. Unfortunately, the small fraction of **9** that appears to undergo dehydrogenation chemistry seemingly extrudes HBN$t$Bu which oligomerizes to form N-$t$-butylborazine and poly-$t$-butylborazylene. This was corroborated by the work of Wright and co-workers, who showed that dehydrocoupling of $t$BuH$_2$N•BH$_3$ with Al(NMe$_2$)$_3$ as a catalyst resulted in mixtures of the trimers **10** and **11** and polymers of HBN$t$Bu and (H$_2$BNH$t$Bu)$_3$[27].
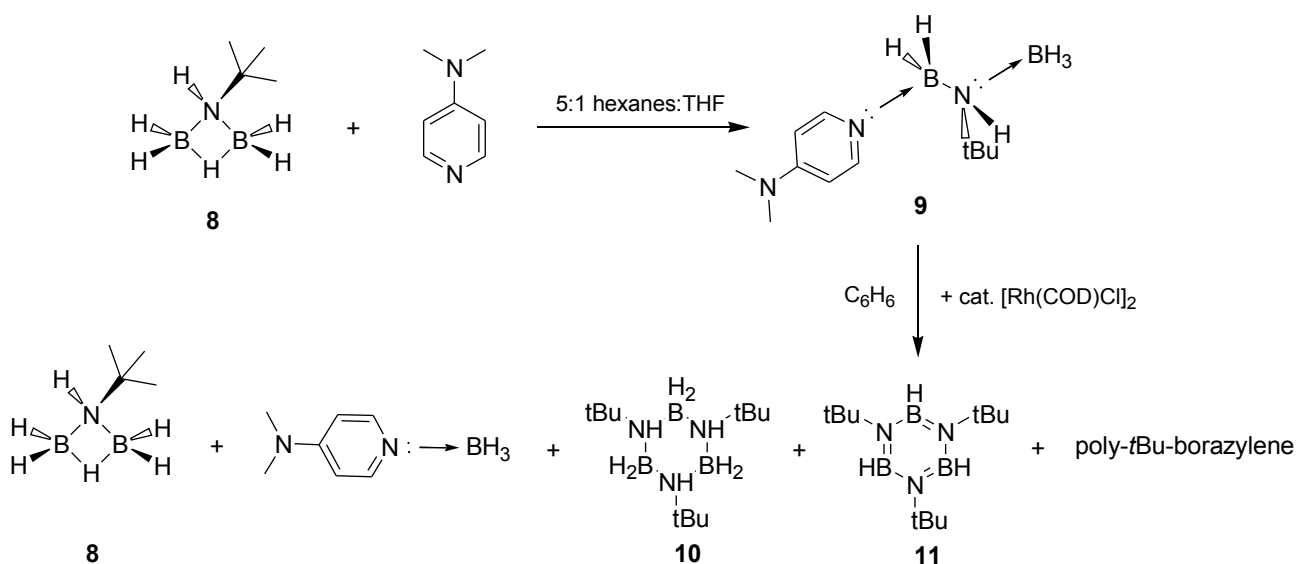


**Scheme 3.2.7**: Synthesis and catalytic dehydrogenation of DMAP•H$_2$BNH$t$Bu•BH$_3$ (**9**).
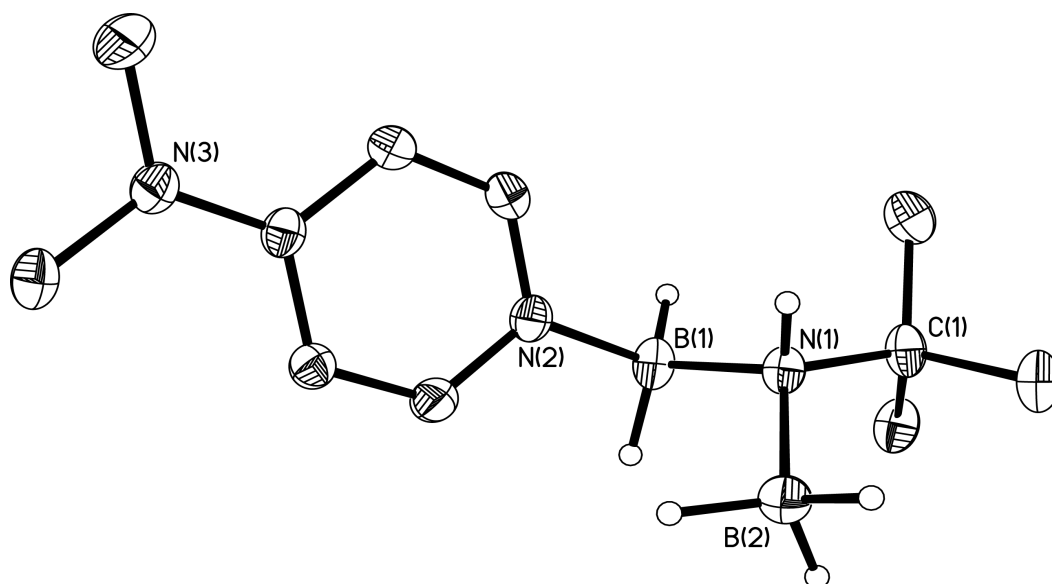
**Figure 3.2.5**: Thermal ellipsoid plot (30 % probability) of DMAP•H$_2$BNH$t$Bu•BH$_3$ (**9**), with carbon-bound hydrogen atoms omitted for clarity. The boron bound hydrogen atoms were located from the electron difference map. Selected bond lengths [Å] and angles [°]: B(1)-H 1.11(2) and 1.11(2), B(2)-H 1.14(2), 1.17(2), and 1.16(2), N(2)-B(1) 1.583(2), B(1)-N(1) 1.593(2), N(1)-B(2) 1.623(2), N(1)-C(1) 1.519(2), N(2)-B(1)-N(2) 108.95(13), B(1)-N(1)-C(1) 112.87(12), B(1)-N(1)-B(2) 110.57(14), N(2)-B(1)-N(1)-B(2) torsion angle 76.66(18).

It is known that N-heterocyclic carbenes have a tendency to act as Brønstead bases to form stable imidazolium cations. In a previous study, we showed that H$^-$ attack on an imidazolium ring cation can yield neutral aminals of the general form NHC$H_2$ (**12**, Scheme 3.2.8, NHC = N-heterocyclic carbene), and it has been shown by Roesky and co-workers that IPr can extract H$^-$ and H$^+$ from H$_3$N•BH$_3$ to give the same aminal product [13a,b].
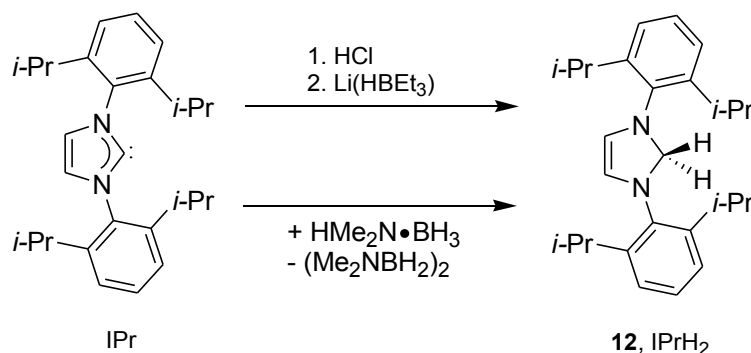


**Scheme 3.2.8**: Two possible routes for the formation of the N-heterocycle aminal IPrH$_2$ via H$^+$ and H$^-$ abstraction.

In an attempt to perform the same transformation, compound **3**, IPr•$H_2BNH_2$•$BH_3$, was reacted with IPr. Upon combining **3** with IPr, the known N-heterocycle, IPrH$_2$ (**12**), was observed as well as the heretofore unknown IPr•$H_2BNH_2$•$BH_3$ adduct (**13**). The fate of HBNH produced from this dehydrocoupling event is currently an area under investigation in our group. While the formation of this adduct does not add further insight into the reactivity of inorganic ethene, it demonstrates that the linear chain $BH_2NH_2BH_3$ is more stable in the presence of strong nucleophiles than the cyclic isomer, μ-aminodiborane ($NH_2B_2H_5$). This allows synthetic access to adducts that were otherwise unobtainable (Scheme 3.2.6), increasing the scope of this method.
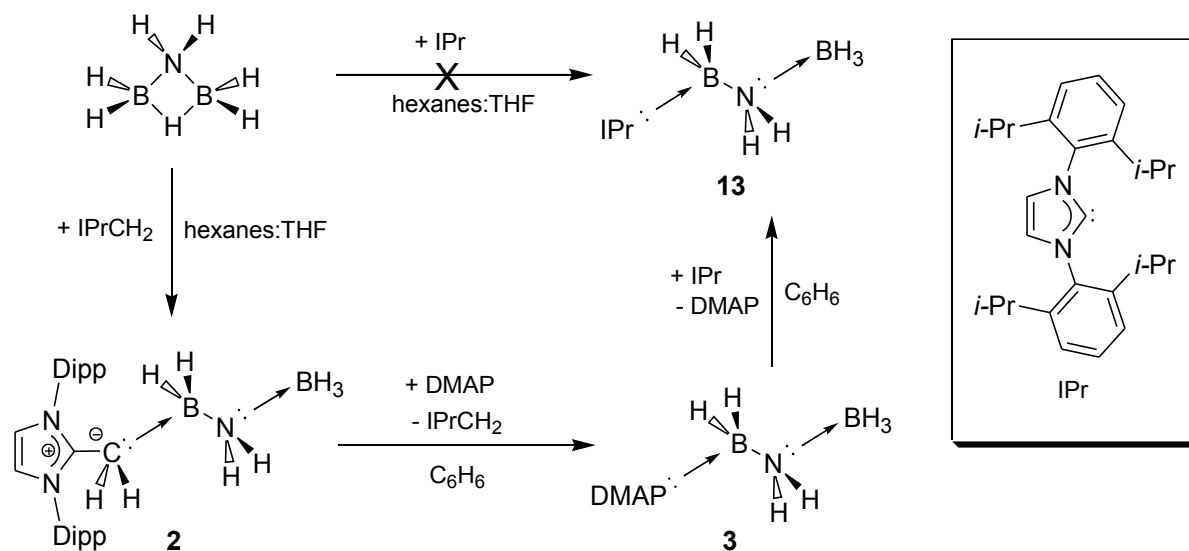


**Scheme 3.2.9:** Alternate synthetic route to obtain IPr•$H_2BNH_2$•$BH_3$

## 3.3 Conclusions

In summary we have developed a general donor-acceptor method for trapping the parent inorganic ethene ($H_2BNH_2$), which is a logical chemical precursor to a molecular adduct of boron nitride. Initial dehydrogenation studies have demonstrated that $H_2BNH_2$ units can be converted to HBNH in the presence of suitable dehydrogenation catalysts, which was shown to trimerize into borazine. This work has opened up new avenues for study of these once unstable molecules, adding insight into the dehydrogenation chemistry of amine boranes in the fields of both boron-nitride materials and hydrogen storage. Future work will involve exchanging the terminal Lewis acid $BH_3$ group in these adducts with less reactive Lewis acid partners in the attempts to induce full dehydrogenation to isolate the elusive BN molecule in the form of a stable complex.

### 3.4 Experimental Section.

**General.** All reactions were performed using standard Schlenk line techniques under an atmosphere of nitrogen or in an inert atmosphere glove box (Innovative Technology, Inc.). Solvents were dried using Grubbs-type solvent purification system manufactured by Innovative Technology, Inc. [28], degassed (freeze-pump-thaw method) and stored under an atmosphere of nitrogen prior to use. Ammonia borane and $t$BuNH$_2$•BH$_3$ was purchased from Aldrich, and Me$_2$NH•BH$_3$, BH$_3$•THF, and p-dimethylaminopyridine (DMAP) were purchased from Alfa Aesar and used as recieved. 1,3-Bis-(2,6-diisopropylphenyl)-imidazol-2-ylidene (IPr) and 1,3-Bis-(2,6-diisopropylphenyl)-imidazol-2-methylidene (IPrCH$_2$) were prepared following literature procedures [29, 30]. $^1$H and $^{11}$B NMR spectra were collected on a Varian iNova-400 spectrometer, and $^{13}$C{$^1$H} NMR spectra were collected on a Varian VNMRS-500 spectrometer. Samples were referenced externally to SiMe$_4$ ($^1$H, $^1$H{$^{11}$B}, $^{13}$C{$^1$H}) and BF$_3$•OEt$_2$ ($^{11}$B, $^{11}$B{$^1$H}). Elemental analyses were performed by the Analytical and Instrumentation Laboratory at the University of Alberta. Infrared spectra were recorded on a Nicolet IR100 FTIR spectrometer as Nujol mulls between NaCl plates. Melting points were measured in sealed glass capillaries under nitrogen using a MelTemp melting point apparatus and are uncorrected.

**X-ray Crystallography.** Crystals suitable for X-ray diffraction studies were removed from a vial (in glove box) and immediately coated with thin layer of hydrocarbon oil (Paratone-N). A suitable crystal was then mounted on glass fiber, and quickly placed in a low temperature stream of nitrogen on the X-ray diffractometer [31]. All data were collected using a Bruker APEX II CCD detector/D8 diffractometer using Mo Kα or Cu Kα radiation, with the crystals cooled to -100 °C. The data were corrected for absorption through Gaussian integration from the indexing of the crystal faces [32]. Crystal structures were solved using direct methods (**3**, **5**, and **7**: SHELXD [33]; **6**: SHELXD [34]), and refined using SHELXS-97. The assignment of hydrogen atoms positions were based on the sp$^2$

or sp$^3$ hybridization geometries of their attached carbon atoms, and were give thermal parameters 20% greater than those of their parent atoms.


**Synthetic Procedures.**

**Synthesis of Aminodiborane, NH$_2$B$_2$H$_5$ (1)**: Ammonia-borane (61.7 mg, 2.13 mmol) was taken up as a slurry in 15 mL of hexanes, and 1.0 M BH$_3$•THF (2.00 mL, 2.00 mmol) was added. The resulting cloudy solution was stirred for 3 days at room temperature to yield a colourless solution. The solution volume was concentrated by half under vacuum and filtered. The presence of NH$_2$B$_2$H$_5$ can be deteremined by diluting a small aliquot with C$_6$D$_6$ for $^{11}$B NMR analysis. $^{11}$B NMR (128 MHz, C$_6$D$_6$): δ = -26.6 ppm [d of t, $^1J_{BH}$ = 27 Hz (B-H bridging) and 138 Hz (B-H terminal)].


**Synthesis of IPrCH$_2$•H$_2$BNH$_2$•BH$_3$ (2)**: A solution of IPrCH$_2$ (0.859 g, 2.13 mmol) in 3 mL hexanes was added to a purified solution of NH$_2$B$_2$H$_5$ (made from 66.0 mg of NH$_3$BH$_3$, 2.13 mmol) in 5:1 hexanes:THF to give a white slurry which was stirred at room temperature for 2 hours. The mother liquor was decanted, and the white precipitate was washed with 2 x 6 mL portions of hexanes and toluene. The product was dried under vacuum, to give **2** as a white powder (0.587 g, 62%).

$^1$H NMR (400 MHz, CDCl$_3$): δ = 7.52 (t, 4H, $^3J_{HH}$ = 7.5 Hz, Ar*H*), 7.34 (d, 2H, $^3J_{HH}$ = 7.5 Hz, Ar*H*), 7.00 (s, 2H, -N-C*H*), 2.56 (septet, 2H, $^3J_{HH}$ = 6.5 Hz, -C*H*(CH$_3$)$_2$), 1.88 (br t, 2H, $^3J_{HH}$ = 4.0 Hz, IPrC*H*$_2$), 1.41 (s, 2H, assignment made by selective $^1$H{$^{11}$B} decoupling, -B*H*$_2$NH$_2$BH$_3$) 1.35 (d, 12H $^3J_{HH}$ = 6.5 Hz, -CH(C*H*$_3$)$_2$), 1.16 (d, 12H, $^3J_{HH}$ = 6.5 Hz, -CH(C*H*$_3$)$_2$), 1.06 (s, 3H, assignment made by selective $^1$H{$^{11}$B} decoupling, -BH$_2$NH$_2$B*H*$_3$). $^{13}$C{$^1$H} (125 MHz, CDCl$_3$): δ = 162.3 (Ar*C*), 145.7 (Ar*C*), 131.4 (Ar*C*), 130.8 (Ar*C*), 124.7 (-N-CH), 121.3 (-N-C(*C*H$_2$)-N-), 28.9 (-*C*H(CH$_3$)$_2$), 25.7 (-CH(*C*H$_3$)$_2$), 22.6 (IPr*C*H$_2$). $^{11}$B (128 MHz, CDCl$_3$): δ = -14.7 (br t, $^1J_{BH}$ = 94.5 Hz, -*B*H$_2$NH$_2$BH$_3$), -21.9 (br q, $^1J_{BH}$ = 86.9 Hz, -BH$_2$NH$_2$*B*H$_3$). IR (Nujol / cm$^{-1}$): 3340 (s, νNH), 2351 (s,

vBH), 2304 (s, vBH), 2219 (s, vBH). Anal. Calcd. for $C_{28}H_{45}B_2N_3$: C, 75.52; H, 10.19; N, 9.44. Found: C, 74.02; H, 11.24; N, 8.49. Mp (°C) 148 – 149 (melts).

**Decomposition of IPrCH₂•H₂BNH₂•BH₃ (2) in Solution:**  To investigate its decomposition, compound **2** (75.3 mg, 0.168 mmol) was dissolved in 8 mL of THF and stirred at room temperature. An aliquot of solution was removed and analyzed by $^{11}$B NMR spectroscopy every hour. Initial measurements (<15 min.) showed no signs of decomposition. After 24 hours ca. 50% had decomposed into [IPrCH₃⁺][BH₄⁻] by integration of the $^{11}$B NMR spectrum. After 48 hours ca. 90% had decomposed into the same product. Volatiles were removed in-vacuo and white residue was analyed by $^1$H and $^{11}$B NMR to yield a crude sample of [IPrCH₃⁺][BH₄⁻], containing 10% of **2**.

**NMR Data for [IPrCH₃⁺][BH₄⁻]:** $^1$H NMR (400 MHz, CDCl₃): δ = 8.18 (s, 2H, -N-C*H*), 7.65 (t, 4H, $^3J_{HH}$ = 8.0 Hz, Ar*H*), 7.44 (d, 2H, $^3J_{HH}$ = 8.0 Hz, Ar*H*), 2.34 (septet, 2H, $^3J_{HH}$ = 6.8 Hz, -C*H*(CH₃)₂), 2.14 (s, 3H, IPrC*H₃*), 1.32 (d, 12H, $^3J_{HH}$ = 6.8 Hz, -CH(C*H₃*)₂), 1.23 (d, 12H, $^3J_{HH}$ = 6.8 Hz, -CH(C*H₃*)₂), 0.33 (q, 4H, $^1J_{BH}$ = 81.5 Hz, B*H₄*⁻). $^{11}$B (128 MHz, CDCl₃): δ = -40.6 (pentet, $^1J_{BH}$ = 81.3 Hz, *B*H₄⁻). $^{13}$C{$^1$H} (125 MHz, CDCl₃): δ = 145.7 (Ar*C*), 144.9 (Ar*C*), 132.6 (Ar*C*), 129.0 (Ar*C*), 126.2 (Ar*C*), 125.4 (Ar*C*), (-N-*C*H), 29.2 (-*C*H(CH₃)₂), 24.6 (-CH(*C*H₃)₂), 23.4 (-CH(*C*H₃)₂), 10.9 (IPr*C*H₃).

**Reaction of IPrCH₂•H₂BNH₂•BH₃ (2) with B(C₆F₅)₃:** Compound **2** (45.4 mg, 0.101 mmol) and B(C₆F₅)₃ (52.1 mg, 0.100 mmol) were taken up in 8 mL of toluene as a slurry, and 1 mL of THF was added to dissolve the starting materials. After 3 hours the volatiles were removed under vacuum to yield a white residue. The tentative primary product of the reaction is [IPrCH₃⁺][HB(C₆F₅)₃⁻]; the $^{13}$C NMR spectrum was in agreement with values for the IPrCH₃⁺ cation [18d], while $^{11}$B and $^{19}$F NMR confirmed the presence of the HB(C₆F₅)₃⁻ anion [18a-c]. The aryl region of the $^1$H spectrum displayed a complicated splitting pattern, making it difficult to use for product identification. In a

separate reaction, 5.6 mg (0.012 mmol) of **2** and 6.4 mg (0.012 mmol) of $B(C_6F_5)_3$ were dissolved in 0.8 mL of toluene and 2 drops of THF. The solution was immediately sealed in a J.Young NMR tube and monitored via $^{11}B$ NMR spectroscopy. After 5 minutes, 90% of the $B(C_6F_5)_3$ had been consumed and converted into $[HB(C_6F_5)_3^-]$, with a second product at -19 ppm (~10%, br s). After 3 hours all of the starting materials had been converted into $[HB(C_6F_5)_3^-]$ (90% yield by integration); $BH_3 \cdot THF$ was present in solution (8% by integration), confirming that the terminal $BH_3$ group was displaced in the reaction before the formation of $[IPrCH_3^+][HB(C_6F_5)_3^-]$. There were several unidentified peaks in the aromatic region of the $^1H$ NMR spectrum thus making it difficult to assign diagnostic resonances, however the major product was confirmed by $^{13}C\{^1H\}$, $^{11}B$ and $^{19}F$ NMR.

**NMR Data for [IPrCH$_3^+$][HB(C$_6$F$_5$)$_3^-$]:** $^{11}B$ NMR (128 MHz, CDCl$_3$): $\delta$ = -25.4 (d, $^1J_{BH}$ = 93.3 Hz, H*B*(C$_6$F$_5$)$_3^-$). $^{19}F$ (500 MHz, CDCl$_3$): $\delta$ = -133.52 (d, $^3J_{FF}$ = 21.8 Hz, Ar*F*), -163.8 (t, $^3J_{FF}$ = 20.7 Hz, Ar*F*), -166.8 (m, $^3J_{FF}$ = 16.6 Hz, Ar*F*). $^{13}C\{^1H\}$ (125 MHz, CDCl$_3$): $\delta$ = 145.1 (Ar*C*), 144.8 (Ar*C*), 132.7 (Ar*C*), 129.1 (Ar*C*), 125.6 (-N-*C*H), 29.3 (-*C*H(CH$_3$)$_2$), 24.3 (-CH(*C*H$_3$)$_2$), 23.2 (-CH(*C*H$_3$)$_2$), 10.6 (IPr*C*H$_3$).


**Thermolysis of IPrCH$_2$•H$_2$BNH$_2$•BH$_3$ (2):** A small amount of **2** (approx. 5 mg) was dissolved in 1 mL of C$_6$D$_6$ and sealed in a J. Young NMR tube under 1 atm of nitrogen. The solution was heated at 100 °C for 24 hours to yield a clear colourless solution with a small amount of undissolved **2**. $^1H$ and $^{11}B$ NMR analysis showed only the presence of **2** with no sign of decomposition.


**Synthesis of DMAP•H$_2$BNH$_2$•BH$_3$ (3)**: A solution of p-dimethylaminopyridine (0.0918 g, 0.75 mmol) in 5 mL of 5:1 hexanes:THF was added to a solution of NH$_2$B$_2$H$_5$ (made from 23.2 mg of NH$_3$BH$_3$, 0.75 mmol) in 10 mL of 5:1 hexanes:THF solvent mixture. The resulting mixture clouded to give a white slurry after 8 hours. The mother liqour was then decanted, and the white solid was washed with 6 mL portions of hexanes, diethyl ether and toluene. The product was dried under

vacuum, giving **3** as a white powder (0.0920 g, 75%). Crystals of **3** suitable for X-ray crystallography (colourless needles) were obtained by cooling a saturated dichloroethane / diethylether solution to -35 °C.

$^1$H NMR (400 MHz, CDCl$_3$): δ = 8.08 (d, 2H, $^3J_{HH}$ = 7.3 Hz, Ar*H*), 6.57 (d, 2H, $^3J_{HH}$ = 7.3 Hz, Ar*H*), 3.13 (s, 6H, -N(C*H$_3$*)$_2$), 2.79 (s, 2H, assignment made by selective $^1$H{$^{11}$B} decoupling, -B*H$_2$*NH$_2$BH$_3$), 2.19 (br s, 2H, -BH$_2$N*H$_2$*BH$_3$), 1.26 (t, 3H, assignment made by selective $^1$H{$^{11}$B} decoupling, $^3J_{HH}$ = 4.4 Hz, -BH$_2$NH$_2$B*H$_3$*). $^{13}$C{$^1$H} (125 MHz, CDCl$_3$): δ = 155.8 (Ar*C*), 147.4 (Ar*C*), 106.2 (Ar*C*), 39.6 (Ar-N(*C*H$_3$)$_2$). $^{11}$B (128 MHz, CDCl$_3$): δ = -3.7 (t, $^1J_{BH}$ = 99.5 Hz, -*B*H$_2$NH$_2$BH$_3$), -21.8 (q, $^1J_{BH}$ = 91.9 Hz, -BH$_2$NH$_2$*B*H$_3$). IR (Nujol / cm$^{-1}$): 3301 (w, νNH), 2364 (w, νBH), 2297 (w, νBH), 2243 (w, νBH). Mp (°C) 138 – 139 (melts).


**Thermolysis of DMAP•H$_2$BNH$_2$•BH$_3$ (3).** 10 mg of **3** was dissolved in 0.5 mL of THF and sealed in a J. Young NMR tube under an atmosphere of nitrogen. The sample was heated at 100 °C for 24 hours. The in-situ $^{11}$B NMR analysis showed the presence of the known DMAP-BH$_3$ adduct and borazine (doublet at 30.6 ppm, $^1J_{BH}$ = 141.1 Hz) in a 3:1 ratio by integration of peaks, with trace starting material. Volatiles were removed in-vacuo and the white residue (5 mg) was identified as DMAP-BH$_3$ by NMR.

**NMR Data for DMAP•BH$_3$ [25]:** $^1$H NMR (400 MHz, CDCl$_3$): δ = 8.05 (d, 2H, $^3J_{HH}$ = 7.6 Hz, Ar*H*), 6.49 (d, 2H, $^3J_{HH}$ = 7.6 Hz, Ar*H*), 3.08 (s, 6H, -N(C*H$_3$*)$_2$). $^{11}$B (128 MHz, CDCl$_3$): δ = -13.9 (q, $^1J_{BH}$ = 92.7 Hz, -*B*H$_3$).


**Dehydrogenation of DMAP•H$_2$BNH$_2$•BH$_3$ (3):** i) To a solution of **3** (34.2 mg, 0.207 mmol) in 5 mL of THF was added 1.0 mg of [Rh(COD)Cl]$_2$ (0.002 mmol, cat. 1 mol%). The solution was initially clear yellow, and turned black-green after 2 hours. An aliquot of the solution was then analyzed by $^{11}$B NMR at the initiation of reaction and after 60 hrs, showing only the presence of **3**

and no other soluble products. The mother liqour was decanted and dried in vacuo to recover 71% of starting material.

ii) 20.7 mg (0.125 mmol) of **3** and 6.2 mg of NiBr$_2$•DME (0.02 mmol, 16 mol% cat., DME = dimethoxyethane) were dissolved in 6 mL of THF to yield a golden brown solution that quickly turned black. The mixture was stirred for 48 hours to yield a clear colourless solution with black precipitate. $^{11}$B NMR analysis of this clear solution showed that 50% of the starting material remained, with the major product DMAP-BH$_3$ (40%) and borazine (10%).

iii) 19.8 mg (0.120 mmol) of **3** and 8.1 mg of CuBr•DMS (0.04 mmol, 32 mol% cat., DMS = dimethylsulfide) were dissolved in 6 mL of THF to yield a light yellow solution that quickly turned black after 10 minutes. The mixture was stirred for 48 hours to yield a clear colourless solution with black metallic precipitate. $^{11}$B NMR of this clear solution showed no signs of starting material, with the major products DMAP-BH$_3$ (65%) and borazine (30%), and one unidentified product (5%, br s, 5.5 ppm).

iv) 21.5 mg (0.130 mmol) of **3** and 6.0 mg of CuBr (0.04 mmol, 32 mol% cat.) were dissolved in 6 mL of THF to yield a pale yellow solution that turned black after 2 hrs. The mixture was stirred for 48 hours to yield a clear colourless solution with black metallic precipitate. $^{11}$B NMR of this clear solution showed no signs of starting material, with the major products DMAP-BH$_3$ (65%) and borazine (30%), and one unidentified product (5%, br s, 5.5 ppm).


**Synthesis of dimethylaminodiborane, (CH$_3$)$_2$NB$_2$H$_5$ (4)**: Me$_2$NH•BH$_3$ (0.1620 g, 2.74 mmol) was dissolved in 6 mL of 5:1 hexanes:THF and combined with 1.0 mg of [Rh(COD)Cl]$_2$. Immediately the solution turned clear yellow, and within 2 hours the solution was dark black-green. The mixture was stirred for 16 hours at room temperature and filtered through a plug of silica to remove colloidal rhodium [23c]; the presence of [Me$_2$NBH$_2$]$_2$ was confirmed by $^{11}$B NMR, showing a triplet at 4.75 ppm ($^1J_{BH}$ = 112.8 Hz) . One equivalent of 1.0 M (2.7 mL, 2.70 mmol.) H$_3$B•THF solution

was added, and the clear colourless mixture was heated at 60 °C for 8 hours to quantitatively yield **4** by ^{11}B NMR (128 MHz, THF): $\delta$ = -17.5 (br t, $^1J_{BH}$ = 146.9 Hz).


**Synthesis of DMAP•H₂BN(CH₃)₂•BH₃ (5)**: A solution of p-dimethylaminopyridine (0.3359 g, 2.75 mmol) in 5 mL of 5:1 hexanes:THF was combined with a 15 mL solution of $N(CH_3)_2B_2H_5$ prepared *in-situ* (from 2.74 mmol of $Me_2NH•BH_3$). The clear colourless solution turned to a pale yellow slurry and the reaction was stirred for 8 hours at room temperature. The volatiles were removed under vacuum, and the solid material was washed with 4 mL portions of hexanes, diethyl ether, and benzene. Volatiles were removed under vaccuum to give **5** as a pale yellow solid (0.332 g, 63%). Crystals of **5** suitable for X-ray crystallography (colourless prisms) were grown by cooling a concentrated hexane/THF solution to -35 °C.

^{1}H NMR (500 MHz, $C_6D_6$): $\delta$ = 8.17 (d, 2H, $^3J_{HH}$ = 6.0 Hz, Ar*H*), 5.55 (d, 2H, $^3J_{HH}$ = 6.0 Hz, Ar*H*), 2.61 (s, 6H, -BH₂N(C*H*₃)₂BH₃), 2.55 (s, 2H, assignment made by selective $^1H\{^{11}B\}$ decoupling in $CDCl_3$, -B*H*₂NH₂BH₃), 1.86 (s, 6H, -N(C*H*3)2), 1.32 (t, 3H, assignment made by selective $^1H\{^{11}B\}$ decoupling in $CDCl_3$, $^3J_{HH}$ = 4.4 Hz, -BH₂NH₂B*H*₃). $^{13}C\{^1H\}$ (125 MHz, $C_6D_6$): $\delta$ = 155.2 (Ar*C*), 148.8 (Ar*C*), 105.2 (Ar*C*), 50.6 (-BH₂N(*C*H₃)₂BH₃), 38.2 (-N(*C*H₃)₂). $^{11}B$ (128 MHz, $C_6D_6$): $\delta$ = 2.5 (t, $^1J_{BH}$ = 101.5 Hz, -*B*H₂NH₂BH₃), -10.8 (q, $^1J_{BH}$ = 94.5 Hz, -BH₂NH₂*B*H₃). IR (Nujol / cm⁻¹): 2394 (w, $\nu$BH), 2354 (w, $\nu$BH), 2330 (w, $\nu$BH), 2281 (w, $\nu$BH). Anal. Calcd. for $C_9H_{21}B_2N_3$: C, 56.04; H, 10.97; N, 21.78. Found: C, 55.98; H, 10.94; N, 21.43. Mp (°C): 131 – 131.5 (melts).


**Attempted Thermolysis of DMAP•H₂BN(CH₃)₂•BH₃ (5):** 10 mg of **5** dissolved in 1 mL of THF was sealed in a J. Young NMR tube under an atmosphere of nitrogen and heated to 100 °C for 24 hours. ^{11}B NMR analysis of the reaction mixture showed only the presence of starting material with no decomposition.

**Reaction of 5 with B(C₆F₅)₃**: Compound **5** (11.8 mg, 0.061 mmol) and B(C$_6$F$_5$)$_3$ (31.4 mg, 0.061 mmol) were combined in 4 mL of toluene to yield a yellow solution. After 2 hours, the volatiles were removed under vacuum to yield 39.1 mg of a pale yellow solid. NMR spectroscopy was performed on the putative product [DMAP•HBNMe$_2$•BH$_3$$^+$][H(BC$_6$F$_5$)$_3$$^-$]. $^1$H NMR (400 MHz, C$_6$D$_6$): δ = 7.58 (d, 2H, $^3J_{H-H}$ = 7.6 Hz, Ar$H$), 5.79 (d, 2H, $^3J_{H-H}$ = 7.6 Hz, Ar$H$), 2.09 (s, 6H, -N(C$H_3$)$_2$). $^{11}$B NMR (400 MHz, C$_6$D$_6$): δ = -14.7 ppm (q, $^1J_{B-H}$ = 142 Hz), -16.9 ppm (d, $^1J_{B-H}$ = 166 Hz), -24.8 ppm (d, $^1J_{B-H}$ = 88 Hz).

**Synthesis of IPrCH₂•H₂BN(CH₃)₂•BH₃ (6)**: A solution of IPrCH$_2$ (0.988 g, 2.45 mmol) in 3 mL of hexanes was added to a solution of N(CH$_3$)$_2$B$_2$H$_5$ (prepared from 0.1453 g (2.46 mmol) Me$_2$N•BH$_3$ as described previously). The clear solution turned to a pale yellow slurry, and the reaction was stirred at room temperature for 4 hours. The mother liquor was decanted and the precipitate was washed with hexanes (2 x 4 mL). The product was dried under vaccuum to give **6** as a pale yellow powder  (0.988 g, 85%). Crystals of **6** suitable for X-ray crystallography (yellow prisms) were grown by cooling a saturated hexanes/dichloroethane solution to -35 °C.

$^1$H NMR (500 MHz, CDCl$_3$): δ = 7.52 (t, 4H, $^3J_{HH}$ = 7.1 Hz, Ar$H$), 7.33 (d, 2H, $^3J_{HH}$ = 7.1 Hz, Ar$H$), 6.98 (s, 2H, -N-C$H$), 2.58 (septet, 2H, $^3J_{HH}$ = 7.0 Hz, -C$H$(CH$_3$)$_2$), 1.96 (br t, 2H, $^3J_{HH}$ = 6.0 Hz, IPrC$H_2$), 1.97 (s, 2H, assignment made by selective $^1$H{$^{11}$B} decoupling, -B$H_2$NH$_2$BH$_3$), 1.82 (s, 6H, -BH$_2$N(C$H_3$)$_2$BH$_3$), 1.39 (d, 12H, $^3J_{HH}$ = 7.0 Hz, -CH(C$H_3$)$_2$), 1.16 (d, 12H, $^3J_{HH}$ = 7.0 Hz, -CH(C$H_3$)$_2$), 1.05 (s, 3H, assignment made by selective $^1$H{$^{11}$B} decoupling, -BH$_2$NH$_2$B$H_3$). $^{13}$C{$^1$H} (125 MHz, CDCl$_3$): δ = 162.3 (Ar$C$), 145.7 (Ar$C$), 131.2 (Ar$C$), 131.0 (Ar$C$), 124.6 (-N-C$H$), 121.2 (-N-C$C$H$_2$), 51.61 (-N(C$H_3$)$_2$), 29.0 (-$C$H(CH$_3$)$_2$) , 25.8 (-CH(C$H_3$)$_2$), 22.6 (IPrC$H_2$). $^{11}$B (128 MHz, CDCl$_3$): -7.7 (br t, $^1J_{BH}$ = 89.5 Hz, -$B$H$_2$NH$_2$BH$_3$), -13.1 (br q, $^1J_{BH}$ = 80.1 Hz, -BH$_2$NH$_2$$B$H$_3$). IR (Nujol / cm$^{-1}$): 2335 (w, νBH), 2295 (w, νBH). Mp (°C) 158 - 159 (melts).

**Thermolysis of IPrCH$_2$•H$_2$BN(CH$_3$)$_2$•BH$_3$ (6):** A solution of **6** (10 mg) in 0.5 mL of C$_6$D$_6$ was sealed in a J. Young NMR tube under an atmosphere of nitrogen, and heated to 65 °C for 24 hours. $^{11}$B and $^1$H NMR spectroscopy showed no signs of decomposition. The sample was then heated at 100 °C for 24 hours. The reaction mixture was analyzed by $^{11}$B and $^1$H NMR. The only identifiable product by *in situ* $^{11}$B NMR spectroscopy was the dimer [Me$_2$NBH$_2$]$_2$ (triplet at 4.75, $^1J_{BH}$ = 113 Hz), with trace starting material (9% by integration). The *in situ* $^1$H NMR spectrum showed seven different carbene environments, including free carbene (7% by integration).

**Synthesis of IPr•H$_2$BN(CH$_3$)$_2$•BH$_3$ (7):** A solution of N(CH$_3$)$_2$B$_2$H$_5$ was prepared as described above (from 0.82 mmol N(CH$_3$)$_2$HBH$_3$, and 0.81 mmol BH$_3$•THF). To this clear colourless solution (approx. 10 mL), was added 6 mL of a hexanes solution of IPr (308 mg, 0.81 mmol). The golden brown mixture was initially opaque, but became clear after 12 hours. The volatiles were removed in vacuo, yielding crude **7** as a light brown powder (321 mg, 85%). The product was further purified by recrystallization from a saturated solution of 1:1 THF:hexane (96.0 mg, 25%). Crystals obtained by this method (light yellow prisms) were suitable for X-ray crystallography.

$^1$H NMR (400 MHz, C$_6$D$_6$): δ = 7.19 (t, 4H, $^3J_{HH}$ = 8.0 Hz, Ar*H*), 7.10 (d, 2H, $^3J_{HH}$ = 7.9 Hz, Ar*H*), 6.54 (s, 2H, -N-C*H*), 2.98 (septet, 2H, $^3J_{HH}$ = 6.8 Hz, -C*H*(CH$_3$)$_2$), 2.20 (s, 2H, assignment made by selective $^1$H{$^{11}$B} decoupling, -B*H$_2$*NH$_2$BH$_3$), 2.09 (s, 6H, -BH$_2$N(C*H$_3$*)$_2$BH$_3$), 2.00 (s, 3H, assignment made by selective $^1$H{$^{11}$B} decoupling, -BH$_2$NH$_2$B*H$_3$*), 1.44 (d, 12H, $^3J_{HH}$ = 6.7 Hz, -CH(C*H$_3$*)$_2$), 0.99 (d, 12H, $^3J_{HH}$ = 6.7 Hz, -CH(C*H$_3$*)$_2$). $^{13}$C{$^1$H} (125 MHz, C$_6$D$_6$): δ = 161.9 (N-*C*-N), 146.2 (Ar*C*), 135.4 (Ar*C*), 130.6 (Ar*C*), 124.3 (-N-*C*H), 123.2 (Ar*C*), 54.6 (-BH$_2$N(*C*H$_3$)$_2$BH$_3$), 29.1 (-*C*H(CH$_3$)$_2$), 26.2 (-CH(*C*H$_3$)$_2$), 22.4 (-CH(*C*H$_3$)$_2$). $^{11}$B{$^1$H} (128 MHz, C$_6$D$_6$): δ = -10.0 (br s, -BH$_2$N(CH$_3$)$_3$*B*H$_3$), -11.3 (br s, -*B*H$_2$N(CH$_3$)$_2$BH$_3$). IR (Nujol / cm$^{-1}$): 3168 (w, νNH), 3134 (w, νNH), 3104 (w, νNH), 2438 (w, νBH), 2334 (w, νBH), 2269 (w, νBH), 2237 (w, νBH). Anal. Calcd. for C$_{29}$H$_{47}$B$_2$N$_3$: C, 75.83; H, 10.31; N, 9.15. Found: C, 75.97; H, 10.77; N, 8.28. Mp (°C): 179 – 180

(melts).

**Synthesis of t-butylaminodiborane, (*t*Bu)HNB₂H₅ (8):** $t$BuNH₂•BH₃ (174.1 mg, 2.00 mmol) was taken up as a slurry in 10 mL of hexanes, and 1.0 M BH₃•THF (2.00 mL, 2.00 mmol) was added to the stirring mixture. The resulting cloudy solution was stirred for 3 days at room temperature to yield a colourless solution. The solution volume was concentrated by half under vacuum and filtered. The presence of N$t$BuHB₂H₅ can be determined by diluting a small aliquot with $C_6D_6$ for ¹¹B NMR analysis. (¹¹B NMR 128 MHz, $C_6D_6$): δ = -26.4 ppm (t of d, $^1J_{BH}$ = 30 Hz (B-H bridging) and 127 Hz (B-H terminal)).

**Synthesis of DMAP•H₂BN(tBu)H•BH₃ (9)**: A solution of p-dimethylaminopyridine (0.329 g, 2.00 mmol) was added to a solution of $t$BuNHB₂H₅ (made from 2.00 mmol $t$BuH₂N•BH₃) in 10 mL of 5:1 hexanes:THF. The resulting mixture clouded to give a white slurry after 8 hours. The mother liqour was then decanted, and the white solid was washed with 4 mL portions of 5:1 hexanes:THF. The product was dried under vaccuum, giving **9** as a white powder (0.321 g, 73%). Crystals of **9** suitable for X-ray crystallography (colourless prisms) were obtained by cooling a saturated THF / hexanes solution to -35 °C.

¹H NMR (400 MHz, CDCl₃): δ = 8.07 (d, 2H, $^3J_{HH}$ = 7.6 Hz, Ar$H$), 6.53 (d, 2H, $^3J_{HH}$ = 7.6 Hz, Ar$H$), 3.10 (s, 6H, -N(CH₃)₂), 1.82 (br s, 2H, assignment made by selective ¹H{¹¹B} decoupling in CDCl₃, -B$H$₂NH₂BH₃), 1.80 (br s, 1H, -N$H$($t$Bu)), 1.79 (br s, 3H, assignment made by selective ¹H{¹¹B} decoupling in CDCl₃, -BH₂NH₂B$H$₃), 1.31 (s, 9H, -NC(C$H$₃)₃). ¹³C{¹H} (125 MHz, CDCl₃): δ = 155.6 (Ar$C$), 147.8 (Ar$C$), 106.3 (Ar$C$), 54.6 (-N$C$(CH₃)₂), 39.4 (-N($C$H₃)₂), 28.3 (-NC($C$H₃)₂). ¹¹B (128 MHz, $C_6D_6$): δ = -3.4 (t, $^1J_{BH}$ = 90 Hz, -$B$H₂NH$t$BuBH₃), -21.7 (q, $^1J_{BH}$ = 90 Hz, -$B$H₂NH$t$BuBH₃). IR (Nujol / cm⁻¹): 3211 (w, ν NH), 3131 (w, ν NH), 3078 (w, ν NH), 2388 (w, ν BH), 2357 (w, ν BH), 2281 (w, ν BH), 2255 (w, ν BH). Anal. Calcd. for $C_{11}H_{25}B_2N_3$: C, 59.79; H, 11.40; N,

19.02. Found: C, 60.59; H, 14.73; N, 10.47. Mp (°C): 132 - 133 (melts).

**Reaction of 3 with IPr to form 13**: IPr (110.0 mg, 0.23 mmol) and **3** (18.9 mg, 0.15 mmol) were taken up in 5 mL of benzene, and stirred at room temperature to yield a clear golden solution after 8 hours. The volatiles were removed in vacuo to yield a pale yellow solid, and the solid was washed with 10 mL of hexanes, and then 5 mL of a 1:1 hexanes:benzene solvent mixture. The remaining solid was dried under vacuum to yield **13** as a white solid (10.4 mg, 21%).

$^1$H NMR (500 MHz, CDCl$_3$): δ = 7.17 (t, 4H, $^3J_{\text{H-H}}$ = 7 Hz, Ar$H$), 7.08 (d, 2H, $^3J_{\text{HH}}$ = 7 Hz, Ar$H$), 6.42 (s, 2H, Ar$H$), 2.90 (septet, 2H, $^3J_{\text{HH}}$ = 6.8 Hz, -C$H$(CH$_3$)$_2$), 2.25 (s, 2H, assignment made by selective $^1$H{$^{11}$B} decoupling, -B$H_2$NH$_2$BH$_3$), 2.11 (s, 3H, assignment made by selective $^1$H{$^{11}$B} decoupling, -BH$_2$NH$_2$B$H_3$), 1.85 (s, 2H, -BH$_2$N$H_2$BH$_3$), 1.43 (d, 12H, $^3J_{\text{HH}}$ = 6.8 Hz, -CH(C$H_3$)$_2$), 0.98 (d, 12H, $^3J_{\text{HH}}$ = 6.7 Hz, -CH(C$H_3$)$_2$). $^{13}$C{$^1$H} (125 MHz, C$_6$D$_6$): δ = 146.1 (Ar$C$), 133.7 (Ar$C$), 130.8 (Ar$C$), 128.3 (Ar$C$), 124.5 (-N-$C$H), 122.7 (Ar$C$), 28.8 (-$C$H(CH$_3$)$_2$), 25.8 (-CH($C$H$_3$)$_2$), 22.9 (-CH($C$H$_3$)$_2$). $^{11}$B{$^1$H} (128 MHz, CDCl$_3$): δ = -18.2 (br s), -19.4 (br s). IR (Nujol / cm$^{-1}$): 3211, 3150 (w, νNH), 2444, 2170, 2201, 2197 (w, νBH). Mp (°C): 144 - 145 (melts).

## 3.5 Crystallographic Tables for Chapter 3

**Table 3.5.1.** Crystallographic Data for Compounds **3**, **5** and **6**.

|  | 3 | 5 | 6 |
|---|---|---|---|
| empirical formula | $C_7H_{17}B_2N_3$ | $C_9H_{21}B_2N_3$ | $C_{31}H_{51}B_2ClN_3$ |
| fw | 164.86 | 192.91 | 522.82 |
| cryst. dimens. (mm) | $0.23 \times 0.13 \times 0.06$ | $0.38 \times 0.36 \times 0.31$ | $0.61 \times 0.36 \times 0.27$ |
| cryst. syst. | monoclinic | orthorhombic | monoclinic |
| space group | $P2_1/n$ | $P2_12_12_1$ | $P2_1/n$ |
| unit cell |  |  |  |
| $a$ (Å) | 11.2392 (2) | 8.4065 (6) | 10.2412 (5) |
| $b$ (Å) | 7.4511 (1) | 10.0395 (8) | 12.9371 (7) |
| $c$ (Å) | 12.1976 (2) | 14.3963 (11) | 24.8848 (13) |
| $\alpha$ (°) |  |  |  |
| $\beta$ (°) | 101.0881 (9) |  | 99.8480 (10) |
| $\gamma$ (°) |  |  |  |
| $V$ (Å$^3$) | 1002.41 (3) | 1215.01 (16) | 3248.4 (3) |
| Z | 4 | 4 | 4 |
| $\rho_{calcd}$ (g cm$^{-3}$) | 1.092 | 1.055 | 1.069 |
| $\mu$ (mm$^{-1}$) | 0.496 | 0.062 | 0.140 |
| T (K) | 173(1) | 173(1) | 173(1) |
| $2\theta_{max}$ (°) | 140.02 | 55.04 | 50.50 |
| total data | 1822 | 10623 | 22840 |
| unique data ($R_{int}$) | 1822 (0.0000) | 2782 (0.0354) | 5886 (0.0286) |
| observed data a [$I > 2\sigma(I)$] | 1637 | 2418 | 4738 |
| params. | 140 | 150 | 376 |
| $R_1$ [$I > 2\sigma(I)$][a] | 0.0336 | 0.0359 | 0.0570 |
| $wR_2$ [all data][a] | 0.0956 | 0.0886 | 0.1725 |
| difference map $\Delta\rho$ (e Å$^{-3}$) | 0.156 / −0.146 | 0.165 / −0.120 | 0.386 / −0.627 |

[a] $R_1 = \Sigma||F_o| - |F_c|| / \Sigma|F_o|$; $wR_2 = [\Sigma w(F_o^2 - F_c^2)^2 / \Sigma w(F_o^4)]^{1/2}$

**Table 3.5.2.** Crystallographic Data for Compounds **7** and **9**.

| | 7 | 9 |
|---|---|---|
| empirical formula | $C_{32}H_{54}B_2N_3$ | $C_{11}H_{25}B_2N_3$ |
| fw | 502.40 | 220.96 |
| cryst. dimens. (mm) | $0.23 \times 0.23 \times 0.15$ | $0.33 \times 0.15 \times 0.04$ |
| cryst. syst. | monoclinic | monoclinic |
| space group | $P2_1/n$ | $P2_1/c$ |
| unit cell | | |
| $a$ (Å) | 12.7575 (2) | 8.0183 (2) |
| $b$ (Å) | 19.0656 (3) | 18.0715 (4) |
| $c$ (Å) | 13.1625 (2) | 9.9072 (2) |
| $\alpha$ (°) | | |
| $\beta$ (°) | 93.3871 (9) | 91.7241 (13) |
| $\gamma$ (°) | | |
| $V$ (Å$^3$) | 3195.91 (9) | 1434.93 (6) |
| Z | 4 | 4 |
| $\rho_{calcd}$ (g cm$^{-3}$) | 1.044 | 1.023 |
| $\mu$ (mm$^{-1}$) | 0.440 | 0.448 |
| T (K) | 173(1) | 173(1) |
| $2\theta_{max}$ (°) | 141.44 | 141.86 |
| total data | 20925 | 9552 |
| unique data ($R_{int}$) | 5834 (0.0184) | 2706 (0.0393) |
| observed data a [$I > 2\sigma(I)$] | 5320 | 2149 |
| params. | 346 | 171 |
| $R_1$ [$I > 2\sigma(I)$]$^a$ | 0.0555 | 0.0533 |
| $wR_2$ [all data]$^a$ | 0.1623 | 0.1564 |
| difference map $\Delta\rho$ (e Å$^{-3}$) | 0.424 / −0.436 | 0.397 / −0.216 |

$^a$ $R_1 = \Sigma||F_o| - |F_c|| / \Sigma|F_o|$; $wR_2 = [\Sigma w(F_o^2 - F_c^2)^2 / \Sigma w(F_o^4)]^{1/2}$

## 3.6 Theoretical Studies

Calculations of geometry optimization, frequency and energy were performed using Gaussian 09, Revision B01 software [35], using DFT methods and the B3LYP functional with default spin parameters. The ccpVDZ-pp basis set was used for all atoms [36]. Optimizations were done with tight convergence criteria, and no restrictions or constraints were placed on any of the calculated structures. The IPrCH$_2$ donors were simplified by replacing the 2,6-diisopropylphenyl groups with methyl substituents in order to expedite the calculations. The INT=ULTRAFINE keyword was used to generate the grid for electron density. Default parameters were used for all other options. Molecular orbitals and natural bonding orbital (NBO) analyses were done with the built in MO and NBO suites of Gaussian 09 and GaussView3. Theoretical IR frequencieswere obtained using the spectrum generator in Gaussian.

### *IR Spectroscopy*

**Table 3.6.1** Summary of calculated and observed IR stretching frequencies for **2**, ImMe$_2$CH$_2$•H$_2$BNH$_2$•BH$_3$, **3**, **5**, **6** and ImMe$_2$CH$_2$•H$_2$BNMe$_2$•BH$_3$.

|   | vB-H calc. (cm$^{-1}$) | vB-H exp. (cm$^{-1}$) | vN-H calc. (cm$^{-1}$) | vN-H exp. (cm$^{-1}$) |
|---|---|---|---|---|
| **2** | 2370, w<br>2425, w<br>2450, w | 2351, w<br>2304, w<br>2219, w | 3452, w<br>3508, w | 3340, w |
| **3** | 2384, w<br>2415, w | 2364, w<br>2297, w<br>2243, w | 3461, w<br>3514, w | 3301, w |
| **5** | 2386, w<br>2418, w<br>2425, w<br>2441, w | 2394, w<br>2354, w<br>2330, w<br>2281, w | - | - |
| **6** | 2370, w<br>2434, w<br>2464, w | 2335, w<br>2295, w | - | - |

## Results from Theoretical Work

**ImMe$_2$CH$_2$•H$_2$BNH$_2$•BH$_3$**

The following compound was used as a model for IPrCH$_2$•H$_2$BNH$_2$•BH$_3$ (**2**), with the 2,6-diisopropylphenyl groups replaced by methyl substituents.
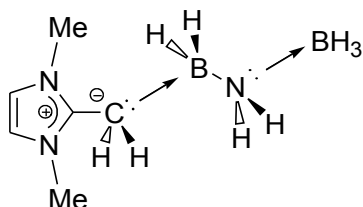


**Table 3.6.2** Calculated bond lengths and angles for the model complex, ImMe$_2$CH$_2$•H$_2$BNH$_2$•BH$_3$, with selected Wiberg bond indices included

|  | d. calc (Å) | θ calc. | Wiberg Bond Index |
|---|---|---|---|
| H$_2$C$_{IPr}$ – B | 1.706 | - | 0.71 |
| B – N | 1.564 | - | 0.70 |
| N – B$_{terminal}$ | 1.638 | - | 0.60 |
| C – B – N | - | 109.5 | - |
| B – N – B | - | 118.3 | - |
| C–B–N–B torsion | - | 180.0 | - |

*NBO Output/Analysis using the cc-pVDZ basis set*

**IMe$_2$CH$_2$-BH$_2$ fragment**

```
6. (1.87623) BD ( 1) C   4 - B  28

              ( 72.83%)   0.8534* C   4 s( 30.06%)p 2.33( 69.93%)d 0.00(  0.01%)
              ( 27.17%)   0.5213* B  28 s( 21.22%)p 3.71( 78.62%)d 0.01(  0.16%)
```

**H$_2$B-NH$_2$ fragment**

```
1. (1.97276) BD ( 1) H   1 - B  28

              ( 54.43%)   0.7378* H   1 s( 99.95%)p 0.00(  0.05%)
              ( 45.57%)   0.6750* B  28 s( 28.38%)p 2.52( 71.58%)d 0.00(  0.04%)

24. (1.98645) BD ( 1) N  21 - H  22

              ( 70.15%)   0.8375* N  21 s( 15.90%)p 5.28( 84.04%)d 0.00(  0.05%)
              ( 29.85%)   0.5464* H  22 s( 99.80%)p 0.00(  0.20%)

27. (1.98291) BD ( 1) N  21 - B  28
              ( 78.52%)   0.8861* N  21 s( 35.97%)p 1.78( 64.01%)d 0.00(  0.02%)
              ( 21.48%)   0.4635* B  28 s( 22.07%)p 3.52( 77.61%)d 0.01(  0.32%)
```

## Terminal NH₂-BH₃ fragment

```
26. (1.97830) BD ( 1) N  21 - B  24

               ( 81.66%)   0.9036* N  21 s( 32.13%)p 2.11( 67.87%)d 0.00(  0.00%)
               ( 18.34%)   0.4283* B  24 s( 17.48%)p 4.70( 82.16%)d 0.02(  0.37%)

28. (1.98934) BD ( 1) B  24 - H  25

               ( 45.95%)   0.6779* B  24 s( 27.88%)p 2.59( 72.08%)d 0.00(  0.04%)
               ( 54.05%)   0.7352* H  25 s( 99.95%)p 0.00(  0.05%)
```



|  |  |  |  |
|---|---|---|---|
| LUMO | HOMO | HOMO-2 | HOMO-3 |
| HOMO-4 | HOMO-5 | HOMO-6 | HOMO-7 |
| HOMO-9 | HOMO-17 | HOMO-18 | HOMO-20 |
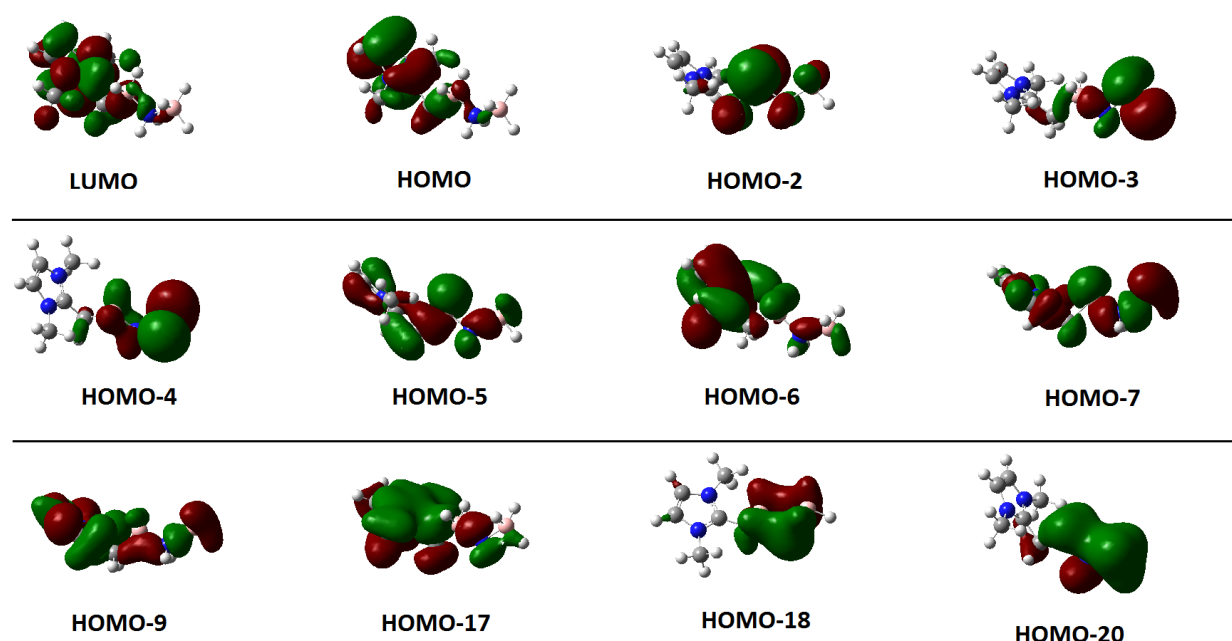
**Figure 3.6.1**: Relevant MO diagrams for the model compound $ImMe_2CH_2 \cdot H_2BNH_2 \cdot BH_3$

## MO Description

| | | |
|---|---|---|
| LUMO | -0.114 a.u. | $ImMe_2CH_2$ $\pi^*$ / $H_2C-BH_2$ σ-bonding |
| HOMO | -0.307 a.u. | $ImMe_2CH_2$ $\pi$ / $H_2C$: donation into an empty p-orbital on $BH_2$ |
| HOMO-2 | -0.342 a.u. | C-H, B-H, N-H, $B_{terminal}$-H σ-bonding |
| HOMO-3 | -0.389 a.u. | $p_{BH2}$ - $p_{NH2}$ σ-bonding interaction / $B_{terminal}$-H σ-bonding |
| HOMO-4 | -0.394 a.u. | $H_2B-NH_2$ $\pi$ symmetry overlap / $B_{terminal}$-H σ-bonding |
| HOMO-5 | -0.399 a.u. | $ImMe_2CH_2$ $\pi$ interaction with $p_{BH2}$ / $p_{H2N}-p_{BH3}$ σ-bonding |
| HOMO-6 | -0.404 a.u. | $ImMe_2CH_2$ $\pi$ system / weak $H_2N-BH_3$ σ-bonding |
| HOMO-7 | -0.446 a.u. | $p_{BH2}-p_{NH2}$ σ-bonding / $p_{NH2}-p_{BH3}$ σ-bonding |
| HOMO-9 | -0.460 a.u. | extended σ interaction between $H_2C$: and p-orbital on N |
| HOMO-17 | -0.536 a.u. | $\pi_{ImMe2CH2}-p_{BH2}$ interaction / $p_{BH2}-p_{NH2}$ σ-bonding |
| HOMO-18 | -0.568 a.u. | $p_{BH2}-p_{NH2}-p_{BH3}$ $\pi$-symmetry bonding interaction |
| HOMO-20 | -0.594 a.u. | $BH_2$ and $BH_3$ $A_1$ bonding combination mixing with p-orbital on N |

**DMAP•H₂BNH₂•BH₃ (3)**
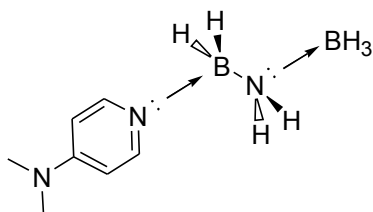


**Table 3.6.3** Comparison of experimental and calculated bond lengths and angles for **3**, with selected Wiberg bond indices included

|  | d. exp (Å) | d. calc (Å) | θ exp. | θ calc. | Wiberg Bond Index |
|---|---|---|---|---|---|
| N$_{DMAP}$– B | 1.5728(15) | 1.594 | - | - | 0.60 |
| B – N | 1.5720(17) | 1.576 | - | - | 0.69 |
| N – B$_{terminal}$ | 1.5939(16) | 1.628 | - | - | 0.63 |
| N$_{DMAP}$– B – N | - | - | 110.44(9) | 109.2 | - |
| B – N – B | - | - | 118.68(9) | 121.8 | - |
| N$_{DMAP}$–B–N–B torsion | - | - | 65.71(13) | 49.3 | - |

*NBO Output/Analysis using the cc-pVDZ basis set*

**H₂B-NH₂ fragment**

```
15. (1.97451) BD ( 1) B  10 - H  11

            ( 46.42%)   0.6813* B  10 s( 29.50%)p 2.39( 70.46%)d 0.00(  0.04%)
            ( 53.58%)   0.7320* H  11 s( 99.94%)p 0.00(  0.06%)

18. (1.96843) BD ( 1) B  10 - N  21
            ( 18.58%)   0.4311* B  10 s( 19.63%)p 4.07( 79.86%)d 0.03(  0.50%)
            ( 81.42%)   0.9023* N  21 s( 35.63%)p 1.81( 64.37%)d 0.00(  0.00%)

19. (1.98771) BD ( 1) N  13 - H  14
            ( 70.43%)   0.8392* N  13 s( 16.21%)p 5.17( 83.74%)d 0.00(  0.05%)
            ( 29.57%)   0.5438* H  14 s( 99.79%)p 0.00(  0.21%)
```

**Terminal NH₂-BH₃ fragment**

```
21. (1.98572) BD ( 1) N  13 - B  16

            ( 80.78%)   0.8988* N  13 s( 33.71%)p 1.97( 66.28%)d 0.00(  0.00%)
            ( 19.22%)   0.4384* B  16 s( 17.87%)p 4.58( 81.77%)d 0.02(  0.36%)

22. (1.98637) BD ( 1) B  16 - H  17
            ( 45.72%)   0.6762* B  16 s( 27.33%)p 2.66( 72.62%)d 0.00(  0.04%)
            ( 54.28%)   0.7367* H  17 s( 99.95%)p 0.00(  0.05%)
```
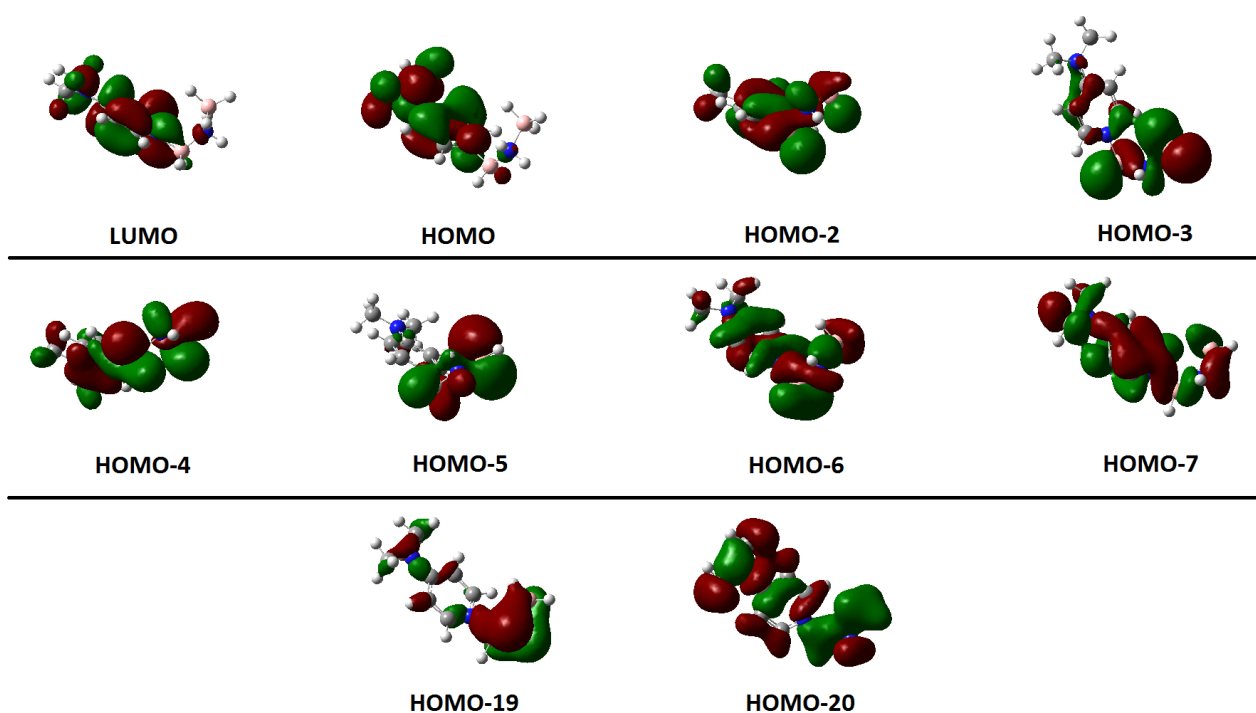
**Figure 3.6.2**: Relevant MO diagrams for DMAP•H$_2$BNH$_2$•BH$_3$ (**3**)

**MO Description**

| | | |
|---|---|---|
| LUMO | -0.160 a.u. | DMAP π, Me$_2$N-Ar π* |
| HOMO | -0.296 a.u. | DMAP π |
| HOMO-2 | -0.386 a.u. | DMAP LP donation into p-orbital on BH$_2$ / N-H and B-H  σ-bonding |
| HOMO-3 | -0.393 a.u. | p$_{BH2}$-p$_{NH2}$ σ-bonding / B$_{terminal}$-H σ-bonding |
| HOMO-4 | -0.397 a.u. | π$_{DMAP}$ mixing with p$_{BH2}$ / p$_{NH2}$-p$_{BH3}$ σ-bonding |
| HOMO-5 | -0.399 a.u. | B-H, N-H, B$_{terminal}$-H σ-bonding |
| HOMO-6 | -0.430 a..u. | π$_{DMAP}$ mixing with p$_{BH2}$ and p$_{NH2}$ / p$_{NH2}$-p$_{BH3}$ σ-bonding |
| HOMO-7 | -0.442 a.u. | slipped π$_{DMAP}$ -p$_{BH2}$ interaction / p$_{BH2}$-p$_{NH2}$ and p$_{NH2}$-p$_{BH3}$ σ-bonding |
| HOMO-19 | -0.568 a.u. | p$_{BH2}$-p$_{NH2}$-p$_{BH3}$ π-symmetry bonding interaction |
| HOMO-20 | -0.587 a.u. | BH$_2$ and BH$_3$ A$_1$ bonding combination mixing with p-orbital on N |

**DMAP•H₂BNMe₂•BH₃ (5)**
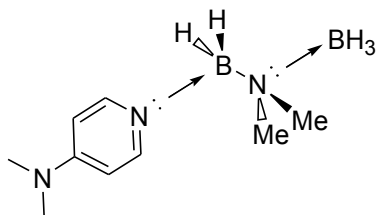


**Table 3.6.4** Comparison of experimental and calculated bond lengths and angles for **5**, with selected Wiberg bond indices included

|  | d. exp (Å) | d. calc (Å) | θ exp. | θ calc. | Wiberg Bond Index |
|---|---|---|---|---|---|
| N$_{DMAP}$– B | 1.5722(19) | 1.595 | - | - | 0.60 |
| B – N | 1.5801(18) | 1.592 | - | - | 0.62 |
| N – B$_{terminal}$ | 1.6020(19) | 1.635 | - | - | 0.58 |
| N$_{DMAP}$– B – N | - | - | 111.32(11) | 111.2 | - |
| B – N – B | - | - | 114.53(11) | 114.7 | - |
| N$_{DMAP}$–B–N–B torsion | - | - | 60.99(15) | 52.4 | - |

*NBO Output/Analysis using the cc-pVDZ basis set*

**DMAP-H₂B fragment**

```
18. (1.96750) BD ( 1) B  10 - N  19

           ( 18.53%)   0.4305* B  10 s( 19.61%)p 4.08( 80.02%)d 0.02(  0.37%)
           ( 81.47%)   0.9026* N  19 s( 36.82%)p 1.72( 63.17%)d 0.00(  0.00%)
```

**H₂B-NMe₂ fragment**

```
15. (1.97521) BD ( 1) B  10 - H  11

           ( 46.92%)   0.6850* B  10 s( 29.82%)p 2.35( 70.09%)d 0.00(  0.09%)
           ( 53.08%)   0.7285* H  11 s( 99.96%)p 0.00(  0.04%)

(1.96013) BD ( 1) B  10 - N  13
           ( 20.08%)   0.4481* B  10 s( 22.07%)p 3.51( 77.57%)d 0.02(  0.35%)
           ( 79.92%)   0.8940* N  13 s( 27.73%)p 2.61( 72.27%)d 0.00(  0.01%)
```

**Terminal NMe₂-BH₃ fragment**

```
19. (1.95995) BD ( 1) N  13 - B  14

           ( 81.75%)   0.9042* N  13 s( 27.83%)p 2.59( 72.17%)d 0.00(  0.01%)
           ( 18.25%)   0.4272* B  14 s( 17.74%)p 4.61( 81.82%)d 0.03(  0.45%)
```
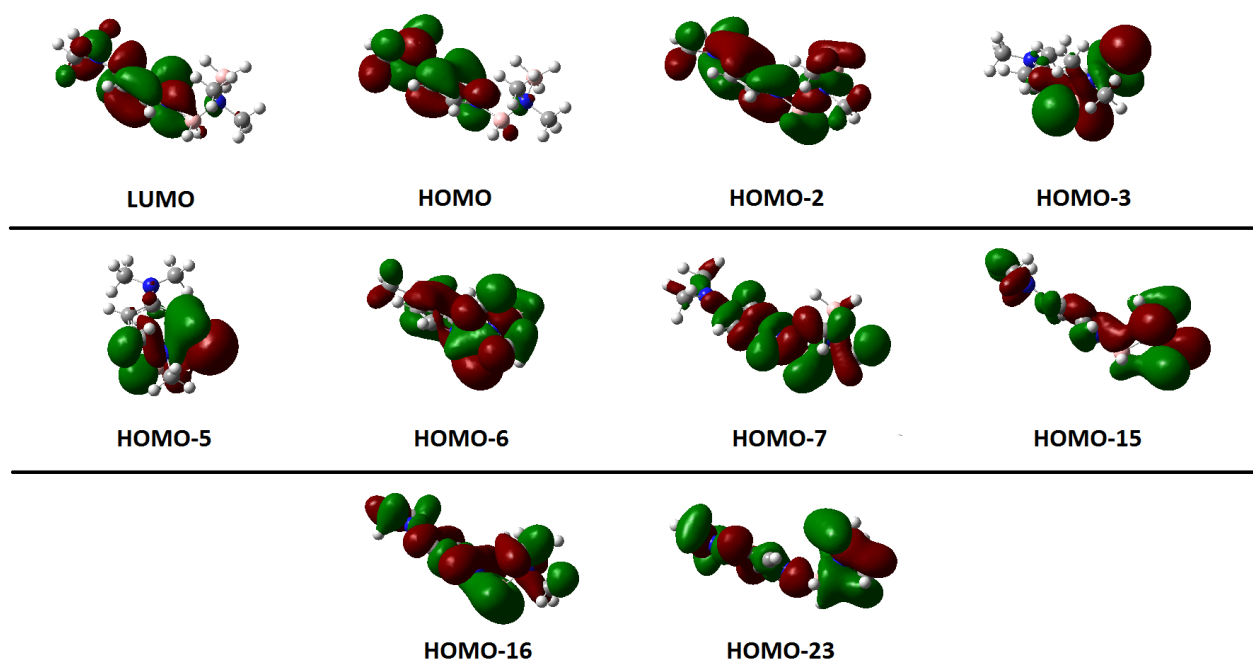
**Figure 3.6.3**: Relevant MO diagrams for DMAP•H₂BNMe₂•BH₃ **(5)**

## MO Descriptions

| | | |
|---|---|---|
| LUMO | -0.160 a.u. | DMAP $\pi$, Me$_2$N-Ar $\pi^*$ |
| HOMO | -0.296 a.u. | DMAP $\pi$ |
| HOMO-2 | -0.353 a.u. | B-H $\sigma$-bonding / p$_{BH2}$-p$_{NMe2}$ and p$_{NMe2}$-p$_{BH3}$ $\sigma$-bonding |
| HOMO-3 | -0.386 a.u. | BH$_2$ and BH$_3$ B-H $\sigma$-bonding w/ weak p$_{NH2}$ mixing. |
| HOMO-5 | -0.398 a.u. | p$_{BH2}$ and p$_{BH3}$ B-H $\sigma$-bonding / p$_N$-p$_{CH3}$ $\sigma$-bonding |
| HOMO-6 | -0.401 a.u. | $\pi_{DMAP}$ mixing with p$_{BH2}$ / p$_{NMe2}$-p$_{BH3}$ $\sigma$-bonding / (C-H)$_{NMe2}$ $\sigma$-bonding |
| HOMO-7 | -0.413 a.u. | DMAP LP donation into p$_{BH2}$ / (C-H)$_{NMe2}$ $\sigma$-bonding |
| HOMO-15 | -0.479 a.u. | slipped $\pi_{DMAP}$-p$_{BH2}$ interaction / (C-H)$_{NMe2}$ $\sigma$-bonding |
| HOMO-16 | -0.504 a.u. | $\pi_{DMAP}$ mixed with A$_1$ combination of BH$_2$ / p$_{NMe2}$-p$_{BH3}$ $\sigma$-bonding |
| HOMO-23 | -0.558 a.u. | DMAP-BH$_2$ $\sigma$-ineraction / p$_{NMe2}$-p$_{BH3}$ $\sigma$-bonding |

**ImMe$_2$CH$_2$•H$_2$BNMe$_2$•BH$_3$**

The following compound was used as a model for IPrCH$_2$•H$_2$BNMe$_2$•BH$_3$ (**6**), with the 2,6-diisopropylphenyl groups replaced by methyl substituents.
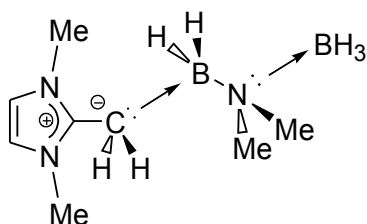


**Table 3.6.5** Comparison of experimental and calculated bond lengths and angles for **6** and the model complex, ImMe$_2$CH$_2$•H$_2$BNMe$_2$•BH$_3$, with selected Wiberg bond indices included

|  | d. exp (Å) | d. calc (Å) | θ exp. | θ calc. | Wiberg Bond Index |
|---|---|---|---|---|---|
| H$_2$C$_{IPr}$ – B | 1.660(3) | 1.709 | - | - | 0.72 |
| B – N | 1.659(9) | 1.587 | - | - | 0.63 |
| N – B$_{terminal}$ | 1.595(12) | 1.652 | - | - | 0.55 |
| C – B – N | - | - | 107.9(4) | 112.5 | - |
| B – N – B | - | - | 116.3(7) | 109.0 | - |
| C–B–N–B torsion | - | - | 51.3(6) | 180.0 | - |

*NBO Output/Analysis using the cc-pVDZ basis set*

**IMe$_2$CH$_2$-BH$_2$ fragment**

```
6. (1.87806) BD ( 1) C    4 - B   26

              ( 72.45%)   0.8512* C    4 s( 30.62%)p 2.27( 69.37%)d 0.00(  0.01%)
              ( 27.55%)   0.5249* B   26 s( 21.31%)p 3.69( 78.54%)d 0.01(  0.15%)
```

**H$_2$B-NMe$_2$ fragment**

```
1. (1.97428) BD ( 1) H    1 - B   26

              ( 53.86%)   0.7339* H    1 s( 99.95%)p 0.00(  0.05%)
              ( 46.14%)   0.6793* B   26 s( 28.39%)p 2.52( 71.57%)d 0.00(  0.04%)

25. (1.95814) BD ( 1) N   21 - B   26
              ( 79.94%)   0.8941* N   21 s( 29.81%)p 2.35( 70.17%)d 0.00(  0.01%)
              ( 20.06%)   0.4479* B   26 s( 21.87%)p 3.56( 77.75%)d 0.02(  0.38%)
```

**Terminal NMe$_2$-BH$_3$ fragment**

```
30. (1.98636) BD ( 1) B   22 - H   25

              ( 45.81%)   0.6768* B   22 s( 26.61%)p 2.76( 73.35%)d 0.00(  0.05%)
```

```
                    ( 54.19%)   0.7361* H  25 s( 99.95%)p 0.00(  0.05%)

24. (1.94645) BD ( 1) N  21 - B  22
                    ( 82.69%)   0.9093* N  21 s( 25.96%)p 2.85( 74.04%)d 0.00(  0.00%)
                    ( 17.31%)   0.4161* B  22 s( 17.26%)p 4.77( 82.31%)d 0.03(  0.43%)
```



| LUMO | HOMO | HOMO-2 | HOMO-3 |

| HOMO-4 | HOMO-5 | HOMO-6 | HOMO-7 |

| HOMO-9 | HOMO-19 | HOMO-22 | HOMO-25 |
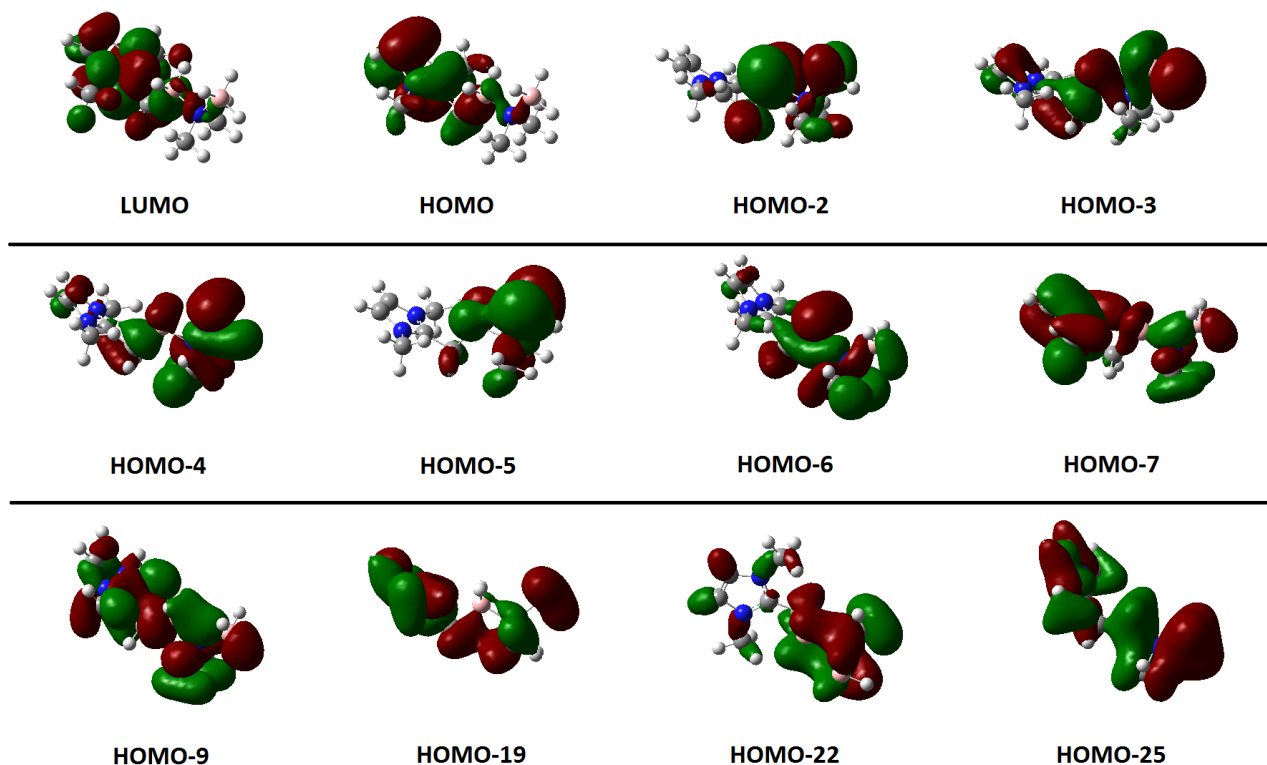
**Figure 3.6.4**:Relevant MO diagrams for the model compound ImMe$_2$CH$_2$•H$_2$BNH$_2$•BH$_3$

## MO Descriptions

| LUMO | -0.114 a.u. | ImMe$_2$CH$_2$ $\pi$* / weak CH$_2$-BH$_2$ $\sigma$-bonding |
|------|-------------|------------------------------------------------------------|
| HOMO | -0.307 a.u. | ImMe$_2$CH$_2$ $\pi$ / p$_{CH2}$-p$_{BH2}$ $\sigma$-bonding |
| HOMO-2 | -0.391 a.u. | C-H, B-H, Bterminal-H $\sigma$-bonding / C$_{NMe2}$ non-bonding |
| HOMO-3 | -0.393 a.u. | LP on CH$_2$ donating into p$_{BH2}$ / p$_{BH2}$ and p$_{BH3}$ mixed w/ p$_{NMe2}$ |
| HOMO-4 | -0.401 a.u. | LP on CH$_2$ donating into p$_{BH2}$ / p$_{BH2}$-p$_{NMe2}$ $\pi$* / p$_{NMe2}$-p$_{BH3}$ $\sigma$-bonding |
| HOMO-5 | -0.402 a.u. | BH$_2$ and BH$_3$ B-H $\sigma$-bonding / p$_N$-p$_{CH3}$ $\sigma$-bonding |
| HOMO-6 | -0.409 a.u. | mixed p$_{CH2}$-p$_{BH2}$-p$_{NMe2}$-p$_{BH3}$ bonding interaction |
| HOMO-7 | -0.443 a.u. | p$_{BH2}$ and p$_{BH3}$ mixed w/ p$_{NMe2}$ / p$_N$-p$_{CH3}$ $\sigma$-bonding |
| HOMO-9 | -0.458 a.u. | ImMe$_2$CH$_2$ $\pi$ interaction with p$_{BH2}$ mixed w/ p$_{NMe2}$ and p$_{BH3}$ |
| HOMO-19 | -0.520 a.u. | Extended interaction between p$_{CH2}$ and p$_{NMe2}$ / BH$_3$ $\sigma$-bonding |
| HOMO-22 | -0.545 a.u. | p$_{BH2}$-p$_{NMe2}$-p$_{BH3}$ $\pi$-symmetry bonding interaction |
| HOMO-25 | -0.614 a.u. | BH$_2$ and BH$_3$ A$_1$ bonding combination mixing with p-orbital on N |

126

## 3.7 References

[1] For a relevant review on ammonia-borane, see: F. H. Stephens, V. Pons, R. T. Baker. *Dalton Trans.* **2007**, 2613.

[2] M. Matus, S.-Y. Liu, D. A. Dixon. *J. Phys. Chem. A.* **2010**, *114*, 2644.

[3] a) M. G. Hu, R. A. Geanangel, W. W. Wendlandt. *Thermochimica Acta.* **1978**, *23*, 249. b) C. R. Eddy, B. D. Sartwell. *J. Vac. Sci. Technol. A.* **1995,** *13*, 2018 (and references contained therein).

[4] C. T. Kwon, H. A. McGee Jr. *Inorg. Chem.* **1970,** *9*, 2458.

[5] E. R. Lory, R. F. Porter. *J. Am. Chem. Soc.* **1973**, *95*, 1766.

[6] a) C. A. Thompson, L. Andrews, *J. Am. Chem. Soc.* **1995**, *117*, 10125. b) C.A. Thompson, L . Andrews, J. M. L. Martin, J. El-Yazal. *J.Phys. Chem.* **1995**, *99*, 13839.

[7] a) R. H. Wentorf, Jr. *J. Chem. Phys.* **1957**, *26*, 956. b) L. Vel, G. Demazeau, J. Etourneau. *Materials Science and Engineering B.* **1991**, *10*, 149 (and references contained therein).

[8] a) V. L. Solozhenko, V. Ya. Leonidov. *J. Phys. Chem.* **1988**, *62*, 1646.

[9] S. Rudolpho. *American Ceramic Society Bulletin.* **2000**, *79*, 50.

[10] a) R. Zedlitz, M. Heintze, M. B. Schubert. *J. Non-Cryst. Sol.* **1996**, *198-200*, 403. b) Z. Pan, H. Sun, Y. Zhang, C. Chen. *Phys. Rev. Lett.* **2009**, *102*, 055503. c) K. Watanabe, T. Taniguchi, H. Kanda. *Nature Mater.* **2004**, *3*, 404. d) S. Y. Shapoval, V. T. Petrashov, O. A. Popov, A. O. Westner, M. D. Yoder, Jr., C. K. C. Lok. *Appl. Phys. Lett.* **1990**, *57*, 1885. e) A. Weber, U. Bringmann, R. Nikulski, C.-P. Klages. *Diamond Relat. Mater.* **1993**, *2*, 201. f) T. Ichiki, T. Yoshida. *Appl. Phys. Lett.* **1994**, *64*, 851. g) T. Ichiki, T. Momose, T. Yoshida. *J. Appl. Phys.* **1994**, *75*, 1330.

[11] Y. Kubota, K. Watanabe, O. Tsuda, T. Taniguchi. *Science* **2007**, *317*, 932.

[12] K. C. Thimer, S. M. I. Al-Rafia, M. J. Ferguson, R. McDonald, E. Rivard, *Chem. Commun.* **2009**, 7119.

[13] a) S. M. I. Al-Rafia, A. C. Malcolm, S. K. Liew, M. J. Ferguson, E. Rivard. *J. Am. Chem. Soc.* **2011**, *133*, 777. b) A. Jana, C. Schulzke, H. W. Roesky. *J. Am. Chem. Soc.* **2009**, *131*, 4600.

[14] S. M. I. Al-Rafia, A. C. Malcolm, R. McDonald, M. J. Ferguson, E. Rivard. *Chem. Commun.* **2012**, *48*, 1308.

[15] S. M. I. Al-Rafia, A. C. Malcolm, S. K. Liew, R. McDonald, M. J. Ferguson, E. Rivard. *Angew. Chem. Int. Ed.* **2011**, *50*, 8354.

[16] K. W. Bodekker, S. G. Shore, R. K. Bunting. *J. Am. Chem. Soc.* **1966,** *88*, 4396.

[17] S. M. I. Al-Rafia, A. C. Malcolm, S. K. Liew, M. J. Ferguson, R. McDonald, E. Rivard, *Chem. Commun.* **2011**, *47*, 6987.

[18] Literature NMR values for $HB(C_6F_5)_3^-$ see: a) P. A. Chase, D. W. Stephan. *Angew. Chem. Int. Ed.* **2008**, *47*, 7433. b) S. J. Geier, D. W. Stephan. *J. Am. Chem. Soc.* **2009**, *131*, 3476. c) R. C. Neu, E. Y. Ouyang, S. J. Geier, X. Zhao, A. Ramos, D. W. Stephan. *Dalton. Trans.* **2010**, *39*, 4285. d) S. M. I. Al-Rafia, M. J. Ferguson, E. Rivard. *Inorg. Chem.* **2011**, *50*, 10543. Data for [IPrMe$^+$][Cl$^-$]: $^1$H NMR (400 MHz, CDCl$_3$): δ = 8.52 (s, 2H, -N-C*H*), 7.60 (t, 4H, $^3J_{HH}$ = 7.6 Hz, Ar*H*), 7.44 (d, 2H, $^3J_{HH}$ = 7.6 Hz, Ar*H*), 2.34 (septet, 2H, $^3J_{HH}$ = 9.2 Hz, -C*H*(CH$_3$)$_2$), 2.08 (s, 3H, IPrC*H$_3$*), 1.28 (d, 12H, $^3J_{HH}$ = 6.8 Hz, -CH(C*H$_3$*)$_2$), 1.18 (d, 12H, $^3J_{HH}$ = 6.8 Hz, -CH(C*H$_3$*)$_2$). $^{13}$C{$^1$H} (125 MHz, CDCl$_3$): δ = 145.0 (Ar*C*), 144.4 (Ar*C*), 132.5 (Ar*C*), 129.2 (Ar*C*), 127.1 (Ar*C*), 125.3 (-N-*C*H), 29.1 (-*C*H(CH$_3$)$_2$), 24.6 (-CH(*C*H$_3$)$_2$), 23.4 (-CH(*C*H$_3$)$_2$), 10.81 (IPr*C*H$_3$). MS (EI): m/z = 403.3 (M$^+$). Anal. Calcd. for C$_{28}$H$_{39}$ClN$_2$: C, 76.59; H, 8.95; N, 6.38. Found: C, 76.56; H, 8.87; N, 6.56.

[19] Y. Wang, B. Quillian, P. Wei, C. S. Wannere, Y. Xie, R. B. King, H. F. Schaefer, P. v. R. Schleyer, G. H. Robinson. *Chem. Mater.* **2007**, *129*, 12412.

[20] W. T. Klooster, T. F. Koetzle, P. E. M. Siegbahn, T. B. Richardson, R. H. Crabtree. *J. Am. Chem. Soc.* **1999**. *121*, 6337.

[21] X. Chen, J-C. Zhao, S.G. Shore. *J. Am. Chem. Soc.* **2010**. *132*, 10658. Bond lengths were extracted from cif files in the electronic supporting information, as no crystallographic tables were published.

[22] J.-S. Li, C.-R. Zhang, B. Li, F. Cao, S.-Q. Wang. *Eur. J. Inorg. Chem.* **2010**, 1763.

[23] a) C. A. Jaska, I. Manners. *J. Am. Chem. Soc.* **2004**, *126*, 2698. b) C. A. Jaska, I. Manners. *J. Am. Chem. Soc.* **2004**, *126*, 9776. c) Manners and co-workers discovered via mercury amalgamation that [Rh(COD)Cl]₂ acts as a heterogeneous catalyst by forming colloidal rhodium in the presence of ammonia boranes; C. A. Jaska, I. Manners. *J. Am. Chem. Soc.* **2004**, *126*, 1334.

[24] a) W. Luo, P. G. Campbell, L. N. Zakharov, S-Y Liu. *J. Am. Chem. Soc.* **2011**, *133,* 19326. b) P. G. Campbell, L. N. Zakharov, D. J. Grant, D. A. Dixon, S-Y Liu. *J. Am. Chem. Soc.* **2010**, *132*, 3289.

[25] A. Jana, R. Azhakar, G. Tavčar, H. W. Roesky, I. Objartel, D. Stalke. *Eur. J. Inorg. Chem.* **2011**, 3686.

[26] J. Li, S. Bernard, V. Salles, C. Gervais, P. Miele. *Chem. Mater.* **2010**, *22*, 2010.

[27] M. M. Hansmann, R. L. Melen, D. S. Wright. *Chem. Sci.* **2011**, *2*, 1554.

[28] A. B. Pangborn, M. A. Giardello, R. H. Grubbs, R. K. Rosen, F. J. Timmers. *Organometallics* **1996**, *15*, 1518.

[29] L. Jafarpour, E. D. Stevens, S. P. Nolan. *J. Organomet. Chem.* **2000**, *606*, 49.

[30] A. Dumrath, X.-F. Wu, H. Neumann, A. Spannenberg, R. Jackstell, M. Beller. *Angew. Chem. Int. Ed.* **2010**, *49*, 8988.

[31] H. Hope, Prog. *Inorg. Chem.* **1995**, *43*, 1.

[32] R. H. Blessing. *Acta Cryst.* **1995**, *A51*, 33.

[33] Schneider, T. R., Sheldrick, G. M. *Acta Crystallogr.* **2002**, *D58*, 1772.

[34] Sheldrick, G. M. *Acta Crystallogr.* **2008**, *A64*, 112.

[35] Gaussian 09, Revision **B.01**, M. J. Frisch, G. W. Trucks, H. B. Schlegel, G. E. Scuseria, M. A. Robb, J. R. Cheeseman, G. Scalmani, V. Barone, B. Mennucci, G. A. Petersson, H. Nakatsuji, M. Caricato, X. Li, H. P. Hratchian, A. F. Izmaylov, J. Bloino, G. Zheng, J. L. Sonnenberg, M. Hada, M. Ehara, K. Toyota, R. Fukuda, J. Hasegawa, M. Ishida, T. Nakajima, Y. Honda, O. Kitao, H. Nakai, T. Vreven, J. A. Montgomery, Jr., J. E. Peralta, F. Ogliaro, M. Bearpark, J. J. Heyd, E.

Brothers, K. N. Kudin, V. N. Staroverov, R. Kobayashi, J. Normand, K. Raghavachari, A. Rendell, J. C. Burant, S. S. Iyengar, J. Tomasi, M. Cossi, N. Rega, J. M. Millam, M. Klene, J. E. Knox, J. B. Cross, V. Bakken, C. Adamo, J. Jaramillo, R. Gomperts, R. E. Stratmann, O. Yazyev, A. J. Austin, R. Cammi, C. Pomelli, J. W. Ochterski, R. L. Martin, K. Morokuma, V. G. Zakrzewski, G. A. Voth, P. Salvador, J. J. Dannenberg, S. Dapprich, A. D. Daniels, Ö. Farkas, J. B. Foresman, J. V. Ortiz, J. Cioslowski, D. J. Fox, Gaussian, Inc., Wallingford CT, 2009.

[36] a) K. A. Peterson. *J. Chem. Phys.* **2003**, *119*, 1109. b) K. A. Peterson, D. Figgen, E. Goll, H. Stoll, M. Dolg. *J. Chem. Phys.* **2003**, *119*, 11113. c) K. A. Peterson, C. Puzzarini. *Theor. Chem. Acc.* **2005**, *114*, 283. d) K.A. Peterson, D. Figgen, M. Dolg, H. Stoll. *J. Chem. Phys.* **2007**, *126*, 124101. e) K. A. Peterson, B. C. Shepler, D. Figgen, H. Stoll. *J. Phys. Chem. A.* **2006**, *110*, 13877. f) D. Figgen, K. A. Peterson, M. Dolg, H. Stoll. *J. Chem. Phys.* **2009**, *130*, 164108.

# Chapter 4

# Summary and future work

## 4.1 Summary and future work for Chapter 2: Platinum-containing polymers for use in polymer-based photovoltaic applications

Chapter 2 describes the synthesis of phosphine-bound Pt-containing complexes with directly bound thienyl residues. The 5-position of the aromatic thienyl groups were brominated to allow for cross-coupling (and polymerization) of aryl-bromide groups to transpire, via C-C bond formation. Specifically, the synthesis of the complex $(Bu_3P)_2Pt(SC_4H_2Br)_2$ was accomplished by transmetallation of $(COD)PtCl_2$ with 2-bromo-5-trimethylstannylthiophene, followed by displacement of the labile COD ligand with $Bu_3P$. Polymerization attempts using Yamamoto coupling were the most successful, yielding polymeric materials with molecular weights $(M_w)$ between 3000 and 38 000 g/mol. Due to the high solubility of the materials generated, it was difficult to separate residual monomers or low molecular weight oligomers from the polymeric materials. The total Pt content of the materials remains unknown, and the optical absorption profiles showed band edge absorptions around 400 - 500 nm, which falls short of the standards set by other polymer-based photovoltaics that use less costly P3HT polymer variants. Alternatively, the utility of these polymers as light emitting diode materials is a potential avenue of chemical exploration.

It was discovered during the initial polymerization attempts that $(Bu_3P)_2Pt(SC_4H_2Br)_2$ displayed solvent and temperature dependant *cis-trans* isomerism. Thus, when using different solvent and temperature combinations, the isomeric form of the polymerizable monomer is difficult to predict, potentially resulting in isomerically impure materials. To control the geometry of the Pt-centre, the chelating phosphines dppe and dppp were used in place of $Bu_3P$, forming isomerically pure *cis*-(dppe)Pt($SC_4H_2Br)_2$ and *cis*-(dppp)Pt($SC_4H_2Br)_2$. Attempts to induce primative, model coupling reactions with the terminal aryl-Br residues proved unsuccessful, implying that the *cis*-form of these complexes are not susceptible to standard cross-coupling reactions. Additionally, phosphine exchange and undesirable reaction between the Pt complex and the employed $Pd(PPh_3)_4$ catalyst imply that these complexes are not conducive to polymerization under standard Sonogashira, Stille, Kumada and Yamamoto type coupling chemistry.

The implications of this work have led us to believe that an isomerically pure *trans*-Pt complex may be desirable to achieve polymerization of $(R_3P)_2Pt(SC_4H_2)_2$ type monomers (R = bulky solubilizing substituent). Initial attempts at synthesizing such complexes has begun by replacing $PBu_3$ phosphines with $PAr'_3$ (Ar' = 3,5 - diisopropylphenyl), leading to complexes that rest solely in the *trans* geometry. Future work will involve obtaining pure samples of this compound, followed by attempts to polymerize with the previously successful Yamamoto homocoupling of the monomer unit.

One avenue of cross-coupling that was not attempted on this system was Suzuki coupling. The reason for this is simply due to the lack of the required precursor, 2-pinacolatoboro-5-trimethylstannylthiophene, to form the complexes of the form $(R_3P)_2(SC_4H_2B[pin])_2$ ([pin] = $O(Me_2)CC(Me_2)O$; R = Bu or Ar) (Scheme 4.1). It would be of value to explore the potential for cross-coupling with this functionality, as Pd-catalysts would not react with the Pt-complexes, but rather with the co-monomer (in this case, 2,5-dibromothiophene or 2,5-dibromo-3-hexylthiophene (although catalyst deactivation via ligand scrambling remains as a possibility). To combat the potential phosphine scrambling, a bulky phosphine ($PAr'_3$) can be used to induce trans-geometry at the Pt centre, as well to generate a new 2-coordinate $Pd^{(0)}$ catalyst $[(PAr'_3)_2Pd^{(0)}]$. The cross-coupling of this new sterically encumbered Pt-complex, $(PAr'_3)_2Pt(SC_4H_2B[pin])$, using $[(PAr'_3)_2Pd^{(0)}]$ as a catalyst would eliminate any possible complications from phosphine exchange.
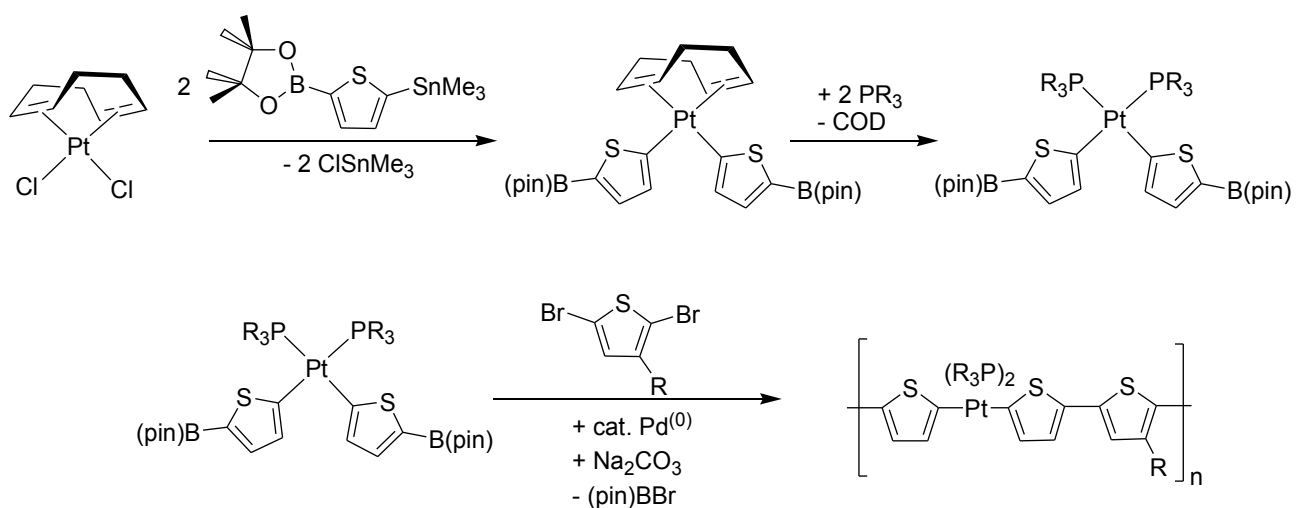
**Scheme 4.1**: Synthetic route towards a pinacol-borane functionalized Pt-thienyl complex, for use in Suzuki type cross-coupling reactions. [(pin) = O(Me$_2$)CC(Me$_2$)O; R = Bu or Ar]

**4.2 Summary and future work for Chapter 3: Isolation of inorganic ethene (H₂BNH₂): en route to boron nitride**

Chapter 3 describes the synthesis of donor-acceptor adducts of the parent inorganic ethene, $H_2BNH_2$, with the general form $LB\bullet H_2BNH_2\bullet LA$ (LB = Lewis base, LA = Lewis acid). The goal of the work was to generate a molecular precursor containing an isolated $H_2BNH_2$ unit that could be dehydrogenated to yield isolated molecular boron nitride ($B\equiv N:$). The successful isolation of of an adduct of $H_2BNH_2$ was achieved via ring-opening of aminodiborane, $NH_2B_2H_5$, with the Lewis bases, $IPrCH_2$ and DMAP, to yield the adducts $IPrCH_2\bullet H_2BNH_2\bullet BH_3$ and $DMAP\bullet H_2BNH_2\bullet BH_3$, respectively.  It was shown that the $IPrCH_2$ adduct would decompose in THF solution, and demonstrated limited or no solubility in other solvents, making it difficult to characterize by X-ray crystallography, or to carry out controlled chemical reactions. However, the DMAP adduct was indefinitely stable in both the solution and solid state.

The adduct, $DMAP\bullet H_2BNH_2\bullet BH_3$, was dehydrogenated with catalytic amounts of $Me_2S\bullet CuBr$ and $(DME)\bullet NiBr_2$ to yield the Lewis base-acid adduct, $DMAP\bullet BH_3$, and borazine $[(HBNH)_3]$. The presence of borazine indicated that the central $H_2BNH_2$ unit was indeed releasing one equivalent of $H_2$ to yield the parent iminoborane (HBNH) which was subsequently extruded and underwent trimerization to give $(HBNH)_3$. In an attempt to prevent the extrusion and trimerization of the iminoborane unit (HBNR), a *tert*-butyl group was installed at the nitrogen centre to yield the sterically encumbered adduct $DMAP\bullet H_2BNH(tBu)\bullet BH_3$. This complex was subsequently dehydrogenated to yield a mixture of products, including $DMAP\bullet BH_3$, $(HBNtBu)_3$, and $[H_2BNH(tBu)]_3$; thus it was noted that increasing the steric bulk at nitrogen did not prevent the formation of oligomeric iminoboranes. These data when taken with the fact that the parent borazines had been difficult to produce in large quantities and in good yields, indicate that these donor-acceptor adducts may be a convenient one-pot source of borazine for further exploratory chemistry.

It was suspected that the teriminal $H_2N\text{-}BH_3$ unit could also participate in dehydrogenation chemistry, leading to undesirable side-reactions. In order to prevent this, displacement of the terminal $BH_3$ unit with a Lewis acid that is not susceptible to hydrogen loss was necessary. In order to verify if the terminal $BH_3$ unit could be displaced with other Lewis acids, we reacted $IPrCH_2 \cdot H_2BNH_2 \cdot BH_3$ with $B(C_6F_5)_3$, however the only observed product was the methylimidazolium salt, $[IPrCH_3^+][HB(C_6F_5)_3^-]$, demonstrating simultaneous $H^-/H^+$ loss from the parent molecule. The N-methylated analogues, $IPrCH_2 \cdot H_2BNMe_2 \cdot BH_3$, $DMAP \cdot H_2BNMe_2 \cdot BH_3$, as well as $IPr \cdot H_2BNMe_2 \cdot BH_3$ were synthesized to prevent this from occurring, however the clean displacement of $BH_3$ by $B(C_6F_5)_3$ has thus far been unsuccessful.

Future work of this project will involve determining methods of directly preparing B-N donor-acceptor adducts with $B(C_6F_5)_3$ and other strong Lewis acids such as metal carbonyls ($W(CO)_5$, $Cr(CO)_5$). For example, the synthesis of donor-acceptor adducts of $H_2BNH_2$ with $B(C_6F_5)_3$ as the Lewis acid are currently underway in the Rivard group, via the route shown in Scheme 4.2. Long-term future goals involve initiating the controlled solution phase release of BN (amorphous or hexagonal) at low temperature and pressure, for potential use in novel substrate coatings or as a low-cost feed stock for cubic BN.
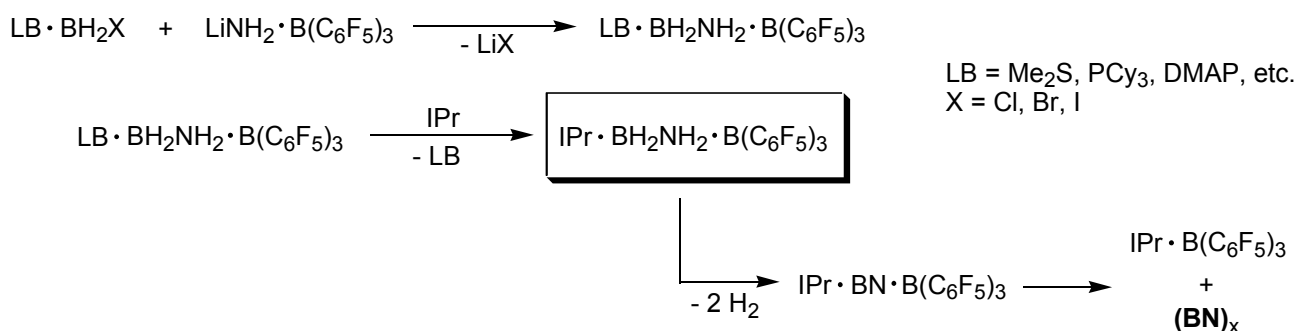


**Scheme 4.2**: Proposed direct synthetic route for obtaining donor-acceptor adducts of $H_2BNH_2$ with $B(C_6F_5)_3$ as the terminal Lewis acid.

*- fin -*